UNIVERSITY OF TEXAS ARLINGTON

LABORATORY TESTING OF ENGINEERED MEDIA FOR BIOFILTRATION SWALES

(Project No. TRN6835)

FINAL REPORT

Prepared for:

North Central Texas Council of Governments
616 Six Flags Dr.
Arlington, Texas 76011

Submitted by

Habib Ahmari, Ph.D., P.E.
Ashish Bhurtyal
Srinivas Prabakar, Ph.D.
Qazi Ashique Mowla
Saman Baharvand, Ph.D., EIT
Hassan Alsaud

The University of Texas at Arlington, Arlington, Texas, USA

September 2023

DISCLAIMER

The contents of this report reflect the views of the authors, who are responsible for the facts and the accuracy of the data presented herein. The contents do not necessarily reflect the official view or policies of the North Central Texas Council of Governments (NCTCOG). While every effort has been made to ensure the accuracy of information provided in this report, this material is not intended to be a substitute for the actual guidelines and specifications for the design of stormwater best management practices (BMPs), nor for assessing their performance in enhancing water quality.

This report does not constitute a standard, specification, or regulation, and is not intended for constructing, bidding, or permit purposes.

The authors do not endorse products or manufacturers. Trade or manufacturers' names appear herein solely because they are considered essential to the object of this report.

ACKNOWLEDGEMENT

This project was supported by the North Central Texas Council of Governments (NCTCOG): Blue-Green-Gray program as part of Project TRN6835, “Laboratory Testing of Engineered Media for Biofiltration Swales”. The authors are grateful for the support and guidance provided by Ms. Jody Purvis Loza, Program Manager of NCTCOG. The authors are also thankful for the technical guidance provided by Dr. Ranjan Muttiah (City of Fort Worth), Ms. Heather Firn (Trinity River Authority of Texas), and Mr. Eric Nelson (Arcosa Lightweight). Their assistance was central to the successful completion of this research project.

Table Contents

List of Figures

List of Tables

EXECUTIVE SUMMARY

Runoff from roads, highways, and bridges represents a significant source of pollutants released into the waters of the United States. Sediment removal stands out as a primary objective within Best Management Practices (BMPs) due to the far-reaching impact of sediment on water quality and its role in degrading aquatic habitats. Many states have adopted the goal of removing a minimum of 80% of the total suspended solids (TSS) load from roadway runoff, following guidance from the Environmental Protection Agency (EPA). However, it is important to note that not all conventional BMPs possess the capability to achieve this level of TSS removal, which is necessary to meet water quality criteria. Furthermore, in densely developed urban areas where land resources are limited, the installation of conventional BMPs often becomes either impractical or cost-prohibitive. Although several emerging technologies with smaller footprints are available and can be deployed in such areas, it is essential to recognize that the installation, operation, and maintenance costs of these systems are significantly higher than those associated with conventional sediment removal structures.

In this project, a comprehensive laboratory investigation centered on the utilization of expanded shale as a filter medium in bioswales was carried out. Bioswales are renowned for their capacity to enhance water quality by effectively mitigating pollutants such as total suspended solids (TSS) and turbidity. While conventional filter media, including rocks, sand, and mulch, have been employed in bioswales to bolster infiltration capabilities, the potential of engineered expanded shale as an alternative medium remains relatively unexplored and under-documented.

The laboratory study consisted of three distinct groups of experiments, which are as follows: drainage experiments to determine the drainage capacity of the soil media used in the study; suspended sediment experiments to evaluate the capability of expanded shale in removing TSS and turbidity; and chemical experiments to measure the removal efficiency of expanded shale in eliminating substances such as nitrogen, phosphorus, and zinc.

These experiments were conducted in a rectangular plexiglass river flume, measuring 15 ft in length, ft in width, and 1.5 ft in depth. Expanded shale mixed with sandy clay soil was used as infiltration media. The reduction of TSS, turbidity, nitrogen, phosphorus, and zinc was assessed under different inflow rates, sediment loading, chemical loading, and infiltration layer dimensions.

The results from sediment experiments demonstrate the efficacy of expanded shale in the removal of both TSS and turbidity across all tested conditions. The mean weighted average removal efficiency for TSS was recorded at 42%, 43%, and 68% for the middle section of the channel, overflow, and infiltrated flow, respectively. Similarly, the mean weighted turbidity removal rates were calculated as 17%, 15%, and 40% for the middle section, overflow, and infiltrated flow, respectively. Notably, approximately 42% of TSS and 17% of turbidity were removed within the first half of the flow length.

The results from chemical experiments indicate that the bioswale has the capacity to reduce nitrogen, phosphorus, and zinc, though the outcomes vary under different flow conditions. Of particular note is the finding that reducing the inflow rate led to a substantial increase in the removal efficiency of these chemicals. In low inflow experiment conditions (without overflow), the bioswale demonstrated maximum removal efficiencies of 80% for nitrogen, 75% for phosphorus, and 90% for zinc.

Flow and sediment dynamics over the soil media were investigated using advanced flow visualization techniques and computer simulations. These methods provided valuable insights into the intricate relationships between flow patterns and sediment behavior within the bioswale, ultimately revealing its efficiency in removing pollutants from stormwater.

The combination of laboratory physical modeling, flow visualization, and computer simulations allowed for a comprehensive exploration of the bioswale's function and efficiency in pollutant removal. This multi-faceted approach provided a deeper understanding of the complex dynamics at play, contributing to the study's findings and insights for the improved design of stormwater management practices like bioswales.

1. INTRODUCTION

Urbanization and increased imperviousness in associated watersheds increase the volume and alter the timing of runoff, impacting the physical characteristics and water quality of the receiving waters. Stormwater runoff from urban areas significantly contributes to surface water quality impairment, typically containing substantial quantities of pollutants, including nitrogen, phosphorus, sediments, heavy metals, biochemical oxygen demand (BOD), pesticides, and herbicides. In addition to these pollutants, the increased quantity of stormwater discharged from rapidly urbanizing areas also poses a significant threat to aquatic ecosystems due to physical alterations in the characteristics of receiving waters.

The primary purpose of stormwater management programs is to mitigate adverse impacts on receiving waters by retaining and treating stormwater on-site using Best Management Practices (BMPs). Examples of these practices include stormwater harvesting to reduce flood-causing stormwater volumes and the implementation of infiltration, biofiltration, or bioretention systems to reduce volume and peak flow, retain pollutants, improve water quality, and minimize the adverse impact on receiving waters. However, in densely developed urban areas where land resources are limited, installing conventional BMPs can be impractical due to space constraints or excessive life-cycle costs. Several emerging technologies with smaller footprints are available, but their pollutant removal efficiencies and life-cycle costs have yet to be determined.

Linear BMPs are commonly used for flow control and runoff treatment in transportation infrastructures such as roadways and bridges. Examples of linear BMPs include bioswales, infiltration ditches, and vegetation strips. Water treatment in bioswales results from a combination of filtration, potential plant uptake, sedimentation, adsorption, and infiltration processes. Like other infiltration BMPs, bioswales are prone to clogging. Gravel and sand/gravel mixes, which are commonly used to minimize clogging in infiltration BMPs, have very low hydraulic conductivity. Larger materials such as crushed stones and gravel are used as filter media for stormwater systems, providing much higher hydraulic conductivity. However, they have very low water retention, making them unsuitable as planting media. Bioswale infiltration can be enhanced by amending the underlying soil with engineered materials like expanded shale. The challenge in engineering, construction, and maintenance lies in the assumptions about filtering media capture efficiencies, treatment configurations, and clogging life-cycle, often derived from vendors or unverified sources.

Even though expanded shale has been used as a soil amendment in stormwater BMPs, its effectiveness in improving water quality parameters, especially suspended sediment concentration and turbidity, has not been studied and documented.

In this project, a small-scale engineered filtration media made of expanded shale was installed and closely monitored in a controlled laboratory environment located within the Fluid Mechanics and Hydraulics Laboratory at the University of Texas at Arlington. This controlled setting allowed for the rapid and precise testing of various physical configurations, including inflow-outflow

dynamics, bypass mechanisms, filtering media dimensions, and pollutant loading rates. These parameters would be challenging to investigate and monitor effectively in real-world field conditions. A total of 40 scenarios were examined, and water samples were collected at different time intervals and locations to assess the effectiveness of expanded shale in removing pollutants from stormwater. Key governing factors, such as the rate of inflow, properties and thickness of the soil medium, infiltration conditions, and influent concentration, were considered as variables when formulating these scenarios. The laboratory study consisted of three distinct groups of experiments: drainage experiments to determine the drainage capacity of the soil media used in the study; suspended sediment experiments to evaluate the capability of expanded shale in removing total suspended solids (TSS) and turbidity (Tu); and chemical experiments to measure the removal efficiency of expanded shale in eliminating substances such as nitrogen, phosphorus, and zinc.

Flow dynamics over the soil media were examined through a flow visualization technique. To capture data on flow patterns at various locations along the experimental flume, a Particle Image Velocimetry (PIV) system was employed. This data was subsequently used to interpret the observations and findings from the laboratory experiments.

Furthermore, flow and sediment dynamics were analyzed using the Flow-3D computer model. Eight different simulations were carried out to replicate sediment transport within the flume, employing the same geometry as in the laboratory experiments. The results of these simulations were complementary to those obtained from the physical modeling.

The data derived from laboratory experiments, flow visualization, and computer simulations were integrated for a comprehensive exploration of the bioswale's function and efficiency in pollutant removal. This multi-faceted approach provided a deeper understanding of the complex dynamics at play, contributing to the study's findings and insights for the improved design of stormwater management practices like bioswales.

1.1 Report Outline

Chapter 1 serves as an introduction to the research project. In Chapter 2, a comprehensive literature review covering stormwater control measures and associated best management practices is presented. This chapter explores a wide range of stormwater pollutants and their potential impacts on receiving waterbodies. A special focus is placed on the introduction of expanded shale, its performance, and the critical role it plays in the integration of effective stormwater management practices. Chapter 3 contains information on the design of the experimental setup, the methodology employed, and the various test scenarios considered. The outcomes of laboratory experiments are detailed in Chapter 4. Chapters 5 and 6 present the findings from the evaluations of flow and sediment dynamics, conducted through flow visualization and computer simulations, respectively. Chapter 7 summarizes the project, offers conclusions, and provides recommendations for the improved design of bioswales.

2. LITERATURE REVIEW

The urbanization and increased imperviousness of associated watersheds increase the volume and alter the timing of runoff, impacting the physical characteristics and water quality of receiving streams. Stormwater runoff from urban areas significantly contributes to the impaired surface water quality of the nation's water resources. It typically contains substantial quantities of pollutants such as nitrogen, phosphorus, sediments, heavy metals, biochemical oxygen demand (BOD), pesticides, and herbicides. In addition to these pollutants, the increased quantity of stormwater discharged from rapidly urbanizing areas also poses a threat of significant impact on aquatic ecosystems due to physical alterations in the receiving waters' characteristics.

The primary purpose of stormwater management programs is to mitigate adverse impacts on receiving waters by retaining and treating stormwater on-site using best management practices (BMPs). Examples of such practices include: i) stormwater harvesting to reduce the volume that causes flooding, and ii) infiltration, bio-filtration, or bio-retention systems to reduce volume and peak flow, retain pollutants, improve water quality, and lessen adverse impacts on receiving waters.

Pollutants can be removed from stormwater by utilizing source control BMPs. Basins, ponds, wetlands, infiltration facilities, filtering systems, and swales are examples of BMPs implemented to treat stormwater runoff before entering receiving waters. Suspended sediments and other pollutants are eliminated from stormwater runoff through processes like gravity settling, filtration, biological uptake, and media or soil adsorption [1]. Some flow control practices, such as infiltration basins, vegetated open channels, detention, and retention ponds, can also function as stormwater treatment BMPs.

Linear BMPs are commonly used for flow control and runoff treatment of transportation infrastructures such as roadways and bridges. Bioswales, infiltration ditches, and vegetation land strips are examples of linear BMPs. Water treatment by bioswales is a combined effect of filtration, potential plant uptake, sedimentation, adsorption, and infiltration processes [2].

This chapter provides an overview of the literature on stormwater control measures and associated best management practices. It discusses various stormwater pollutants and their implications in receiving waterbodies. The review focuses on introducing expanded shale, its performance, and the need to incorporate expanded shale into stormwater management practices.

2.1 Effects of Urbanization on Stormwater Quality

Urbanization has fundamentally transformed the natural hydrology of watersheds, both large and small, through the introduction of new hydrological, ecological, and environment-related mechanisms that exert an impact on water quality [3]. The densely populated urban areas, paved surfaces, and constructed flow paths and streambeds within urban landscapes have led to significant alterations in the inherent hydrological systems [4]. The urban surfaces have notably accelerated the mobilization of pollutants due to increased surface runoff and enhanced hydraulic

efficiency of artificial channels [5]. The increased runoff contributes to a greater accumulation of pollutants within receiving waterbodies during storm events.

The rise in urbanization has resulted in hydrologic modifications such as dam construction, river channelization, and flow diversion, which give rise to environmental problems ranging from eutrophication to flooding. Issues encompassing sediments, nutrients, and pathogens are not solely linked to urbanization; they also involve time shifts from a hydrological perspective [6]. Both stormwater quantity and quality are concerns associated with the challenges induced by urbanization [7].

Moreover, interactions at the source level, such as vehicles releasing pollutants into the atmosphere, can subsequently lead to their deposition on paved surfaces. This can result in the same pollutant being associated with two distinct sources, such as brake-induced dust particles and tire dust, both of which contain heavy metals and sediment. Consequently, identifying the precise source of pollutants becomes complex. Additionally, the task of pinpointing pollutant sources is further compounded by phenomena like suspension and re-suspension [8]. These interconnected phenomena contribute to the intricate challenge of comprehensively studying the impact of urbanization and untangling the sources of pollutants [9].

Due to increased industrial activities, natural gases and particles, including pollen, microorganisms, and wind-blown debris, enter the atmosphere. Over time, these entities combine or undergo transformations, giving rise to complex urban pollutants like aerosols and trace gases. Similarly, heavy metals originating from vehicle abrasion, oil spillage, construction site debris, and corrosion induced by acid rain emerge as common sources of pollutants within urban catchments, being washed or carried away by rainwater [10].

For the assessment of urban stormwater runoff quality, various water quality parameters come into play. These encompass total suspended solids (TSS), chemical oxygen demand (COD), pH, heavy metals, nitrates, and phosphate. These factors have been considered in studies focused on evaluating the quality of urban stormwater runoff [11],[12],[13].

2.1.1 First-Flush

The term *first-flush* refers to the initial runoff generated from a surface during precipitation. The concentration of pollutants within this initial runoff is influenced by the time span between rainfall events. Longer dry intervals between events tend to result in higher levels of pollutants being present [14]. A comprehensive investigation into first-flush phenomena in urban catchments revealed that a significant portion of pollutant mass is contained within the initial volume of runoff [15]. However, the attributes of first-flush, including flow rate and concentration, exhibit substantial variation across diverse sites and climates [16].

In the study of first-flush in stormwater runoff, key water quality parameters taken into account include suspended solids, chemical oxygen demand (COD), total phosphorus, heavy metals, and

total nitrogen [13],[16],[17]. These studies reveal that stormwater treatment strategies tailored for first-flush scenarios can effectively capture a significant portion of pollutants.

The US Department of Agriculture [18] has also indicated that the initial runoff from a site tends to be highly contaminated. Treating this initial runoff, or first-flush, often proves sufficient to address water quality concerns. However, if the runoff contains harmful substances, additional treatment measures might be necessary. It is equally crucial to recognize the influence of peak flow rates and overall volume in these contexts.

2.1.2 Pollutants Origin and Indicator Pollutants

Urban areas, characterized by reduced perviousness, have become notable sources of non-point source pollutants. Such pollutants arise from a combination of both natural origins and anthropogenic activities, constituting significant contributors to urban water pollution. The diverse forms in which pollutants manifest in stormwater can primarily be attributed to the various sources from which they originate [7].

The term *solid pollutant* encompasses various types of solid particulate matter, which can exist as freely floating, suspended, or dissolved solids. Among these, solid particles encompassing both suspended and dissolved solids were found to comprise 72% of pollutants in stormwater runoff [19]. Frequently, solid particles serve as carriers for other pollutants like metals, gases, and microorganisms, which may become attached to these solid particles. These particles generally encompass soil particles from construction sites, debris, floating matter, and at times, litter that accompanies flowing water. Suspended solids impede the penetration of light and concurrently act as conveyors for other pollutants that can inflict harm on aquatic ecosystems [20]. Consequently, suspended sediment serves as a key indicator pollutant in the context of stormwater runoff [7], [20].

2.2 Stormwater Management

Prior to the early 1970s, stormwater management practices predominantly revolved around conveyance considerations [21]. The prevalent approach, known as *conventional stormwater infrastructure* or *gray infrastructure management*, primarily involved quickly bypassing stormwater away from urban areas [22]. However, these practices largely neglected the vital treatment aspect of runoff. Over time, there emerged an understanding of the necessity to counteract this trend by disengaging from the traditional focus on water quantity and instead embracing water quality improvement strategies such as retention, detention, and infiltration of stormwater. This shift aimed to achieve a more harmonious natural water balance best practices [21],[23].

In 1998, the concept of a sustainable urban drainage system (SUDS) was developed by D'Arcy. The SUDS framework encompasses three core principles: water quality, water quantity, and the underlying habitat. This integrated approach has been widely adopted, particularly in European countries [23]. Similarly, in the United States, the term *best management practice* (BMP) is

utilized to refer to pollution-preventing mechanisms employed for stormwater management under the framework of the Pollution Prevention Act.

2.2.1 Best Management Practices (BMPs)

The inception of stormwater best management practices (BMPs) can be traced back to the early 1990s in the United States. This development was catalyzed by the legal mandate to address the imperative of ensuring stormwater quality control. The effective management of stormwater runoff yields several positive outcomes, including the safeguarding of habitats, flood mitigation, improved water quality within receiving water systems, preservation of water resources, and the protection of public health [24].

BMPs encompass a wide array of practices that can be broadly classified as physical, chemical, structural, or managerial measures, often incorporating a combination of these practices. They serve as tools to curtail or prevent stormwater pollution by regulating the volume, timing, and quality of stormwater runoff [24]. As such, BMPs are strategically employed to reduce peak flow or peak volume, guided by their specific implications and objectives.

2.2.2 Need for BMPs

The conventional sewer network, constructed primarily for hydraulic control, has been evolving to accommodate diverse objectives and local needs. These expanded objectives frequently encompass tasks such as flood mitigation, urban ecology enhancement, public health considerations, and improved water quality [21]. Similarly, conventional stormwater control techniques, which primarily revolve around flow control, entail the collection of peak flows, providing local drainage, and safely conveying the runoff to receiving bodies of water. However, these methods are generally proficient at altering peak timing and reducing runoff rates, but they do not effectively address the reduction of stormwater volume. Thus, alongside conventional controls, there is a growing imperative to incorporate strategies that specifically target stormwater volume reduction.

In practice, this necessitates the implementation of BMPs that incorporate on-site infiltration. These BMPs have the advantage of being able to occupy smaller footprints compared to conventional treatment systems, such as detention ponds [25]. Flow control measures, including bioretention, constructed wetlands, flow separators, vegetative swales, and porous pavement, are commonly employed. These approaches bring about alterations in flow characteristics and simultaneously treat water through a combination of processes like sedimentation, infiltration, adsorption, and plant uptake [26],[27].

2.2.3 Application of BMPs

Stormwater pollution was recognized as a significant contributor to the compromised water quality of the nation's waterbodies [27]. Subsequent to this recognition, BMPs have been integrated into design manuals for engineers practicing across the United States, with regulations overseeing their implementation.

The efficacy assessment of any BMP's implementation should be rooted in comprehensive management strategies, considering factors such as costs and overall effectiveness within a larger system, rather than solely focusing on the application of individual BMPs [28]. For instance, while designed for pollution reduction, BMPs could concurrently address objectives such as flood control [26]. Additionally, there are scenarios where BMPs are utilized to mitigate the adverse impacts of runoff ensuing from post-construction activities [29].

In cases where the site's specific requirements encompass the promotion of natural flow patterns, enhanced infiltration, and the preservation of aesthetics, alongside the primary objective of improving water quality, implementing infiltration-based BMP techniques becomes relevant [28]. Similarly, in situations characterized by limited infiltration capacity due to factors like low native soil infiltration rates and a high groundwater table, bioretention-based BMPs can be a viable solution [30]. Bioretention approaches in such cases rely on a combination of evaporation for flow reduction and extended infiltration for mitigating flow.

Barret et al. [31] underscored the need for effective treatment systems to meet design standards, often necessitating the consideration of first-flush for stormwater runoff treatment. However, concerning highway runoff, the study suggested examining constant pollutant concentration for a single storm event. Various studies also point out that BMPs, frequently designed to target the treatment of first-flush, present an opportunity to address high concentrations of diverse pollutants, including total suspended solids (TSS), chemical oxygen demand (COD), biological oxygen demand (BOD), turbidity, heavy metals, and nutrients [13],[16],[17].

2.2.4 Types of BMPs

BMPs are categorized according to their *geometric properties* and the *goal of practice*. These classifications are elaborated upon in the subsequent sections.

2.2.4.1 Classification Based on Geometric Properties

BMPs can be categorized based on their physical characteristics and design components. These characteristics primarily pertain to the distinct structural features of the practice. According to the EPA, BMPs are classified into point, linear, and area BMPs [24].

Point BMPs. Practices that collect and treat water from upstream at a designated location, utilizing a combination of detention, infiltration, sedimentation, and pollutant conversion mechanisms, fall under the category of point BMPs. Constructed wetlands, infiltration basins, and similar structures exemplify point BMPs.

Linear BMPs. Streams or channels that facilitate the filtration of pollutants across their course, the infiltration through porous media, the uptake by vegetation, and the retention of aesthetic appeal within the area are classified as linear BMPs. Examples of linear BMPs include grass swales, wet swales, and vegetated filter strips.

Area BMPs. Practices centered around land management strategies aimed at fulfilling water quality and quantity standards by modifying the permeability of existing surfaces and integrating

pollutant management techniques fall within the domain of area BMPs. Examples of area BMPs include green roofs and permeable pavements, which are widely implemented measures.

2.2.4.2 Classification Based on Goal of BMPs

BMPs can be designed according to the specific objectives they aim to achieve. These objectives can be categorized into three distinct classifications: flow control BMPs, pollutant source control BMPs, and treatment control BMPs [27],[30].

Flow Control BMPs. These practices are strategically designed to effectively manage both the volume and timing of stormwater runoff. In doing so, these BMPs work to reduce the likelihood of pollutant collection and stream bank erosion by limiting the generation of stormwater runoff. They achieve this by promoting enhanced infiltration and incorporating on-site water storage solutions. Detention basins, rain barrels, vegetated filter strips, and infiltration wells are examples of such BMPs.

Pollutant Source Control BMPs. These BMPs are designed to intercept and remove pollutants prior to their being washed away by stormwater runoff. These practices operate by reducing runoff pollutants through nonstructural measures. They involve fostering public engagement and awareness to curtail and regulate existing practices that contribute to urban runoff pollution. This encompasses measures such as limiting chemical usage, identifying and regulating sanitary practices within the community, and promoting informed behavior in proximity to urban areas. Activities such as sweeping impervious surfaces, minimizing the application of pesticides and herbicides, proper waste disposal, and raising public consciousness about pollution all fall under the umbrella of pollutant source control BMPs.

Treatment Control BMPs. These practices are designed to alleviate the adverse impact of stormwater runoff on receiving waterbodies by employing a combination of physical, chemical, and biological processes to capture and treat contaminants. They are typically designed based on a specified target concentration or amount of pollutants that is deemed safe for release into natural water streams. The efficacy of treatment control BMPs hinges on the integration of one or multiple pollutant removal mechanisms. These mechanisms encompass a spectrum of processes, including sedimentation, flotation, filtration, infiltration, adsorption, plant uptake, and chemical reactions.

2.2.5 Low Impact Development BMPs

Low Impact Developments (LID) and green infrastructure (GI) encompass a range of practices aimed at limiting the volume of stormwater runoff. These approaches not only seek to reduce runoff but also to reinstate or construct natural processes that effectively manage water quality and the encompassing habitat and ecosystem within a given watershed or environment [30],[32],[33].

LID BMPs specifically encompass those methods that adeptly treat stormwater on-site by harnessing natural processes, including infiltration, biological retention, and evapotranspiration. Key to LID are features that utilize either natural or engineered media to reduce runoff and foster infiltration, all operating within the framework of a Water Quality Management Plan (WQMP).

This plan mandates on-site runoff volume retention, pollutant reduction tailored to different types of pollutants, and the implementation of specific BMPs addressing these pertinent pollutants [30].

In terms of stormwater treatment, methods such as bioretention, biofiltration, and rain gardens represent the most desired water treatment practices, effectively embodying both infiltration and biofiltration components of LID BMPs.

2.2.6 Selection of BMPs

The choice of BMPs hinges on the specific characteristics of the pollutants present in the flowing water. The selection of BMPs is guided by factors such as sediment sizes, types of pollutants, incoming pollutant concentrations, and the ultimate objective of the intervention [34]. Moreover, the site's inherent limitations also play a pivotal role in determining the suitable treatment BMPs. Considerations such as available space and prevailing site conditions can significantly influence the selection process. For instance, in cases of limited space, bioretention systems may take precedence over grassed channels in urban settings. Similarly, site-specific factors such as groundwater levels, native soil properties, topography, and hydraulic head influence the selection of appropriate BMPs [35].

2.2.7 Treatment Phenomena in BMPs

Various mechanisms determine the efficacy of pollutant control within BMPs. These encompass a range of phenomena, including sedimentation, flotation, filtration, infiltration, sorption, nutrient uptake, biological conversion, and the degradation of chemical compounds. These mechanisms collectively underpin the effectiveness of pollutant control BMPs [26]. For a concise overview, these mechanisms are summarized in Table 2.1.

Flow control BMPs, like bioswales, infiltration wells, and vegetated filter strips, not only serve their primary function of managing flow but also operate as treatment control BMPs. A range of BMPs, each employing distinct treatment mechanisms, are outlined in Table 2.2. This table provides a comprehensive overview of these BMPs along with a fundamental description of the underlying phenomena responsible for the reduction of pollutants.

Table 2.1: Various treatment mechanisms in BMPs [36]

Phenomenon	Descriptions
Sedimentation	Settlement of the particles at the bottom of the channel due to gravity
Infiltration	Movement of water percolating through the soil media promoting recharge and flow reduction
Sorption	The combined chemical process of absorption and adsorption. Absorption is caused due to sediment trapped in the porous surface of soil media; similarly, adsorption is due to physical-chemical interactions. They may include dissolved or particulate matter. Ion exchange and interlocking of particles are common
Filtration	They are gross filtration which is caused due to trapping of particles by vegetation blocking the particle flow direction.
Biological interaction	They may be phenomena such as nitrification, denitrification, plant uptake, or any chemical reaction involving ion exchange

Table 2.2: Summary of various BMPs and their treatment mechanism [37]

BMPs	Descriptions	Treatment Mechanism
Biofiltration systems	Consists of sand or mulches as a filter media, provided with underdrain without soil amendment to drain once infiltrated	Filtration, adsorption, nutrient uptake, assimilation
Enhanced biofiltration system with underdrain	Biofiltration basins with impervious base/with amended soil, drained once infiltrated, underdrain provided	Filtration, adsorption, nutrient uptake, assimilation, ponding-induced settlement
Filter strips[1]	Sloped vegetated land with/without amended soils	Infiltration, sedimentation, adsorption, filtration
Dry detention basins/Retention basins	Shallow depressions typically with dual outlet, i.e., orifice and weir outlets, permanent pool of water	Ponding-induced settling, infiltration, biological uptake, chemical reaction
Wet detention basins	Captures and temporarily stores runoff volume, permanent pool of water	Ponding-induced settling, sedimentation, biological uptake, filtration
Infiltration systems	Captures runoff and infiltrates water gradually, no underdrain system	Natural filtration, sedimentation, adsorption, biological uptake, dilution
Wet swales	Depression with vegetated strip over natural soil, no underdrain provided, near or at water table level, the soil may be amended	Vegetation uptake, adsorption, sedimentation, infiltration
Dry swales/Bioswales	Vegetated channels may or may not be with check dams and underdrains	Infiltration, vegetation uptake, sorption, sedimentation

[1] *Cannot meet 80% TSS reduction performance goal [38],[39]*

2.3 Bioswales

Swales are wide, shallow open channels constructed to receive stormwater runoff at a non-erosive rate in order to enhance water quality through infiltration, sedimentation, and filtering. Swales are classified as filtration BMPs when an underdrain system is employed and as infiltration practices when an underdrain is not installed. Engineered media may be incorporated into filtration swales to improve their performance [40]. Swales can be covered with dense vegetation, typically grass, which serves to decelerate water flows, trap suspended particles, and remove pollutants [41]. Two types of vegetated swales exist: dry swales (or grassed swales) and wet swales (or water quality swales). Schematics of these bioswales are depicted in Figure 2.1.

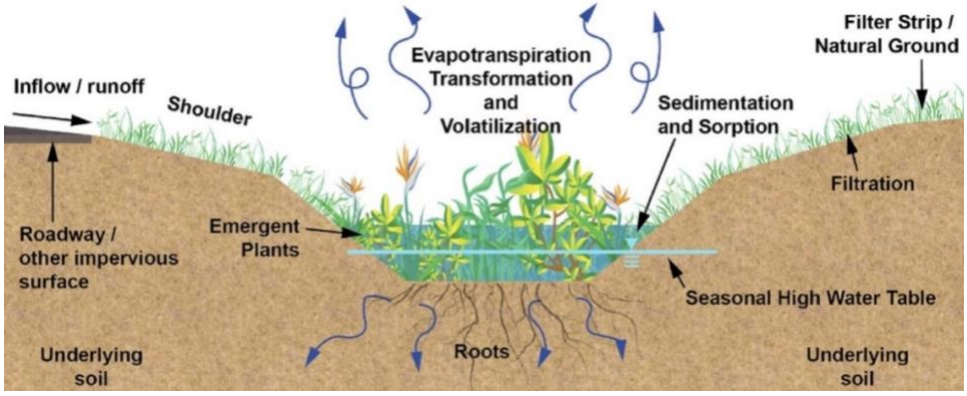

(a)

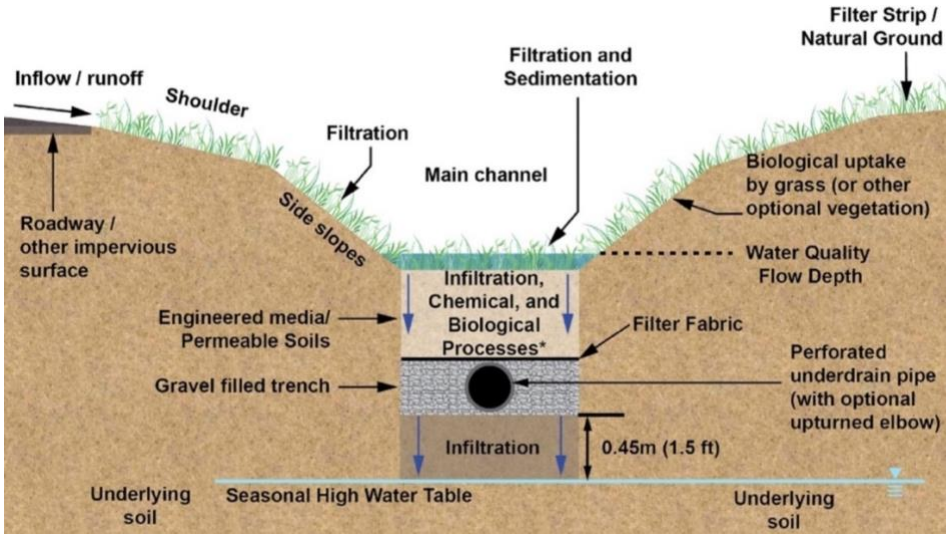

(b)

Figure 2.1: Typical cross sections of (a) wet swales, and (b) dry swales [36]

The dry swale is a vegetated conveyance channel designed to treat and filter stormwater runoff for specific water quality and volume goals. Check dams can be installed within these channels to create ponding, thus reducing the velocity of stormwater runoff within the swale. This velocity reduction enables vegetation to filter runoff pollutants effectively. Ponding also increases the hydraulic residence time, facilitating the gravitational settling of sediment pollutants [42] and enhancing both infiltration and the potential for evapotranspiration [36]. Dry swales typically incorporate an underdrain system that facilitates drainage, ensuring that the ponding duration does not exceed 48 hours. Their design aims to maintain the channel's bottom at least 2 feet above the groundwater level [43]. Consequently, they can also be devised as groundwater recharge facilities. Another advantage of dry swales over wet swales is their ability to manage runoff hotspots from point sources, preventing groundwater contamination [43].

A wet swale functions as a relatively long linear wetland. Wet swales can be planted with emergent wetland plant species to enhance pollutant removal. The primary processes involve settling and nutrient uptake by plants [40]. Engineered soil media mixes are used in wet swales to allow controlled infiltration and facilitate the growth of wetland vegetation. While wet swales are more effective than dry swales in removing pollutants like phosphorus from stormwater, their inability to reduce peak stormwater runoff limits their application in most cases. The constant presence of water in wet swales could also hinder their utilization in urban areas due to potential interference with surrounding infrastructure [36]. Furthermore, because of the large area requirements and mosquito breeding possibilities, wet swales are not suitable for urban landscapes [43],[44] Consequently, dry swales are generally considered as vegetated swales or bioswales [35].

Bioswales are designed to facilitate water infiltration into the surrounding soils and can be constructed over native soils or amended media. The necessary media properties can be determined using soil's gradation curve. If the existing soil exhibits particle sizes with $d_{10} > 0.02$ mm and $d_{20} > 0.06$ mm, it indicates slow filtration rates and necessitates soil amendment [26]. Filtration and infiltration are the primary contributors to pollutant removal in bioswales. These BMPs can be utilized for water quality enhancement, flood control, or a combination of both purposes [26].

Bioswales also facilitate the removal of pollutants from stormwater runoff through vegetation. As the runoff passes through the bioswale, the vegetation's leaves and stems capture pollutants. These pollutants subsequently enter the soil and undergo decomposition or breakdown by soil bacteria [42]. The pollutants that can be captured by bioswales include nutrients (such as phosphates and nitrates), heavy metals (like mercury, lead, and chromium), and polycyclic aromatic hydrocarbons [42],[45].

Bioswales can serve as alternatives or supplementary treatment methods to traditional stormwater management systems. They collect water from impervious surfaces such as paved parking lots, highways, and rooftops, absorbing and partially conveying runoff directly to sewer conveyance infrastructure [46]. Because of the linear structure of bioswales, they are commonly employed for treating and conveying highway stormwater runoff. These swales are designed and positioned along the edges of parking lots or integrated into road medians, curb cutouts, and sidewalks. Their

purpose is to collect and treat stormwater runoff prior to its release into streams or storm drainage systems. During the first flush, a significant amount of pollutants is washed away from the surfaces of roads and pavements with the first rain. Figure 2.2 displays examples of bioswales.

(a)

(b)

(c)

Figure 2.2: Examples of Bioswales: (a) Tarrant County College (South Campus), (b) Texas Health Clearfork Center (Clearfork Main St.), and (c) Fire Dep. Training Academy (W Felix St.), Fort Worth, Texas.

2.3.1 Efficiency of Bioswales

The efficiency of BMPs is closely tied to both the reduction in runoff volume [47],[48],[49] and the specific type of pollutants under consideration. In some cases, treatment systems can inadvertently act as sources of certain pollutants, like total nitrogen [50]. Regardless of pollutant size, infiltration facilitates additional pollutant capture in conjunction with settling and sedimentation processes [51]. Furthermore, the infiltration rate tends to be higher for coarser soil particles compared to finer ones. However, factors such as bulk density and soil layering also play a role in influencing infiltration rates within stormwater infiltration systems [52].

Bioswales are typically more efficient in treating particulate contaminants, while their capacity to treat dissolved contaminants is comparatively lower. Additionally, wet swales have demonstrated a high effectiveness in reducing nitrogen and heavy metals from influents [53]. Research by Hunt et al. (2006) [54] established an inverse relationship between the Phosphorus index (P-index) of the soil media and phosphorus removal. Similarly, the organic content and hydraulic conductivity were observed to influence the total nitrogen removal efficiency. Kim et al. (2003) [55] provided evidence of a 70-80% total nitrogen removal efficiency when utilizing an engineered mix as soil media in a bioretention system. Furthermore, King County (1995) [56] conducted 39 swale surveys, focusing on 32 swales for their study. The research assessed swales' functionality, drainage area, and land use. The findings revealed that under existing conditions, 40% of total suspended solids (TSS) and 17% of total phosphorus removal were achieved in swales considered to be in good or fair condition. Interestingly, the same study indicated that if all swales were in their originally designed good condition, the overall removal efficiency could reach 83% for TSS and 33% for total phosphorus.

In a comparative study on permeable pavement and bioswales conducted by Seters et al. (2006) [57], bioswales were found to be over 50% more effective than conventional asphalt systems in reducing common heavy metals like zinc and lead. However, the study also noted that nutrient concentrations were higher in the bioswale effluent.

Moreover, Fardel et al. (2019) [58] undertook a comprehensive review of 59 studies related to swales. They established correlations among TSS, total trace metals, total nitrogen, and total phosphorus. The study revealed a strong correlation between TSS and total trace metals, including copper, zinc, cadmium, and lead. Swales exhibited a median reduction efficiency of 56% for TSS and 62% for total trace metals. Dissolved trace metals saw a reduction of more than 44%, while nutrients (total nitrogen and total phosphorus) showed a maximum median reduction of only 30%.

For a comprehensive overview of the treatment efficiency of swales in various studies, refer to Table 2.3.

Table 2.3: Summary of the effectiveness of different BMPs in reducing major pollutants

Type of BMP	Runoff Volume (%)	TSS (%)	Total Phosphorus (%)	Total Nitrogen (%)	Metals (%)	Bacteria (%)	No. of Obser.	Reference
Swales	-	40-83	17	-	-	-	33	[56]
Dry swale	55-60	44-83	(–49.2)-68.7[1]	(–25.6)-85.6[1]	18-92.6	-	-	[59]
Bioretention	96.5	60	31	32.2	31.4-59.5	69-71	23[2]	[60]
Bioretention	67	58	–10	58	-	-	161	[61]
Bioswale	88.8	95	-	97	87	-	-	[19]
Bioretention	-	92	72	80	-	-	42	[47]
Bioswale	23	75	35	30	-	-	30	[62]
Bioswale	83-97	81	-	-	81	-	-	[63]
Various bioretention systems[3]	-	80	67	51	90-94	-	182	[48]
Bioswale[4]	-	56	30	30	62	-	59	[58]
Bioswale with overflow	-	10	-	-	-	59-65	-	[64]
Bioswale with underdrain	-	88	-	-	-	55-75	-	[64]
Grassed swale	-	87	5-83	46-84	88-90	-	-	[43]

[1] *Negative value means an increase in pollutants instead of a decrease.*

[2] *Number of tests or observations varies for different contaminants.*

[3] *Data analysis based on the previous database on various bioretention BMPs*

[4] *TN and TP were studied as nutrients.*

2.4 Design of Bioswales

The bioswales are designed based on the stormwater flow rate to be treated. The flow rate is a function of the contributing drainage area and its impervious cover, rainfall intensity, and bioswale characteristics (cross-sectional geometry, slope, and type of lining) [65]. Other factors to be considered in selecting and designing bioswales are site soil type, depth of groundwater table, flow velocity, shear stress, and discharge [53].

In the following sections, factors affecting bioswale performance and efficiency in removing pollutants are discussed. These factors include contributing drainage area, soil properties of the underlying media, swale geometry, longitudinal slope, design flow, hydraulic residence time, shear stress, swale length, and check dams.

2.4.1 Contributing Drainage Area

Even though a minimum drainage area contributing to bioswale is not restricted, these BMPs are well-suited for small drainage basins. The maximum size of the contributing drainage area is limited to the peak stormwater runoff treated by the bioswale. The peak flow is a function of the channel cross-section, geometry, roughness, longitudinal slope, and flow velocity in the channel. Therefore, the maximum size of the contributing drainage area is limited to the peak flow carrying capacity of the bioswale.

The flow rate subjected to bioswales should account for 80%-95% of the stormwater runoff [65]. A wet swale can be designed to receive stormwater from a drainage area of 1-5 acres, while a dry swale is suitable for drainage areas less than 0.5 acres and does not require any pretreatment [43]. Flow regulation also determines the maximum amount of runoff that can be subjected to bioswale design.

2.4.2 Soil Properties of Underlying Media

Infiltration and hydraulic conductivity greatly influence the treatment capability of BMPs [43],[47],[48]. The soil should permit water infiltration, such that the swale is drained within 48 hours. A field permeability test is strongly recommended if the site soil permeability is unknown.

Soil infiltration can be enhanced by providing an underdrain and sometimes by increasing the depth of the standing water [66]. If the native soil is highly permeable, an underdrain may not be necessary; however, the soil may be amended to achieve the desired hydraulic conductivity and permeability [51].

Soil can be amended with highly porous materials to promote quick drainage and enhance the infiltration rate. Similarly, soil with a coarser fraction is desirable as it can retain more moisture during droughts. Soils with a higher fine-particle fraction are likely to reduce infiltration by clogging the surface, ultimately decreasing infiltration [34]. Hence, gravel and sand-mixed gravel are commonly used in practice due to their comparatively high hydraulic conductivity, which reduces the likelihood of clogging.

USDA [67] suggests that the saturated hydraulic conductivity of infiltrating soils should be at least 0.5 cm/hr (0.2 in/hr), and stored water during peak events should be drained within 72 hours. In general, if the media has an infiltration rate of at least 1.27 cm/hr (0.5 in/hr), bioswales can be designed without an underdrain. An underdrain is optional when the infiltration rate of the underlying soil is $\geq$ 0.2 in/hr. Nevertheless, in both cases, 72 hours of drainage time should be maintained, as is standard for any infiltration system [27],[68] Therefore, precautions should be taken during the construction of bioswales to avoid soil compaction.

Additionally, soil containing any amendment, regardless of its nature (organic or inorganic), is found to increase hydraulic conductivity and water retention, promoting vegetation growth and enhancing pollutant removal efficiency [34],[69].

2.4.3 Swale Geometry

Swale geometry is determined based on the site location, inflow volume, topography, and hydraulic efficiency. The geometry of the swale significantly influences hydraulic efficiency and can change flow depth and velocity even for the same incoming flow. As a rule of thumb, it is suggested that the maximum surface area of the swale should be no more than 1% of the drainage area [27],[51]. The geometric design of bioswales is flexible and can be based on land availability and aesthetic considerations.

Since the recommended flow depth for water quality is limited to 6 inches or equal to the vegetation height, trapezoidal channels are often preferred as they provide a higher wetted perimeter and are less sensitive to side slopes [34]. Moreover, trapezoidal channels are more commonly used in practice due to the clogging and construction challenges associated with V-shaped and parabolic channels. Trapezoidal channel sections with bottom width of 2 to 6 ft and bank slope no steeper than 3H:1V are recommended for bioswales. The channel depth should permit conveyance of 10-year stormwater runoff event while maintaining a minimum of 6 inches of freeboard. The channel depth should be selected such that the height of check dams does not exceed one half of the total channel depth [26].

2.4.4 Longitudinal Slope

The slope of bioswales should be as flat as practically possible for the given site. Generally, flatter slopes ranging from 1 to 2% are preferred. If slope is less than 1%, underdrain is purposed to limit the level of standing water. However, the slope should not exceed 6% or any threshold slope that could lead to bank scouring during a 10-year storm event with 6 inches of flow depth [70]. In such cases, the use of check dams is recommended to reduce flow velocity. Generally, a less steep swale configuration requires greater length, and vice versa.

2.4.5 Design Flows

The flow rate is an important factor that governs the swale design. The size of the contributing watershed and soil properties determine the flow rate. Flow rate may be calculated using the rational method due to its simplicity [26]. However, other methods such as NRCS's TR 55 method can be used [20].

BMPs are typically designed based on more frequent, less intense storm durations, such as the 2-year, 24-hour storm, which is used for water quality purposes. For peak flow conveyance, less frequent and more intense storm intensities are considered, such as the 25-year or 100-year storms. These recommendations can be found in the design manuals of various agencies and authorities, e.g., [39],[56].

Since bioswales need to be designed to accommodate both water quality flow and peak flow during extreme events, the depth of flow within the swale may exceed 6 inches, unless bypass arrangements are included in the swale design [26]. Increasing the depth of flow can promote infiltration, thereby enhancing efficiency, but the depth of water in swales is typically limited to 6

inches or the height of the vegetation for water quality flow. If bypass arrangements are present, the excess flow can be directed to nearby conventional treatment systems, such as detention basins or underground storage systems [39].

For water quality volume calculations, the first one inch of rainfall is typically considered [26],[71]. However, using 1.5 inches of rainfall is also recommended for water quality volume calculations for treatment bioswales, representing the 85th percentile of all storm events [38].

2.4.6 Flow Velocity

Flow velocity plays a crucial role in the efficiency of pollutant removal in bioswales. Maintaining a low flow velocity is essential to ensure maximum retention and settling of pollutants within the swale. Additionally, the design of the bioswale should account for preventing the re-suspension of sediments that have settled during previous storm events. For design flows corresponding to a 2-year storm event, a maximum flow velocity of 4 ft/s is recommended, while for a more extreme 10-year design flow, a maximum flow velocity of 7 ft/s is advised.

Flow rates in swales are generally constrained to a maximum of 5 ft³/s as specified by EPA guidelines [72]. The allowable incoming flow velocity should be carefully considered to prevent erosion of the swale channel, and this depends on the specific soil type. For instance, velocities ranging from 3.5 to 5 ft/s are considered suitable for soils composed of sand, silt, or a combination of both. For soils containing mixtures of clay, velocities between 4.5 to 6 ft/s are deemed acceptable, taking into account the type of vegetation in the area [73]. In cases where vegetation is absent, designers should adhere to a maximum flow velocity of 1 ft/s for water quality purposes, while allowing a higher velocity of 4 ft/s for runoff originating from highways [26]. These velocity limits are established to ensure proper erosion control and pollutant removal while accommodating various soil types and conditions.

The flow depth and velocity within bioswales can be determined using Manning's equation (Equation 2.1), where Manning's roughness coefficient (n) value is considered as 0.2 to 0.3 for water quality flow (WQF) and 0.05 for peak flow events.

$$v = \frac{Q}{A} = \frac{1.49}{n} R^{2/3} S^{0.5} \tag{2.1}$$

where v is flow velocity (ft/s), Q is flow rate (ft^3/s), A is cross-section area of the swale channel (ft^2), n is Manning's roughness coefficient, R is hydraulic radius of the channel (ft), and S is longitudinal slope of the channel.

In situations where flow velocities reach as high as 4 ft/s, measures can be taken to address potential erosion of the underlying soil. One effective approach is to utilize a geofabric to cover the engineered media or soil within the bioswale. This geofabric acts as a protective layer, preventing erosion and maintaining the integrity of the underlying soil structure. This technique is recommended to ensure the stability and effectiveness of bioswales, particularly in cases of extreme flow velocities [26].

2.4.7 Shear Stress

Shear stress refers to the force per unit area exerted by water on the surface of a channel. The applied shear stress can be calculated using Equation 2.2 [74].

$$\tau = \gamma R S \tag{2.2}$$

where τ is average shear stress (lb/ft^2), γ is specific weight of water (lb/ft^3), R is hydraulic radius of the channel (ft), and S is longitudinal slope of the bioswale.

Furthermore, the permissible shear stress represents the highest stress that flowing water can exert on a channel surface without causing erosion or damage. To maintain channel stability, the applied shear stress should always be kept below the permissible shear stress. The specific permissible shear stress value depends on factors such as the type of existing vegetation and the characteristics of the underlying soil. Permissible shear stress values can range from 0.35 lb/ft² to 3.7 lb/ft².

2.4.8 Hydraulic Residence Time

Hydraulic residence time (*HRT*) refers to the average duration that water remains within the swale before moving out. For the purpose of water treatment design, a minimum *HRT* of 5 minutes is recommended [26]. The *HRT* can be calculated numerically using Equation 2.3.

$$HRT = \frac{V}{Q} \times 60 = \frac{L}{v} \times 60 \tag{2.3}$$

where V is volume (ft^3), Q is flow rate (ft^3/s), L is the swale length (ft), v is flow velocity (ft/s), and 60 is used as unit conversion to calculate *HRT* in minutes.

If the calculated *HRT* falls below the minimum threshold of 5 minutes, adjustments can be made to the swale's dimensions, such as extending its length or altering its width, to decrease the flow velocity and achieve a longer *HRT*. Another approach to achieving lower velocity is by reducing the channel slope.

Also, an inter-relationship value, calculated using Equation 2.4, must be satisfied to ensure compliance with the water quality flow requirement. If the calculated value does not satisfy this criterion, the design process is repeated using different configurations [26]. If none of the calculated configurations meet the established criterion, the BMP cannot be classified as a treatment BMP, but it may still serve as a pollutant control BMP.

$$\frac{HRT \times 60}{y_{WQF} \times v_{WQF}} \geq 1300 \tag{2.4}$$

where, *HRT* is hydraulic residence time (min), y_{WQF} is depth for water quality flow (ft), and v_{WQF} is velocity for water quality flow (ft/s), and 60 is the unit conversion factor.

2.4.9 Swale Length

The channel's length is a critical factor in promoting the settlement of suspended particles within the swale. It should be sized in conjunction with the channel's cross-sectional area and the height of check dams to achieve the desired water quality storage volume and residence time [26].

The determination of the swale's length can be approached in two ways. The first method calculates the necessary channel length based on the *HRT* (Equation 2.3), which is a design approach specific to the site's conditions. The second method employs the Aberdeen equation, which is based on the mean size of sediment in the influent, to determine the appropriate swale length.

2.4.9.1 Design Based on HRT (Site-based Design)

This approach involves a series of steps to design a bioswale for its intended purpose:

1. *Design Volume Evaluation:* Determine the design volume of stormwater that needs to be managed, whether it is for water quality flow (*WQF*) or peak flow.
2. *Flow Velocity Calculation:* Calculate the flow velocity for the selected *WQF* using Manning's equation, taking into account factors such as channel geometry and roughness.
3. *Hydraulic Residence Time (HRT) Calculation:* Utilize the calculated flow velocity and the available length of the bioswale to compute *HRT*, which represents the average duration that water remains within the swale.
4. *Minimum HRT Check:* Verify if the calculated *HRT* meets the minimum required criteria, typically set at 5 minutes. This step ensures that water has sufficient time for treatment within the bioswale.
5. *Adjustment of Design Parameters:* If the calculated *HRT* falls short of the minimum requirement, consider adjusting parameters such as the length, width, or slope of the bioswale. These adjustments aim to achieve the desired *HRT*.
6. *Inter-relationship Formula Check:* Assess the new *HRT* obtained after parameter adjustments using the inter-relationship formula (Equation 2.4). This formula helps ensure that the designed bioswale meets the water quality treatment requirements.
7. *Consideration of Check Dams:* In cases where meeting *HRT* criteria becomes challenging, the installation of check dams may be proposed. Check dams can help regulate flow velocity, enhance sediment settling, and contribute to achieving the desired treatment goals.

2.4.9.2 Design Based on Aberdeen Equation (Sediment-settling Based Design)

The methodology comprises the following steps:

1. *Determination of Sediment Properties:* Assess the characteristics of the sediment targeted for treatment, including parameters like mean particle size (d_s) and density of sediment particles (ρ_s).
2. *Calculation of Design Volume:* Determine the required design volume based on the specific application and purpose of the bioswale.
3. *Settling Velocity Calculation:* Utilize the sediment properties to compute the settling velocity (V_s) using Stokes' law (Equation 2.5).

$$V_s = \frac{g}{18\,\mu}(\rho_s - \rho_w)\, d_s^2 \quad (2.5)$$

where g is the acceleration due to gravity, μ is the dynamic viscosity of water, ρ_s is density of sediment particles, and ρ_w is the density of water.

4. *Calculation of Fall Number (N_f)*: Use the calculated settling velocity to determine N_f with the available swale length according to Equation 2.6.

$$N_f = \frac{L\ V_s}{y\ v} \quad (2.6)$$

where L is the swale length, y is the flow depth, V_s is settling velocity, and v is flow velocity.

5. *Calculation of Sediment Removal Efficiency:* Compute the treatment removal efficiency by settling (Tr_s) using Equation 2.7.

$$Tr_s(\%) = \frac{{N_f}^{0.69}}{({N_f}^{0.69} + 4.95)} \times 100 \quad (2.7)$$

If the desired target removal efficiency is not achieved, repeat the process. You can increase the swale length to meet the target or adjust other parameters like width, slope, or incoming flow rate to attain the desired removal efficiency.

2.4.10 Check Dams

Check dams are small structures designed to manage concentrated flow within bioswales. They typically have a maximum height of 2 ft and serve multiple functions, including trapping sediment and heavy metal particles, removing nutrients and chemicals, controlling peak flow, and enhancing infiltration for stormwater runoff [34],[59],[75].

Check dams can be constructed using stones or rock structures and are usually positioned near the downstream end of the swale's length. By increasing the hydraulic residence time, check dams accelerate processes like absorption and nutrient uptake. The longer particles remain in contact with the swale's media due to increased retention time, the greater the potential for pollutant removal. To achieve this, check dams can be placed perpendicular to the flow approximately every 20 feet, especially when the channel slope exceeds 5% or when erosion needs to be minimized. The slope between any two check dams should ideally be limited to 2% to maintain their effectiveness [68].

For water quality flow treatment, the spacing between two check dams should be at least 50 ft [39],[56],[72]. This spacing ensures that the swale has sufficient capacity to accommodate the required water quality treatment processes between each check dam.

The impact of check dams on TSS removal efficiency in bioswales appears to vary based on different studies. For instance, Deletic and Fletcher (2006) [76] found that TSS removal efficiency was higher when check dams were installed perpendicular to the length of the grass swale. However, a study by Stagge et al. (2012) [59] showed contradictory results, suggesting that the

opposite effect could occur. This difference in findings might be attributed to factors such as re-suspension or surface erosion of the channel during extreme events with high influent concentrations. This indicates that the effectiveness of check dams in TSS removal could be influenced by multiple factors, including the specific design, local conditions, and the nature of the influent.

In the context of runoff volume reduction, Winston et al. (2019) [75] highlighted that the introduction of check dams to existing swales improved runoff volume reduction by 17%. However, they also reported that the construction of check dams led to higher instances of clogging and surface irregularities. This underscores the importance of optimizing the design of check dams and implementing effective maintenance practices to ensure their continued efficiency.

Overall, the effectiveness of check dams in bioswales can depend on a variety of factors, including their orientation, the characteristics of the influent, and the overall design and maintenance of the swale system.

2.5 Applicability and Limitations of Bioswales

When evaluating the suitability and effectiveness of BMPs such as bioswales, it is crucial to consider a range of factors including technological feasibility, economic viability, and institutional constraints [77]. Bioswales, for example, require site-specific designs tailored to address specific target pollutants [34]. The suitability of swales can be determined by considering various goals including pollutant removal, flow control, erosion control, and groundwater recharge.

Challenges often arise when treating contaminants in limited spaces, especially in non-point pollution sources like highways and urban areas. While grassed swales can help lower peak concentrations to some extent, they might not effectively reduce the overall contaminant load [70]. Swales have shown effectiveness in treating certain particle sizes and sediment-bound particles, but they might struggle with dissolved solids, nitrogen, and chlorine [65]. Achieving an effective hydraulic design for proper purification near the source can be challenging.

The use of check dams in swales can improve sediment removal efficiency for water quality flow but might decrease hydraulic capacity and induce flow turbulence downstream [43]. Additionally, bioswales might not be suitable for landscapes with steep slopes, and larger areas exceeding 10 acres could require special provisions to enhance flow [70].

Bioswales have limitations due to the restriction on water quality flow depth, which is typically within 6 inches or the height of the vegetation. This limitation affects construction and implementation possibilities, potentially constraining the use of this treatment BMP.

Underlying soil properties (infiltration rate, grain size, etc.) are considered the most important factors affecting the efficiency of bioswales in removing pollutants. If the swale is constructed in low permeability sites, it might not be very effective in removing pollutants. Gravel and sand/gravel mix that are commonly used to minimize clogging of infiltration BMPs have very low hydraulic conductivity. Larger materials such as crushed stones, gravel, etc. are used as the filter

media for stormwater systems. These materials provide much higher hydraulic conductivity, but they have very low water retention which makes them not suitable as plant-growing media. The bioswale infiltration can be increased by amending the underlying soil with engineered materials such as *expanded shale*. Conducting studies to explore the effects of incorporating such materials is crucial in enhancing the potential of bioswales.

2.6 Expanded Shale

Enhancing bioswale infiltration can be achieved through amendments to the underlying soil. Various materials such as sand, gravel, and engineered materials can be used for this purpose. One particularly effective material is expanded shale produced by heating clay or shale in a rotary kiln. This process results in a lightweight, porous aggregate with improved drainage properties. Expanded shale can serve as an amendment to clay soils, enhancing their drainage capabilities. Additionally, it can function as a filtering media, contributing to improved water quality and pollutant removal [78].

Expanded shale can come in various sizes based on particle size distribution, allowing for flexibility in its application. Commercially available classes of expanded shale produced by North American rotary kiln plants include gradations such as 20-5 mm, 13-5 mm, and 10-2 mm [79]. This material possesses several advantageous properties. Expanded shale has a remarkably high specific surface area, low density, and high durability. Additionally, it exhibits significant durability, making it a suitable choice for long-term applications.

One of the notable advantages of using expanded shale is its exceptional drainage properties. Its high drainage capabilities minimize the risk of clogging, a concern in conventional bioswales. Moreover, the increased surface area of expanded shale, which can be up to 45% greater than other materials, provides ample space for microbial colonization and pollutant trapping. This attribute can significantly enhance treatment efficiency [79].

For more detailed information about the properties of expanded shale aggregate used in filtration applications, the readers are referred to the information provided in Table 2.4.

Expanded shale offers multiple benefits that make it a versatile option for various applications. Its ability to improve water quality and function as a filtering medium when mixed with fine clay underscores its versatility. Despite its natural high drainage capacity, it is worth noting that the drainage efficiency of expanded shale can be further augmented by incorporating an underdrain system within bioswales. This combination of expanded shale and underdrains can be particularly effective in managing water flow and enhancing overall performance.

In situations where soil properties may lead to the presence of fine particles, geofabrics can play a crucial role. These fabrics can be strategically installed to prevent these fine particles from entering the underdrainage system. This helps maintain the long-term effectiveness of the underdrain and ensures that the bioswale continues to function optimally in capturing pollutants and promoting proper drainage.

Table 2.4: General properties of expanded shale aggregate used in filtration applications [79]

Aggregate Properties	Test Method	Typical Values for Expanded Shale	Typical Values for Granular Filter Materials
Surface Area	EGME Sorption Method	5 m^2/g - 19 m^2/g	0.001 m^2/g - 3 m^2/g
Specific Gravity	ASTM C127/128	1.25 - 1.85	2.65 - 2.75
Durability Index	ASTM D3744	82 - 93	80 - 99
Magnesium Soundness	ASTM C88	< 6%	< 6%
Acid Solubility	ASTM D3042	1% - 4%	0.3% - 93%
Caustic Solubility	ASTM D1109	0% - 0.9%	0% - 1%
pH	pH Meter	6 - 10	6.5 - 11
Organic Impurities	ASTM C40	< 0.5%	0.5% - 10%
Permeability (Constant Head)	ASTM D2434	50in/hr - 1300 in/hr	1 in/hr - 600 in/hr
Loose Dry Density	ASTM C29	30 lb/ft^3 - 60 lb/ft^3	90 lb/ft^3 - 105 lb/ft^3
Loose Wet Density	ASTM C29	45 lb/ft^3 - 70 lb/ft^3	95 lb/ft^3 - 110 lb/ft^3
Los Angeles Abrasion	ASTM C131	20% - 40%	10% - 45%

2.6.1 Application of Expanded Shale in Stormwater and Wastewater Treatment

The diverse applications of expanded shale in wastewater and stormwater treatment demonstrate its versatility and effectiveness across various scenarios. In wastewater treatment, it finds application in sand filters for systems like intermediate, mound, trickling-recirculating, and septic systems. It is also used in constructed wetlands for re-use or release of treated water, as well as in industrial fluid treatment processes [79].

In stormwater treatment, expanded shale plays a role in sand filters like the Austin surface Sand Filter, Delaware Sand Filter, and DC Underground Fault Sand Filter. Additionally, it is utilized in green infrastructure practices such as bioretention, bioswales, and filter strips, enhancing their pollutant removal capabilities. It contributes to high-flow stormwater devices as a polishing filter, serves as a base filtration material for permeable pavements, and offers enhanced water storage capacity. Infiltration trenches benefit from expanded shale's properties as well [79].

2.6.2 Economic Benefits of Expanded Shale

Economically, the use of expanded shale brings several advantages. Treatment efficiencies are improved, leading to longer filter life cycles with enhanced run times and no loss of performance. It enables filter bed expansions with less backflush water and supports the use of coarser media for bioactive sites while preventing crusting and ponding. From an operational standpoint, lower costs are achieved through more efficient transportation due to its lighter weight. The increased volume per load reduces the number of required trucks, and easier handling in confined spaces

leads to labor savings. Furthermore, expanded shale enables faster placement and longer reaches with loaders or cranes, contributing to lower operating and maintenance expenses [79].

2.6.3 Experimental Studies on Expanded Shale

Expanded shale finds diverse applications, as highlighted in the subsequent sections. Sloan et al. (2002) [80] embarked on enhancing clay soil drainage via the inclusion of expanded shale. Their study introduced fine shale (1-3 mm) and coarse shale (3-6 mm) into the soil media at a 50% shale-to-clay mix ratio by volume. Within a 6-inch total media thickness, Pansy and Scaevola vegetation thrived significantly due to the soil amendment, with coarse-graded expanded shale proving more effective than fine-graded varieties.

Forbes et al. (2004) [81] explored the retention of dissolved phosphorus in long-term constructed wetlands. To optimize soil for phosphorus sorption and desorption, they compared expanded shale and masonry sand against native soil, employing sorption isotherms and pilot-scale cell experiments (Figure 2.3). Expanded shale exhibited superior phosphorus absorption efficiency while retaining high hydraulic conductivity, surface area, and sorption capacity. Importantly, absorbed phosphorus was not released during desorption experiments.

In a subsequent study by Forbes et al. (2005) [82], the focus shifted to the removal efficiency of expanded shale as filtration media for phosphorus removal, building upon the capacity identified in their prior work. They examined various phosphorus forms, observing that expanded shale significantly outperformed sand beds in constructed wetlands.

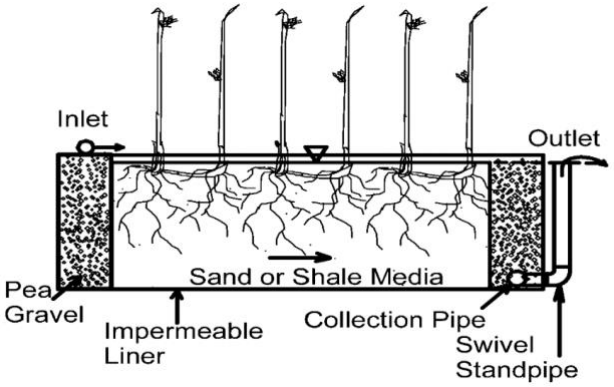

Figure 2.3: Schematic for pilot cells of constructed wetlands [82]

In a small-scale pilot study conducted by the California Department of Transportation (Caltrans), various filtering media were evaluated for their effectiveness in treating stormwater runoff. The tested filtering media included activated aluminum, expanded shale, sand, zeolite, limestone, aluminum oxide, and wollastonite. Among these options, the results highlighted the remarkable performance of expanded shale compared to the other considered filter media. Expanded shale demonstrated superior outcomes in terms of turbidity reduction and phosphorus removal. However, the study found that the effectiveness of nitrogen removal was not satisfactory, similar to other systems that were tested [83].

In a pilot-scale constructed wetland, Mateus and Pinho (2010) [84] assessed the phosphorus-removal capabilities of two types of lightweight expanded clay aggregates. These aggregates had specific weights of 300 kg/m³ and 500-600 kg/m³. Over a six-year laboratory experiment conducted under field conditions, the study demonstrated that aggregates with higher specific weight exhibited superior phosphorus removal performance compared to those with smaller specific weights. The study's conclusion highlighted that although the initial cost of lightweight aggregates might be notably higher than that of common materials like gravel for filling constructed wetlands, their long-term benefits, including high removal efficiencies, excellent hydraulic conductivity, and a conducive substrate for plant growth, justify the initial investment.

Sloan et al. (2010) [85] employed expanded shale (3-6 mm) to enhance water drainage and root aeration in plant soil. They blended organic content soils with varied volume percentages of expanded shale (0%, 15%, 30%, and 50%). Despite increased porosity in low-porous soil blends, the study noted that reduced nutrient content led to poor vegetation growth in expanded shale containers. Hydraulic conductivity enhancement through expanded shale was beneficial mainly for soils with poor drainage and aeration. The expanded shale's slow release of adsorbed phosphorus was also noted, supplying nutrients to vegetation over time. Additionally, expanded shale could supply nutrients to vegetation by releasing adsorbed phosphorus slowly over time in a soil medium. IT acted as an internal reservoir of water, which could be utilized by the vegetation for a prolonged period [86].

Mechleb et al. (2014) [78] undertook laboratory research involving different soil types and ratios of soil to expanded shale (0% to 50%). They employed two compaction methods, demonstrating improved drainage quality and decreased dry density in amended soils with expanded shale. Notably, expanded shale's performance surpassed lime-mixed clay as an engineered media, even with identical particle size distribution (Figure 2.4). Higher hydraulic conductivity was observed in low plasticity index soils.

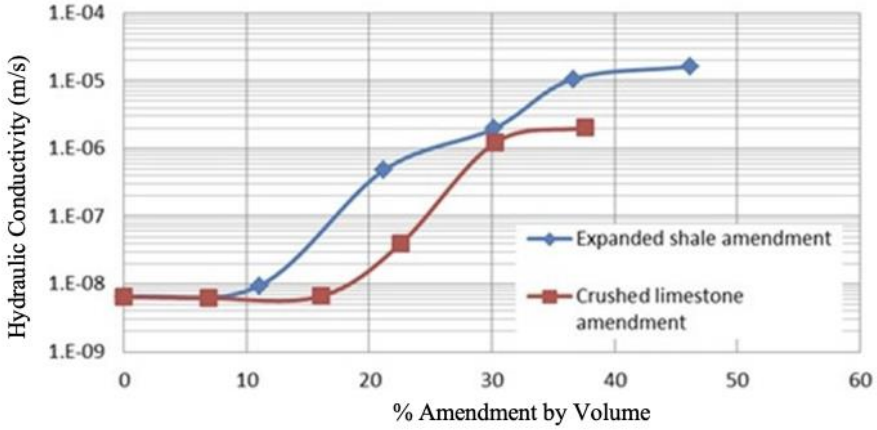

Figure 2.4: Hydraulic conductivity of amended soils with expanded shale and crushed limestone [78]

Furthermore, studies involving the application of expanded shale in permeable pavers have demonstrated improved efficiency in both pollutant removal and hydraulic conductivity [87]. Finally, Li et al. (2016) [88] reported that bioswales without vegetation exhibited 7% to 49% nitrogen removal efficiency during low flow and limited change during high flow. Nitrogen removal was less efficient with higher inflow concentrations, and soil media's pollutant absorption ability remained consistent.

3. LABORATORY EXPERIMENTS

In this project, a small-scale expanded shale engineered filtration media was installed and monitored in a controlled laboratory setting within the Fluid Mechanics and Hydraulics Laboratory at the University of Texas at Arlington. The controlled environment enabled the rapid testing of various physical configurations, including inflow-outflow dynamics, bypass mechanisms, filtering media dimensions, and pollutant loading rates, which would be challenging to implement and monitor in field settings. Multiple scenarios were examined, and water samples were collected at different timeframes and locations to investigate the efficiency of expanded shale in removing pollutants from stormwater. The governing factors, encompassing inflow rate, soil medium properties and thickness, infiltration conditions, and influent concentration, were considered as variables for developing these scenarios.

This study comprised three distinct groups of experiments, including:

1. Drainage experiments aimed at determining the drainage capacity of the soil media utilized in the study.
2. Suspended sediment experiments were conducted to assess the efficacy of expanded shale in removing TSS and Tu.
3. Chemical experiments designed to ascertain the removal efficiency of expanded shale in eliminating substances such as nitrogen, phosphorus, and zinc.

Each of the three groups of experiment utilized the same setup, yet adjustments were implemented to align with the unique requirements of each group.

3.1 Experimental Setup

3.1.1 Experimental Flume

The experiments were conducted in a plexiglass flume with overall dimensions of 16 ft in length, 4 ft in width, and 1.5 ft in depth. Inlet and outlet tanks measuring 2 ft in length, 3 ft in depth, and the same width as the flume were installed at the upstream and downstream ends of the flume.

The inlet tank is designed to facilitate water entry from its bottom through a 4-inch PVC pipe and a perforated horizontal spreader. This design ensures a consistent and even water inflow into the flume. Similarly, the outlet tank has the same dimensions as the inlet tank and functions to collect the water that passes through the flume, redirecting it back to the sump.

The flume's longitudinal slope is adjustable; however, the slope was set at 0.3% to adhere to the recommended slope (<1%) for swales with underdrains, as specified by Caltrans (2020) [26]. Engineered media, consisting of 65% expanded shale and 35% sandy clay, was placed in the flume at varying thicknesses, primarily 6 inches (with a few experiments using 4 inches). Figure 3.1 provides a schematic diagram of the experimental arrangement.

To evaluate the efficiency of expanded shale over time and along the flume, water samples were collected from four designated points within the flume: upstream above the gravel bed, the middle section of the channel, and two downstream outlets.

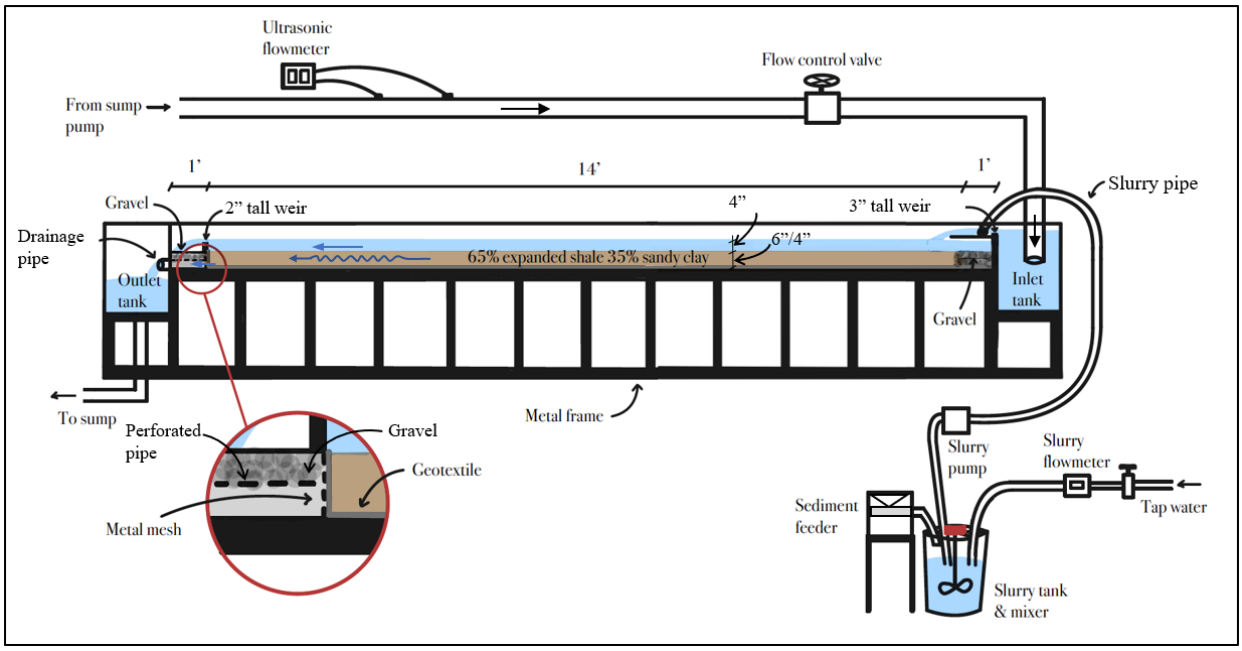

Figure 3.1: Schematic diagram of the experimental river flume (not to scale)

3.1.2 Flow Source and Control

For continuous water supply during the experiments, two underground tanks were utilized as water sources. The water supplied from the pumps within the underground tanks to the flume was regulated by a control valve attached to the 4-inch PVC pipe. The flow was measured using a calibrated Sono-TraK ST30 ultrasonic flowmeter. The flowmeter has an accuracy of ±0.5% and a response time of up to 30 seconds. To verify the flowmeter's dependability, volumetric flow measurements were additionally carried out during each experiment. This involved using the inlet tank in conjunction with a stopwatch.

3.1.3 Inlet Configuration

To ensure uniform flow distribution across the width of the flume's inlet and prevent eddies from entering the flume through the inlet tank, a rectangular contracted weir measuring 3 inches in height was installed upstream of the flume. The crest of the weir was positioned 9 inches above the bottom of the flume. Downstream of the weir, a horizontal wooden plank was placed across the flume to serve as the mixing area. The sediment slurry was introduced into the flume over this surface, against the flow direction, through a ½-inch perforated pipe, as illustrated in Figure 3.2a. The perforated pipe used for the slurry had uniformly spaced holes with a diameter of 0.375 inches, each spaced 2 inches apart. The hole size and arrangement were designed to accommodate the intended slurry rate. Additionally, a horizontal layer of gravel was introduced at the flume entrance

on top of the soil medium to mitigate flow velocity and prevent localized erosion, as depicted in Figure 3.2b.

(a) **(b)**

Figure 3.2: Inlet section components of the experimental setup

3.1.4 Underdrain System

An underdrain system was designed and installed in the flume to enhance the filtration capability of the soil media. This system consisted of 2-inch perforated pipes, with a main pipe running along the length of the flume, and six collectors evenly spaced across the width of the flume (refer to Figure 3.3). The holes in the pipes were spaced to ensure that every two holes maintained a distance equivalent to the diameter of the used pipe (i.e., two holes per every 2 inches).

All pipes were wrapped with non-woven geotextile (as shown in Figure 3.4) to prevent any soil medium material from being washed out. The geotextile had a sieve #80 size rating, indicating that only particles smaller than 0.18 mm could pass through it. The soil media used in this study were much coarser, with over 90% of particles exceeding 0.18 mm in size (refer to Section 3.1.7). Additionally, the silica flour utilized in this study had a maximum size of 0.13 mm (see Section 3.1.6), ensuring that the geotextile did not capture any influent sediment that might have potentially led to clogging. A ball valve was installed at the end of the main pipe. Its primary function was to control the flow through the underdrain system. Fully closing the valve limited the flow to infiltration through the soil medium alone, representing the scenario without an underdrain. Conversely, when the valve was fully open, the flow passed through both the soil medium and the underdrain pipe system, representing cases of swales with underdrain.

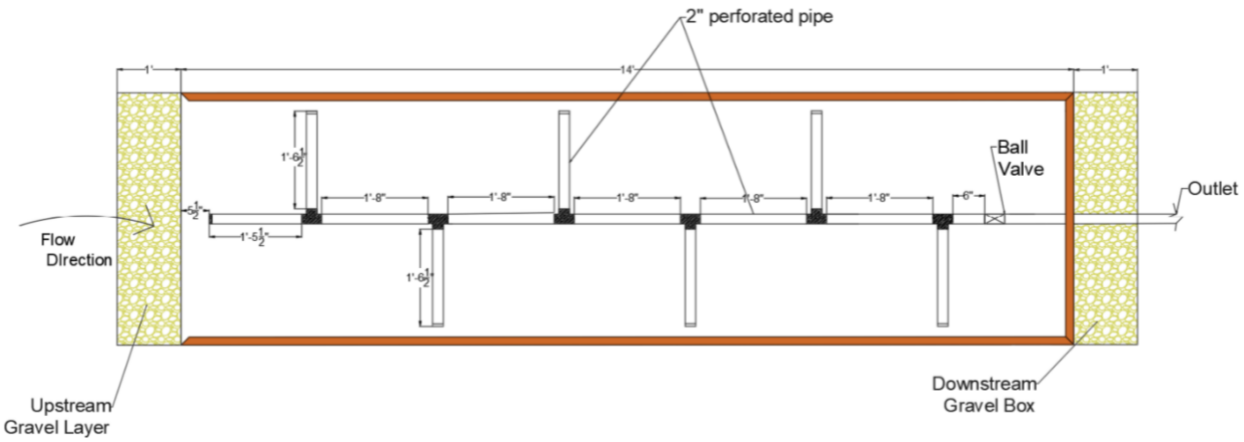

Figure 3.3: Layout of the underdrain system in the experimental flume (plan view)

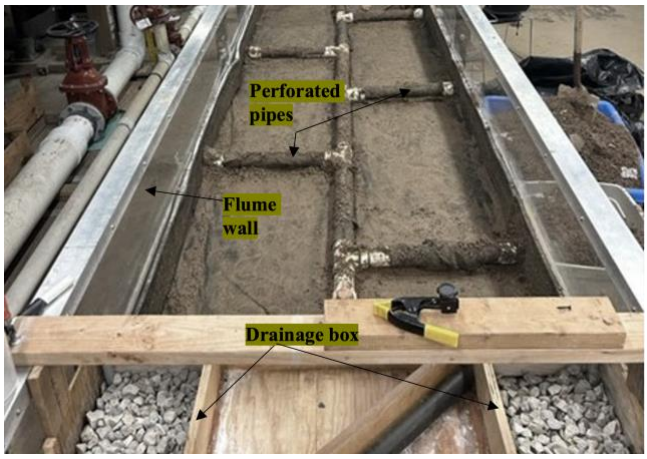

Figure 3.4: Underdrain system before placing soil medium in the flume

3.1.5 Outlet Configuration

At the downstream end of the flume, a rectangular box measuring 1ft in length was installed. This box was filled with coarse gravel and served as a crucial component of the experimental setup (Figure 3.4). Positioned on the upstream face of the box was a 6-inch tall opening that spanned across the flume. This design allowed water to flow through the soil medium and reach the interior of the box. To prevent the soil medium materials from being washed away, both a metal mesh and a non-woven geotextile fabric were placed between the layer of gravel and the soil medium (Figure 3.1). This arrangement facilitated water passage while effectively retaining the soil medium within its designated space. The geotextile fabric possessed a sieve #80 rating, indicating its capability to allow particles smaller than 0.18 mm to pass through. Given that the silica used as influent sediment in this study had a maximum particle size of 0.13 mm (refer to Section 3.1.6), the geotextile fabric did not impede the soil medium's infiltration capacity or its ability to remove sediment.

Furthermore, to facilitate the collection of water that infiltrated through the geotextile from the soil medium, a 2-inch perforated pipe was installed across the drainage box. This perforated pipe was integrated into the system to efficiently guide the flow of infiltrated water to the outlet tank located within the drainage box (as depicted in Figure 3.5).

At the downstream end of the soil medium, on top of the drainage box, a 6-inch tall check dam was installed, causing water to pond in the flume. To enable excess water to overflow into the outlet tank, a 1-ft wide weir was cut out in the check dam's midsection (Figure 3.5). The weir's crest elevation was chosen to ensure that the soil media was always covered by at least 4 inches of water.

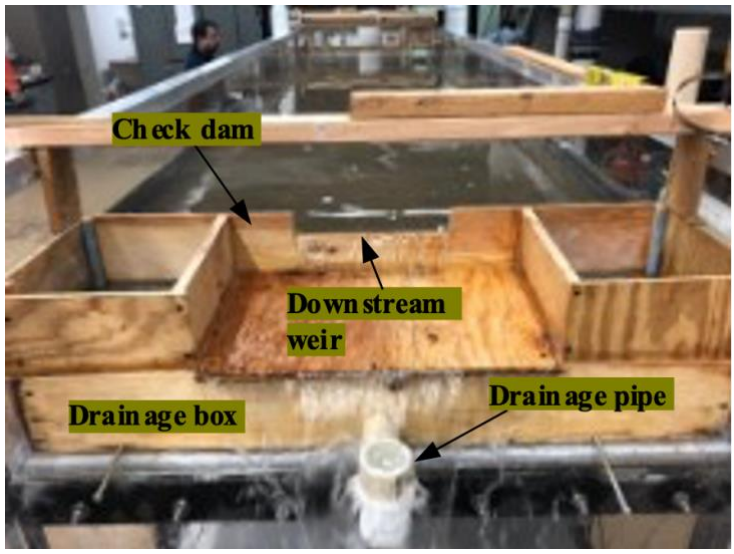

Figure 3.5: Outlet box with underdrain pipe, check dam, and downstream weir

3.1.6 Sediment Slurry Preparation

Silica flour #140/106u was used in preparing the slurry. The consistency of the silica flour's gradation was assessed through three separate tests conducted at the UTA Shimadzu Lab to ensure compliance. The particle size gradation was determined using a Shimadzu nano-particle size analyzer (Shimadzu SALD-7101) employing the laser diffraction method. The gradation curves of the silica flour provided by the manufacturer, AGSCO Corporation, were compared with those established in this study, as depicted in Figure 3.6. The designations “Test 1” to “Test 3” correspond to three distinct gradation tests on the silica, while “Ave” represents the averaged values derived from all three tests.

The gradation curve of the silica flour provided by the manufacturer aligns with the gradation determined in this study up to 0.037 mm in size. However, the manufacturer's gradation data does not extend to particles smaller than 0.037 mm, likely due to the absence of equipment capable of testing at such sizes. Consequently, the sediment gradation data obtained from the UTA Shimadzu

lab was used for data analysis, ensuring greater accuracy. It is important to note that the selection of silica flour for this study was in accordance with the sediment particle size distribution requirements established for experiments assessing total suspended solids removal through filtration within manufactured treatment devices, as outlined by the New Jersey Department of Environmental Protection (NJDEP, 2022) [89]. The comparison between the percentage passing of the selected silica flour and the NJDEP's specified values is presented in Table 3.1. Notably, all sediment classes in this study meet or exceed the minimum percentage passing criteria set by NJDEP, emphasizing the suitability of the chosen silica flour for accurate and valid experimentation.

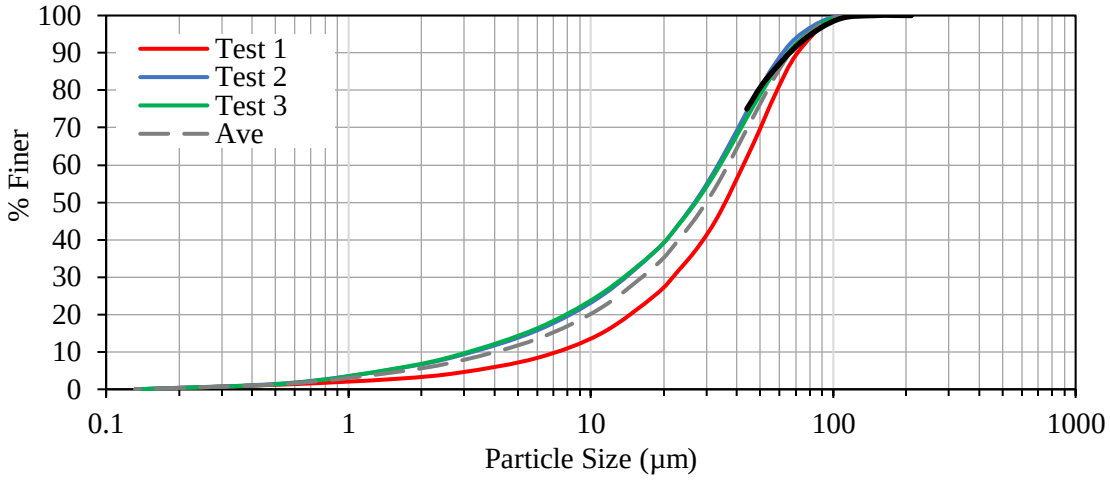

Figure 3.6: Silica flour particle gradation size

Table 3.1: Particle size distribution of the silica flour and NJDEP [89] minimum percentage passing

Particle Size (µm)	% Passing of Silica Flour	NJDEP Minimum % Passing
1000	100	100
500	100	95
250	100	90
150	100	75
100	99	60
75	93	50
50	76	45
20	35	35
8	15	20
5	9	10
2	5	5

Silica flour was mixed with tap water at a precisely controlled rate to achieve the desired concentrations for the slurry mixture. The slurry preparation process utilized a cylindrical tank with a 32-gallon capacity and a horizontal base (Figure 3.7). This tank was equipped with a float valve to regulate the water level within the tank, ensuring a consistent and predetermined depth. To measure the water flow rate entering the slurry tank, an in-line flowmeter was incorporated into the setup (see Figure 3.7). Similarly, a continuous injection of silica flour into the slurry tank was achieved using a Tecweigh volumetric feeder. The selection of this feeder was based on its ability to handle dry materials and its volumetric accuracy, which ranged between 2% and 4% [90].

To ensure a steady and controlled flow of the slurry into the flume, a sump pump was employed to facilitate the injection of the slurry from the slurry tank into the flume at a consistent rate. Additionally, a valve was integrated into the outlet pipe of the sump pump (as depicted in Figure 3.7). During each experiment, this valve was used to collect samples from the slurry to assess and verify its sediment concentration, contributing to the overall accuracy and reliability of the experimental process.

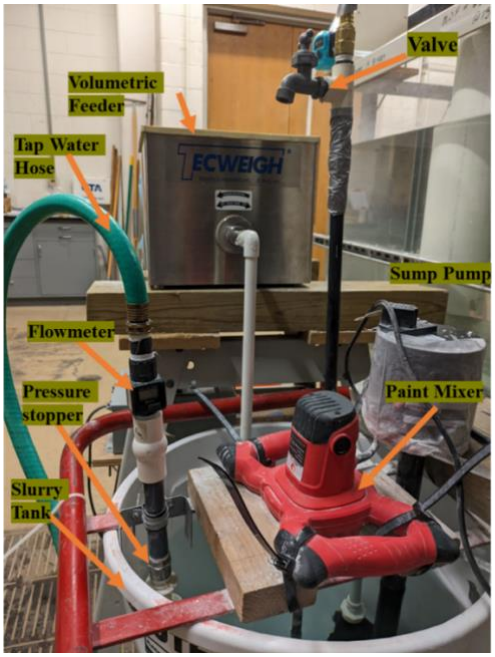

Figure 3.7: Volumetric sediment feeder and slurry preparation tank

3.1.7 Soil Media

Two different soil media mixes were employed in this study. Type 1 consisted of a coarser size of expanded shale, also referred to as G-pile by the manufacturer. Type 2 contained finer expanded shale, also known as J-pile by the manufacturer. Both types maintained the same ratio of expanded shale to sandy-clay, specifically 65% expanded shale and 35% natural sandy-clay.

Sieve analysis was conducted in the UTA Geotechnical Laboratory to determine the gradation of the expanded shale types (G-pile and J-pile) as well as the two soil mixes used in the study. The ASTM D6913 standard (2017) [91] was followed for all sieve tests. Gradation curves for G-pile, J-pile, Type 1 mix, and Type 2 mix were prepared and are illustrated in Figures 3.8 and 3.9.

The median diameters (d_{50}) of the coarse (G-pile) and fine (J-pile) expanded shale materials were approximately 5.5 mm and 2.45 mm, respectively (Figure 3.8). The d_{50} values for Type 1 and Type 2 were 2.25 mm and 1.5 mm according to Figure 3.9.

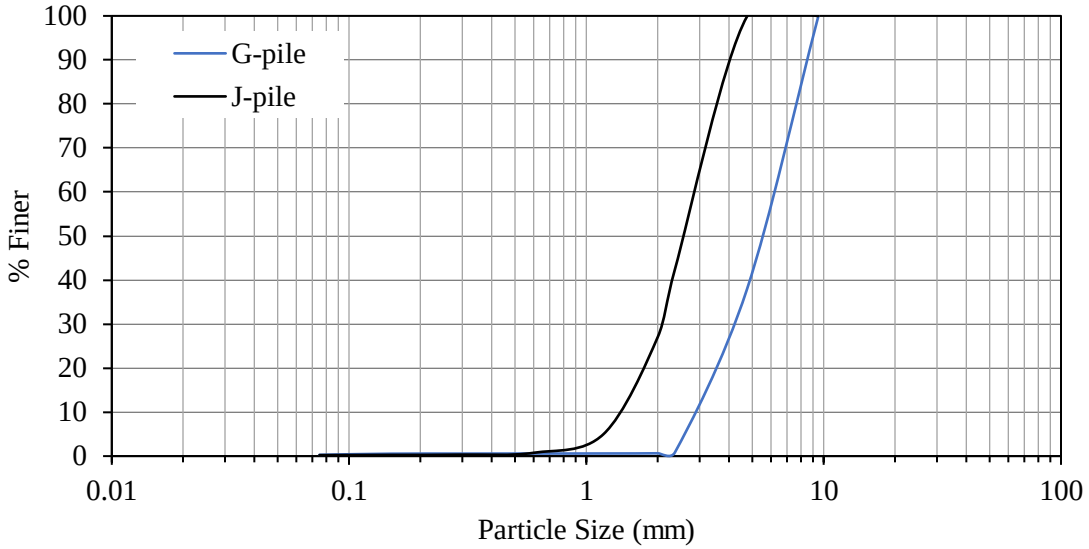

Figure 3.8: Particle size gradation of coarse (G-pile) and fine (J-pile) expanded shale

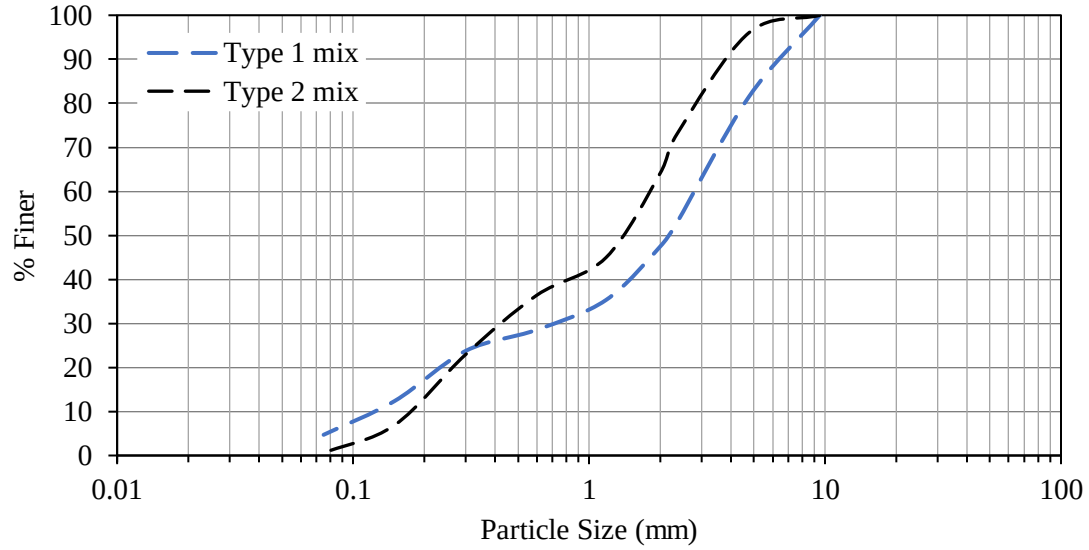

Figure 3.9: Particle size gradation of Type 1 and Type 2 soil mix

3.1.8 Chemicals Slurry Preparation

For chemical tests, water flowing through the flume was mixed with synthetic water containing nitrogen, phosphorus, and zinc. The certified sodium nitrate, zinc nitrate hexahydrate, and 85% phosphoric acid were used in the experiments. The nitrate nitrogen, phosphate phosphorus, and zinc concentrations were measured by the Hach method.

In each experiment, chemicals were mixed in a 10-liter feed tank. Subsequently, these chemicals were pumped at a rate of 1 L/min utilizing a peristaltic pump and combined with tap water, which was pumped from the slurry tank at a rate of 11.3 L/min. The resulting diluted chemical solution was then introduced into the flume inlet area by means of a perforated pipe. It should be noted that the identical perforated pipe and mixing surface that were employed for sediment slurry were also utilized in the chemical tests.

3.2 Experimental Procedure

3.2.1 Selection of Inflows

Three inflows were considered in this study, i.e., 60 Lit/min (low flow), 120 Lit/ min (base flow), and 180 Lit/min (high flow). In the base flow scenario, the inflow rate was determined by adhering to a minimum hydraulic residence time (*HRT*) of 5 min, a requirement outlined in Caltrans (2020) guidelines for bioswale design [26]. The maximum flow velocity was calculated using Equation 2.3, considering a flume length, including the gravel bed, of 15 ft (4.6 m), which yielded a maximum flow velocity of 0.05 ft/s (0.015 m/s) and the flow depth within the flume that was constrained to 0.33 ft (11.4 cm) due to the presence of a check dam installed downstream. With the calculated maximum flow velocity, flow depth, and width, the maximum water quality flow was computed to be 0.066 ft^3/s, equivalent to 112 Lit/min. Taking into account that a portion of the inflow infiltrates through the soil, as discussed in Section 4.1, an inflow rate of 120 Lit/min was selected for the base case scenario.

The base flow rate of 120 Lit/min corresponds to the peak stormwater runoff generated from a drainage area measuring 16,145 ft^2 (1500 m^2) when subjected to a rainfall intensity of 0.5 in/hr (12.7 mm/hr). This rainfall intensity is a commonly employed value in calculations related to water quality flow, as recommended by Barrett et al. (1998) [92] and stormwater management guidelines.

Claytor and Schueler (1996) [93] recommended a minimum hydraulic residence time of 10 minutes to ensure optimal filtration for water quality flow. Consequently, for the low flow scenario, a flow rate of 60 Lit/min was selected. This flow rate resulted in a flow velocity of 0.026 ft/s (0.008 m/s), which is below the maximum allowable velocity of 0.05 ft/s (0.015 m/s).

As some BMPs are designed to address both water quality flow and peak flow reduction, a flow rate of 180 Lit/min was chosen for the high flow scenario. Although this flow rate does not meet the criteria outlined in the inter-relationship formula (Equation 2.4), it can still be safely managed and conveyed through the bioswale system. The swale was modeled to function as a flow reduction

and conveyance system with a flow velocity of 0.078 ft/s (0.024 m/s), corresponding to 180 Lit/min.

3.2.2 Influent Suspended Sediment Concentrations

In order to capture a broad spectrum of typical suspended sediment concentrations in stormwater, two influent suspended sediment concentrations of 100 mg/L and 200 mg/L were chosen. These selections were informed by a literature review of mean concentrations found in highway runoff effluent (Barrett et al. 1998) [92]. By opting for these concentrations, both high and low scenarios were covered, offering a comprehensive representation of the possible range of variability in highway runoff sediment concentrations.

3.2.3 Influent Chemical Concentrations

According to the EPA's preliminary data summary of urban stormwater BMPs, the total nitrogen range found in urban runoff is 0.4-20 mg/L, the total phosphorus range is 0.02-4.30 mg/L, and the total zinc range is 0.01-2.90 mg/L [27]. In this study, the targeted influent concentrations of nitrogen (N), phosphorus (P), and zinc (Zn) were set at 25.0 mg-N/L, 5.0 mg-P/L, and 5.0 mg-Zn/L. These values were deliberately chosen to exceed the upper limits of the aforementioned ranges, allowing us to assess the removal efficiency of chemicals in a worst-case scenario and to provide a buffer for any potential increases in constituent concentrations over time. Furthermore, the calculated removal efficiencies were based on the measured values of the concentrations in the influent and effluent.

3.2.4 Testing Scenarios

3.2.4.1 Drainage Experiments

Prior to conducting suspended sediment and chemical experiments, it was essential to evaluate the drainage capacity of both Type 1 and Type 2 soil media. A total of 16 drainage capacity tests were carried out. These tests involved measuring the flow over the downstream weir (overflow) and flow through the soil media (underflow) for inflow rates of 60, 120, and 180 Lit/min. Furthermore, the drainage rate was assessed under a zero-overflow condition. To achieve this, the inflow rate was gradually increased until a water depth of 4 inches was achieved in the flume without any water spilling over the downstream weir. Both overflow and underflow were quantified using a volumetric flow measurement following the EPA Bucket and Stopwatch method [94]. Every volume measurement was taken for at least 10 seconds and repeated at least three times for reliability. Additionally, the water depth just before the downstream weir was recorded for each experiment that resulted in overflow.

It is worth noting that these drainage capacity tests for Type 1 and Type 2 soil media were conducted under both with underdrain and without underdrain conditions. Importantly, no sediment or chemicals were introduced into the flume during these drainage tests.

3.2.4.2 Suspended Sediment Experiments

Several scenarios were conducted, wherein different factors were selected and their effects on reducing total suspended solids (TSS) and turbidity (Tu) were assessed. These factors included inflow rate, the depth of the filter media, underdrain conditions, influent sediment concentrations, and the type of filter media. By altering and evaluating these variables, a comprehensive understanding of their influence on the system's performance and effectiveness was achieved.

A total of 30 scenarios were conducted in suspended sediment experiments as shown in Table 3.2. Among these, 12 involved an active underdrain system, where the underdrain system control valve remained open during the experiment. The remaining tests were conducted without an underdrain system, i.e., with the underdrain system control valve closed. Two different influent concentrations of 100 mg/L and 200 mg/L were considered. Regarding the thickness of the soil media, both 4-inch and 6-inch depths of soil media were tested in this study. However, as discussed in Section 4.2.1, the 4-inch thickness for the Type 2 soil media was not tested in this study due to the subpar performance observed with the Type 1 soil mix at that thickness in reducing TSS and turbidity.

Each experiment had a duration of 40 minutes, representing the typical rainfall duration and aligning with the requirements set by NJDEP for filtration treatment device tests, which mandate a test duration of more than 30 minutes [89].

Water samples were collected for TSS and turbidity analysis from various parts of the flume. A 10-minute sampling interval was selected based on the requirement for the hydraulic residence time. For this study, the maximum hydraulic residence time was calculated to be 8 minutes for low flow conditions.

Initially, sampling locations were chosen, including the slurry tank, the upstream weir at the inlet, the area upstream of the soil media over the gravel, the middle section of the flume, water exiting the underdrain, and water flowing over the downstream weir (if applicable). After conducting a few preliminary tests, the results showed more uniform mixing over the gravel bed. Therefore, sampling from the upstream weir location was discontinued. Throughout the study, sampling was initiated only after a 4-inch water depth was established over the soil media and during low flow conditions when there was no substantial change in flow depth over time.

Samples were collected using a single grab sample method as defined by USGS (2006) [95]. Each time, a clean 1-liter bottle, washed with distilled water, was used to take a sample with a swift horizontal motion, targeting the middle 2/3rd portion of the flume width to minimize wall effects. All collected samples were tested for TSS and turbidity on the same day. In some instances, samples were kept at room temperature and tested within 24 hours to prevent any changes in sample composition or sediment decay due to undesirable factors, such as sediment decomposition or microbial activities (if present). All the samples collected from the flume were used for TSS tests, and the testing protocol adhered to EPA method 160.2 [96]. Prior to testing, samples were vigorously shaken and swirled. The TSS test was repeated if the values deviated by more than ±20% from the overall mean values to ensure reliability.

Every sample considered for the TSS tests was also subjected to turbidity testing, except for samples from the slurry tank. Notably, samples from scenarios 1 to 3 and experiments with 4-in soil media were not subjected to turbidity testing. All the turbidity tests were performed by a Hach 2100Q portable turbidimeter after it was calibrated using standard samples with turbidity levels of 20, 100, and 800 NTU. Following the calibration, a 10 NTU standard was used to confirm and verify the turbidimeter's calibration, in accordance with the guidelines outlined by EPA [94].

Table 3.2: Summary of suspended sediment test scenarios

Experiment No.	Infiltration Media	Media Thickness (inch)	Drainage Condition	Inflow (Lit/min)	Influent Sediment Concentrations (mg/Lit)
1	Coarse media (G-Pile)	6	With underdrain	60	100
2				120	
3				180	
4				60	200
5				120	
6				180	
7			Without underdrain	60	100
8				120	
9				180	
10				60	200
11				120	
12				180	
13		4	Without underdrain	60	100
14				120	
15				180	
16				60	200
17				120	
18				180	
19	Fine media (J- Pile)	6	With underdrain	60	100
20				120	
21				180	
22				60	200
23				120	
24				180	
25			Without underdrain	60	100
26				120	
27				180	
28				60	200
29				120	
30				180	

Additionally, a subset of the samples was chosen for particle size gradation testing. A SALD-7101 nano-particle size analyzer was utilized to determine the particle size distribution of both silica flour and selected water samples collected during the suspended sediment experiments. The procedure was carefully followed to ensure the accuracy of the UV laser-equipped analyzer. For cleaning the sampling bottles and, when necessary, diluting the samples, distilled water obtained from reverse osmosis was employed. While samples collected from the flume were in liquid form, the dry silica flour was diluted with distilled water before testing. Each sample underwent three evaluations to maintain consistency. For particle size distribution analysis, samples from both the high inflow condition (180 Lit/min) and the low inflow condition (60 Lit/min) were examined. This analysis encompassed samples from experiments conducted with both soil media types and at both high and low sediment concentrations. Samples for each condition were collected and tested at four different sampling locations, with testing occurring at 10-minute intervals.

3.2.4.3 Chemical Experiments

A total of 10 chemical experiments were carried out to determine the efficiency of the soil media in removing nitrogen, phosphorus, and zinc. The experiments were conducted only with Type 2 soil media. A summary of these experiments and their conditions is shown in Table 3.3.

Experiments 1 to 6 were conducted with three inflow rates of 60, 120, and 180 L/min. Each flow was run under two conditions: with the underdrain and without the underdrain. These experiments were conducted for the duration of their corresponding hydraulic residence time (*HRT*) calculated based on the inflow rate. The chemicals were injected for the duration of the experiment, and samples were collected when they arrived at the sampling point.

The samples in the inlet area were taken one minute after the chemical feed started. In the middle section of the flume, samples were collected at approximately half the hydraulic residence time. For instance, in experiments with an *HRT* of 8.8 minutes, the middle samples were collected at approximately 5.4 minutes (=1 min + 4.4 min). The underflow and overflow samples were collected after the hydraulic residence time had elapsed. Therefore, for an *HRT* of 8.8 minutes, the outflow and overflow samples were taken at approximately 9.8 minutes (1 min + 8.8 min)

Experiments 7 to 10 were conducted for a duration of 40 minutes. These experiments were designed to assess the chemical removal efficiency of soil media, simulating scenarios where continuous rainfall runoff passes through the swale in the field. This allowed us to observe how the removal efficiency may change over time.

For each experiment, samples were collected at designated times at the inlet, middle section, overflow, and underflow. The flume was operated for 10 minutes, and the first set of samples was taken at the 10^{th} minute. Subsequent sets of samples were collected at 10-minute intervals, specifically at 10 minutes, 20 minutes, 30 minutes, and 40 minutes.

The pH and conductivity were measured using the Accumate AP85 meter immediately after sampling. Then, the concentrations of nitrate nitrogen, phosphate phosphorus, and zinc were measured using the Hach DR890 Colorimeter following the Hach procedure manual.

Table 3.3: Summary of chemical test scenarios

Experiment No.	Inflow (L/min)	Run time (min)	Overflow (L/min)	Drainage Condition
1	60	8.81	29	With underdrain
2		8.81	48	Without underdrain
3	120	4.41	88	With underdrain
4		4.41	108	Without underdrain
5	180	2.94	148	With underdrain
6		2.94	168	Without underdrain
7	120	40	89	With underdrain
8	60	40	30	With underdrain
9	30	40	0	With underdrain
10	12	40	0	Without underdrain

4. RESULTS OF LABORATORY EXPERIMENTS

4.1 Drainage Capacity Experiments

In this study, two types of expanded shale soil media, namely Type 1 and Type 2, were evaluated for their drainage capacity. Before conducting the sediment and chemicals experiments, the drainage capacity of these media under various flow conditions was determined.

To assess the drainage capacity, three different inflow scenarios were considered, i.e., 60, 120, and 180 Lit/min. During these tests, underflow and overflow rates were measured. The underflow represents the rate at which water is infiltrated through expanded shale media and exits the flume through the outlet drainpipe. This rate indicates how effectively the media can drain water under different flow conditions. The overflow, on the other hand, represents the rate at which water overflows the downstream weir when it reaches soil media maximum infiltration capacity. The overflow rate is essential to understand the capacity of the media to handle high water volumes and to prevent flooding. In addition to the above scenarios, experiments were conducted at zero-overflow condition. The inflow rate was gradually increased until a 4-inch water depth was observed in the flume without water flowing over the downstream weir. This experiment aimed to determine the maximum drainage capacity of the expanded shale media when the water level is maintained at a specific height without overflowing.

In addition to estimating the infiltration capacity, the effect of the underdrain system on the underflow rate was also assessed. For this purpose, the control valve of the underdrain system was kept open during experiments and both underflow and overflow were measured.

Throughout the experiments, the water depth just before the downstream weir was also recorded. This measurement provides information on how the water level changes as it approaches the downstream weir and helps in understanding the flow dynamics in the flume.

The results of the flow rates and depth measurements for Type 1 and Type 2 media are summarized in Tables 4.1 and 4.2, respectively. These tables show that for Type 1 soil media, when the underdrain system was not active (i.e., the control valve was closed), the drainage capacity of soil media was 46.2 Lit/min, and no overflow was recorded. As the inflow increased to 60, 120, and 180 Lit/min (target inflows), the drainage capacity also increased to 48, 53.4, and 55.2 Lit/min. At the highest inflow rate, the drainage capacity increased only by 20% even though the inflow was increased by almost 4 times from 46.2 to 180 Lit/min. The reason for this small increase is simply the crest elevation of the downstream weir which kept the flow depth at around 10 cm (4 inches) over the soil media. As shown in Table 4.1, the flow depth increased only from 10 to 10.69 cm (6.9% increase) as the inflow increased from 46.2 to 182.2 Lit/min.

The drainage capacity of Type 2 soil media was slightly smaller than that of Type 1. It increased from 41.2 Lit/min in zero-overflow condition to 48 Lit/min during maximum inflow, i.e., 180 Lit/min. Overall, the drainage capacity of Type 1 soil media was 10-15% higher than the drainage capacity of Type 2. Considering that the composition of Type 1 soil media is slightly coarser than

Type 2, this small difference between their drainage capacities was expected. The d_{50} of Type 1 and Type 2 are approximately 2.25 mm (0.09 in) and 1.5 mm (0.06 in) (Figure 3.9). This result is in agreement with the previous studies that indicate that soil properties affect the infiltration rate such that coarser materials have higher infiltration (e.g., [71]).

In experiments with an active underdrain system (i.e., the control valve open), the drainage capacity of Types 1 and 2 soil media in zero-overflow experiments increased by 20 and 24 Lit/min (43% and 58%). In the high inflow scenario (180 Lit/min), this increase was 17 and 24 Lit/min (30% and 50%). It should be noted that when underdrain was active, both media had similar underflow rates.

Table 4.1: Drainage capacity of Type 1 and Type soil media (without underdrain system)

Media Type	Target Inflow (Lit/min)	Actual Inflow (Lit/min)	Underflow (Lit/min)	Overflow (Lit/min)	Water Depth (cm)
Type 1	-	46.2	46.2	-	10.0
	60	59.5	48	11.5	10.06
	120	120.2	53.4	66.8	10.38
	180	182.2	55.2	127	10.69
Type 2	-	41.2	41.2	-	10.0
	60	62.1	42	20.1	10.06
	120	120.2	43.8	76.4	10.50
	180	182.2	48	134.2	10.75

Table 4.2: Drainage capacity of Type 1 and Type soil media (with underdrain system)

Media Type	Target Inflow (Lit/min)	Actual Inflow (Lit/min)	Underflow (Lit/min)	Overflow (Lit/min)	Water Depth (cm)
Type 1	60	60.7	60.7	-	10.0
	-	66.5	66.5	-	10.0
	120	120.2	68.4	51.8	51.8
	180	182.2	72	110.2	110.2
Type 2	60	60.7	60.7	-	10.0
	-	70.6	65.4	5.2	10.0
	120	120.2	71.4	48.8	10.25
	180	185.2	72.6	112.6	10.63

4.2 Suspended Sediment Experiments

A total of 30 scenarios were conducted to evaluate the efficiency of the soil media in reducing TSS concentration and turbidity. Water samples were collected from the flume inlet (inflow), the middle section of the flume, underflow (infiltrated water through the soil media and underdrain system), and overflow (water flowing over the downstream weir). Each scenario was conducted for 40 min, and water samples were collected at 10-minute intervals during the experiments. The TSS concentration and turbidity (Tu) of the samples were determined. As an example, Figure 4.1 shows the variation of TSS and Tu with time in experiments with the inflow rate of 120 L/min, influent with concentration of 100 mg/L, and infiltration layer of thickness of 4 inches (10 cm) and 6 inches (15 cm). The average TSS in the flume inlet area was 100 mg/L ± 10 mg/L in both experiments. The average TSS concentrations in the flume's middle section, overflow, and drained water were 55, 58, and 31 mg/L (Figures 4.1a and c).

The removal efficiency of the swale was calculated by comparing the TSS concentration of the inflow with those of the underflow and overflow. For example, in experiments with the 6-in soil media, the TSS was reduced by 45%, 42%, and 69% at these three locations. In experiments with the shallower infiltration layer (4-in), the reduction in TSS was 31%, 37%, and 53%. The reduction in TSS in underflow was mainly due to the infiltration and filtration process, whereas the reduction in TSS in the overflow was largely due to the sedimentation process in the flume.

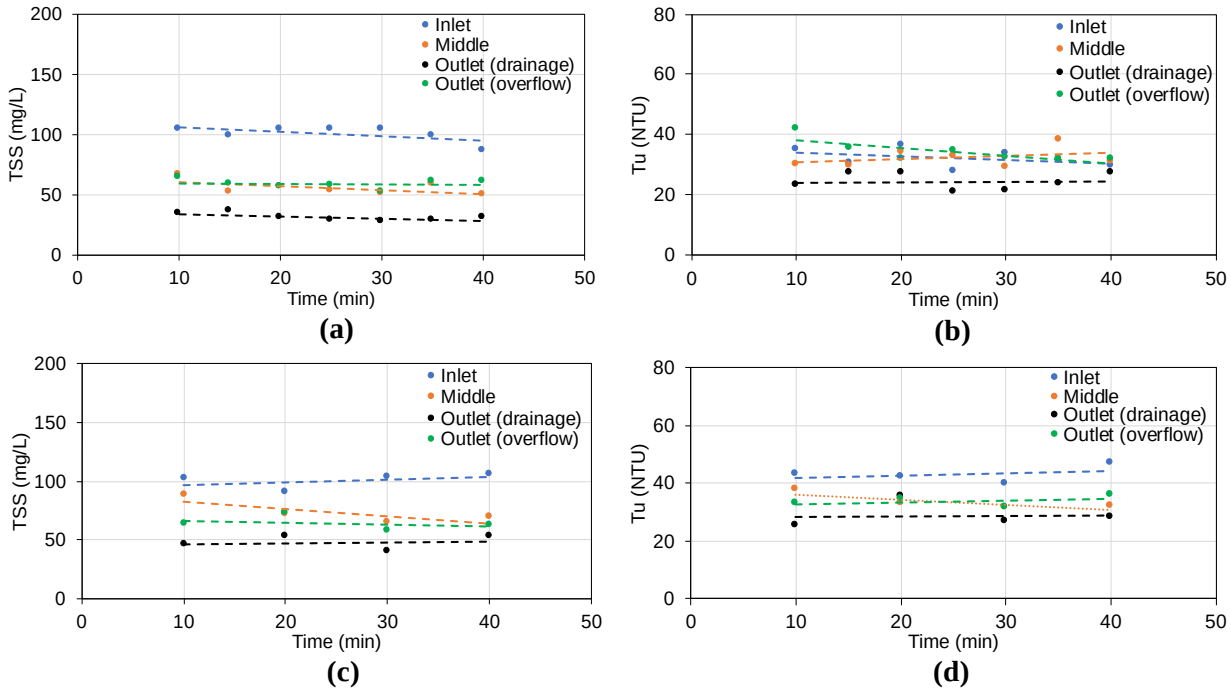

Figure 4.1: TSS and Tu at the inlet, middle section, underflow, and overflow for experiments with the inflow of 120 Lit/min, influent sediment concentration of 100 mg/L, and infiltration layer thickness of 6 inches (a,b) and 4 inches (c,d)

In experiments with a deep infiltration layer (6 inches), the average Tu reduced from 32 NTU in the inlet area to 24 NTU in infiltered water (25% reduction), however; it did not show any reduction in the middle section (32 NTU) and was slightly higher in the overflow (34 NTU). In experiments with the 4-in infiltration layer, the average Tu was 44, 35, 34, and 30 NTU at the inlet, middle section, overflow, and infiltered water, respectively (Figures 4.1b and d). The Tu reduced by 21% in the middle section, 24% in overflow, and 34% in drained water.

The following sections discuss various factors affecting TSS and Tu removal efficiency. These factors include soil media type and thickness, drainage condition, inflow rate, and influent sediment concentration.

4.2.1 Effect of Soil Media on TSS Removal

The effect of soil media thickness, type, and drainage conditions on TSS removal efficiency was investigated and the results are discussed in the flowing sections.

4.2.1.1 Effect of Soil Media Thickness on TSS Removal

Twelve experiments were performed, comprising six experiments with 4-inch and six experiments with 6-inch thickness soil media. The percentage reduction of TSS in underflow and overflow is plotted in Figures 4.2 and 4.3, respectively. Figure 4.2 shows the reduction in TSS concentration in underflow was higher (65-76%) in 6-inch thick media compared to 53-67% in the 4-inch thick media. In both cases, as inflow increased from 60 to 120 Lit/min, the percentage of TSS reduction decreased and then increased with the increase in inflow to 180 Lit/min. Also, an increase in influent concentration from 100 to 200 mg/Lit did not have a significant effect on TSS removal efficiency, and no obvious relationship between these two was found.

As expected, the thickness of soil media had minimal effects on the reduction of TSS in overflow. This effect was more pronounced in low flow experiments whereas it had no effects in experiments with high inflows (Figure 4.3). During low inflows, a larger portion of water entering from the flume inlet passes through the media, so the thickness of soil media plays a larger role in removing sediment. At the same time, due to smaller flow velocity in low inflow experiments, sediment deposition would occur at a higher rate than in high inflow experiments. Therefore, the higher TSS removal in low inflow experiments with 6-inch soil media may not be attributed solely to thicker soil media.

To have a better insight into the effect of soil media thickness on TSS removal, the weighted average TSS reductions of each experiment were calculated, and the results are summarized in Table 4.3. The percentage of TSS removal and the rate of flow in underflow and overflow were used to calculate the weighted average TSS removal. Since the influent sediment concentration did not show any effects on TSS removal, the results of every two experiments with the same inflow but different concentrations (i.e., 100 and 200 mg/L)were averaged. As shown in Table 4.3, regardless of inflow rates, the weighted average TSS removal was always higher in experiments with the 6-in soil media.

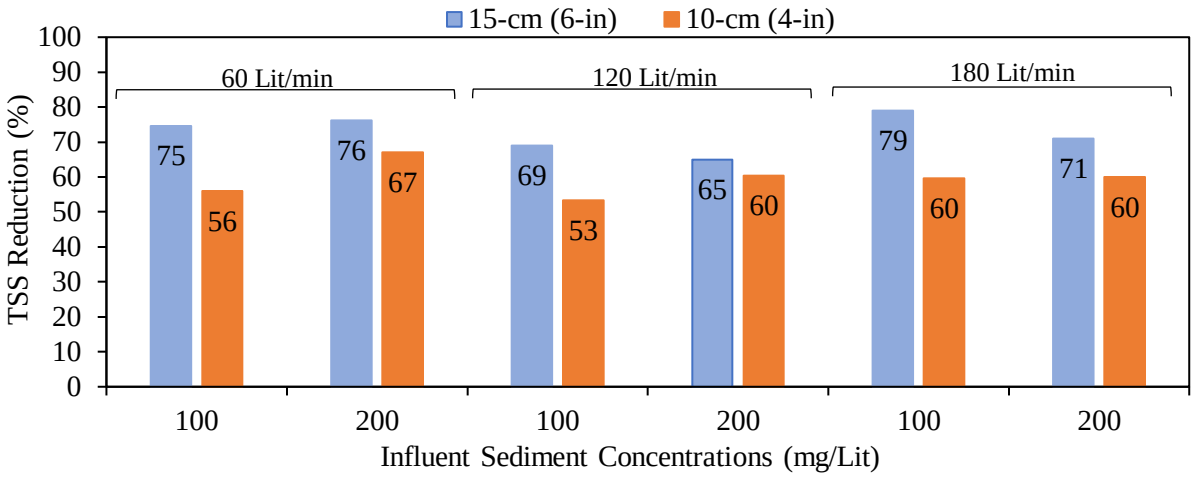

Figure 4.2: Effect of soil media thickness on TSS removal in underflow

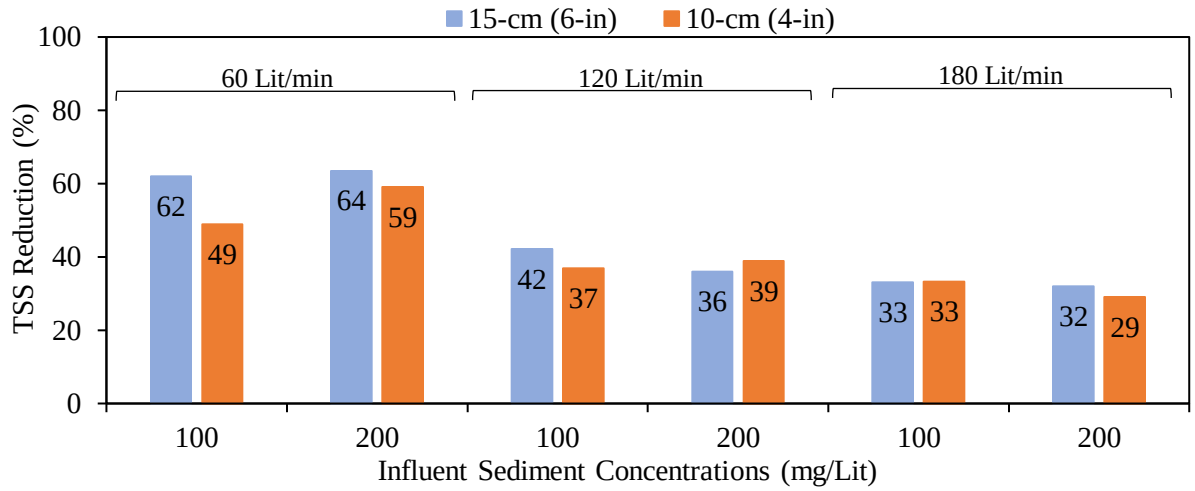

Figure 4.3: Effect of soil media thickness on TSS removal in overflow

Table 4.3: Weighted average TSS removal for soil media with different thickness and under different inflows

Soil Media Thickness (cm (in))	Weighted Average TSS Removal (%)		
	60 (Lit/min)	120 (Lit/min)	180 (Lit/min)
10 (4)	56	40	33
15 (6)	66	42	36

4.2.1.2 Effect of Soil Media Type and Drainage Conditions on TSS Removal Efficiency

Two different soil media types (Type 1 and Type 2) under two drainage conditions (with and without the underdrain system) were tested. Type 1 was a mix of sandy-clay soil and coarse expanded shale whereas Type 2 was a mix of sandy-clay soil with fine expanded shale. The control valve of the underdrain system was kept closed during the experiment without active underdrain and open in experiments with active underdrain. The TSS reductions in underflow and overflow were calculated for these test conditions, and the results are depicted in Figures 4.4 and 4.5. Also, the weighted average TSS reductions of each experiment were calculated, and the results are summarized in Table 4.4 and depicted in Figure 4.6.

In experiments without underdrain, Type 1 performed better than in reducing TSS in underflow in all conditions regardless of inflow rate and influent sediment concentration (Figure 4.4a.). Also, Type 1 had slightly better or equal performance than Type 2 in TSS reduction in overflow (except for one scenario: 120 Lit/min & 200 mg/L). Comparing weighted averaged TSS reduction in experiments without underdrain shows that both types had the same TSS removal percentage for 60 Lit/min and 120 Lit/min (66% and 42%) while Type 1 showed slightly better performance (36%) compared to Type 2 (32%) (Table 4.4, Figure 4.6). Type 1 contains coaster materials that promote drainage leading to higher TSS removal efficiency due to infiltration. Higher drainage also means, a lower overflow rate and lower flow velocity in the flume resulting in a higher reduction in TSS due to sedimentation.

Activating the underdrain system resulted in an overall higher TSS removal. Figure 4.5 shows the effect of the underdrain system on TSS removal efficiency over Type 1 and Type 2 soil media. Type 2 showed a higher TSS reduction in underflow in all scenarios, except for 60 Lit/min & 100 mg/L (Figure 4.5a). However, Type 1 had better performance in TSS removal from overflow during average and high inflow conditions. During low inflow (60 Lit/min), the overflow rate was zero and no comparison could be made (Figure 4.5b). Overall, in experiments with the active underdrain, the weighted average TSS removal by Type 1 was higher than Type 2 for low and average flows (78% vs. 74% and 51% vs. 43%) but it was slightly lower during high flows (46% vs. 47%) (Table 4.4).

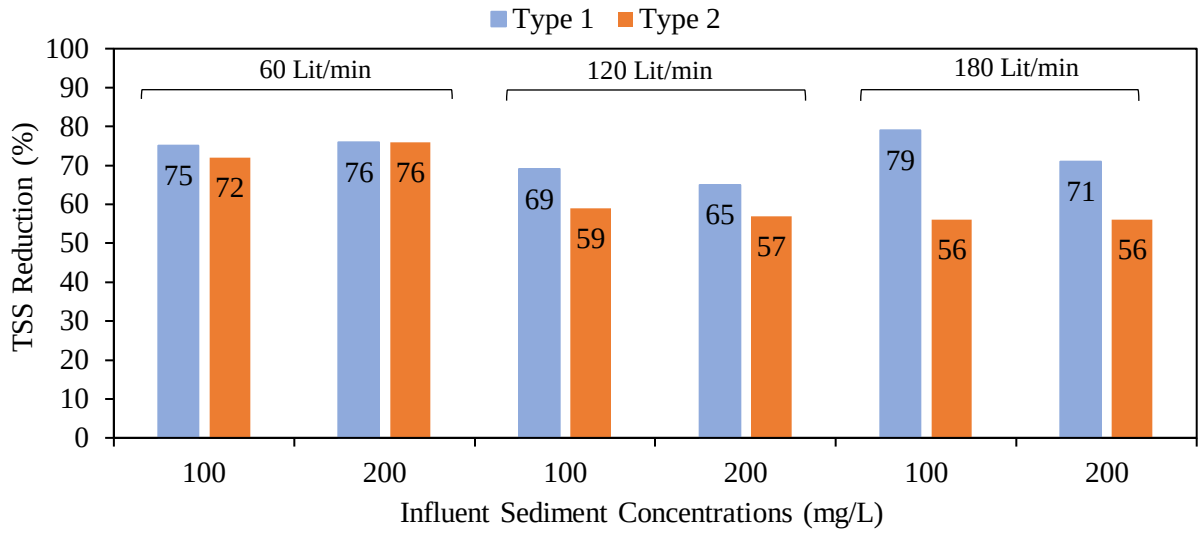

(a)

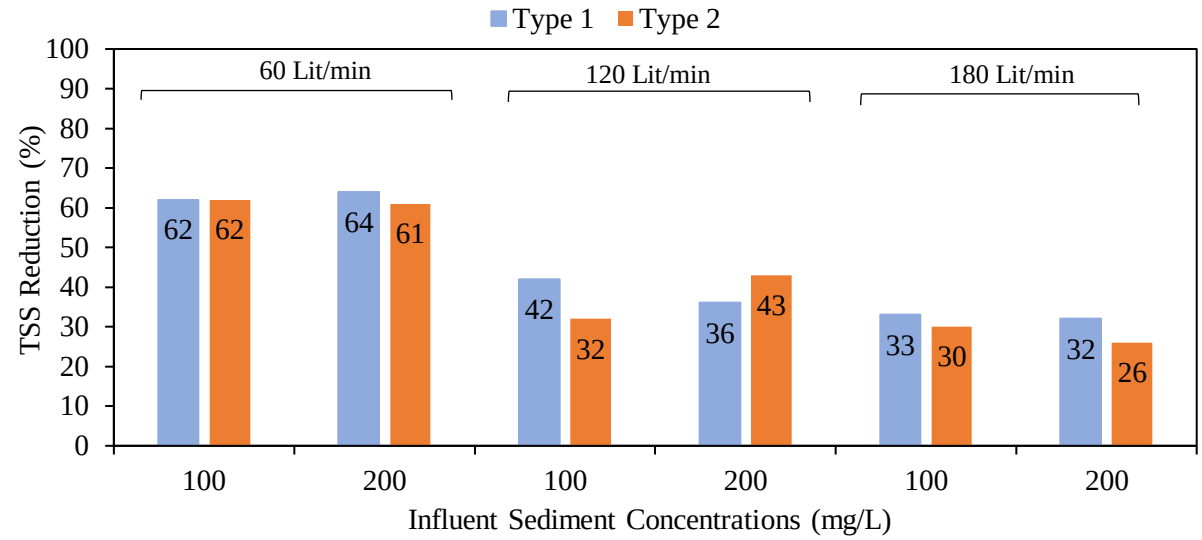

(b)

Figure 4.4*:* Effect of soil media type on TSS removal (a) Underflow, (b) Overflow (without underdrain system)

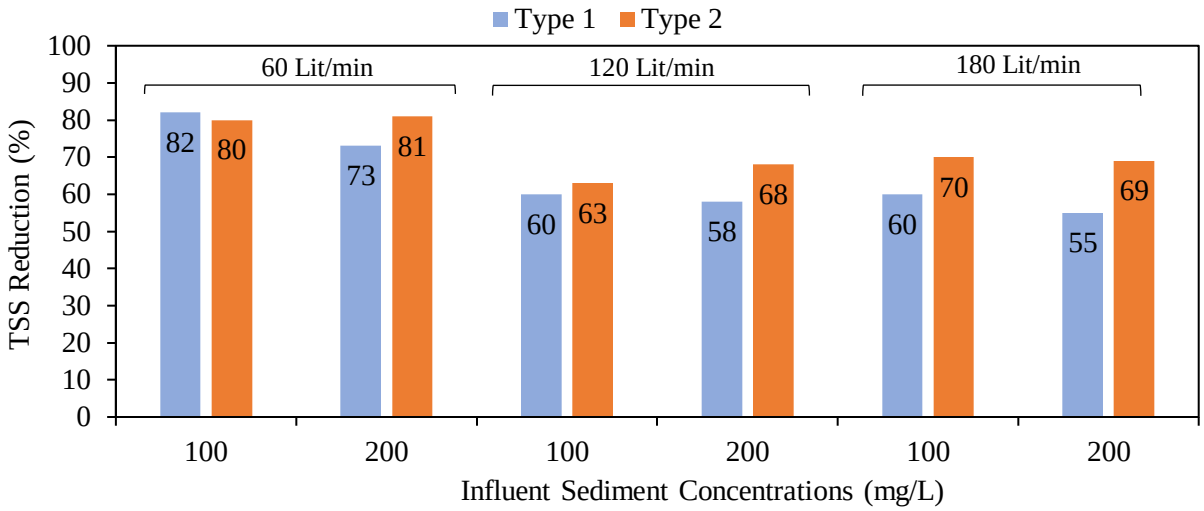

(a)

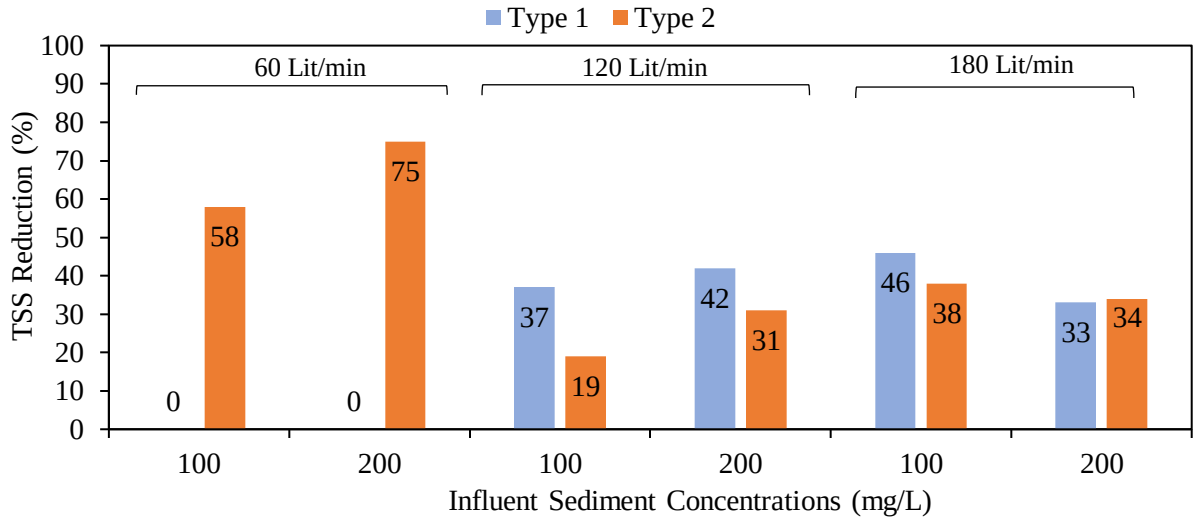

(b)

Figure 4.5: Effect of soil media type on TSS removal (a) Underflow, (b) Overflow (with underdrain system)

Table 4.4: Weighted average TSS removal for Types 1 and 2 media, with and without underdrain, and under different inflows

Media Type/ Drainage Condition	**Weighted Average TSS Removal (%)**		
	60 (Lit/min)	**120 (Lit/min)**	**180 (Lit/min)**
Type 1	72	47	41
Type 2	70	42	39
Without underdrain	66	42	34
With underdrain	76	47	47

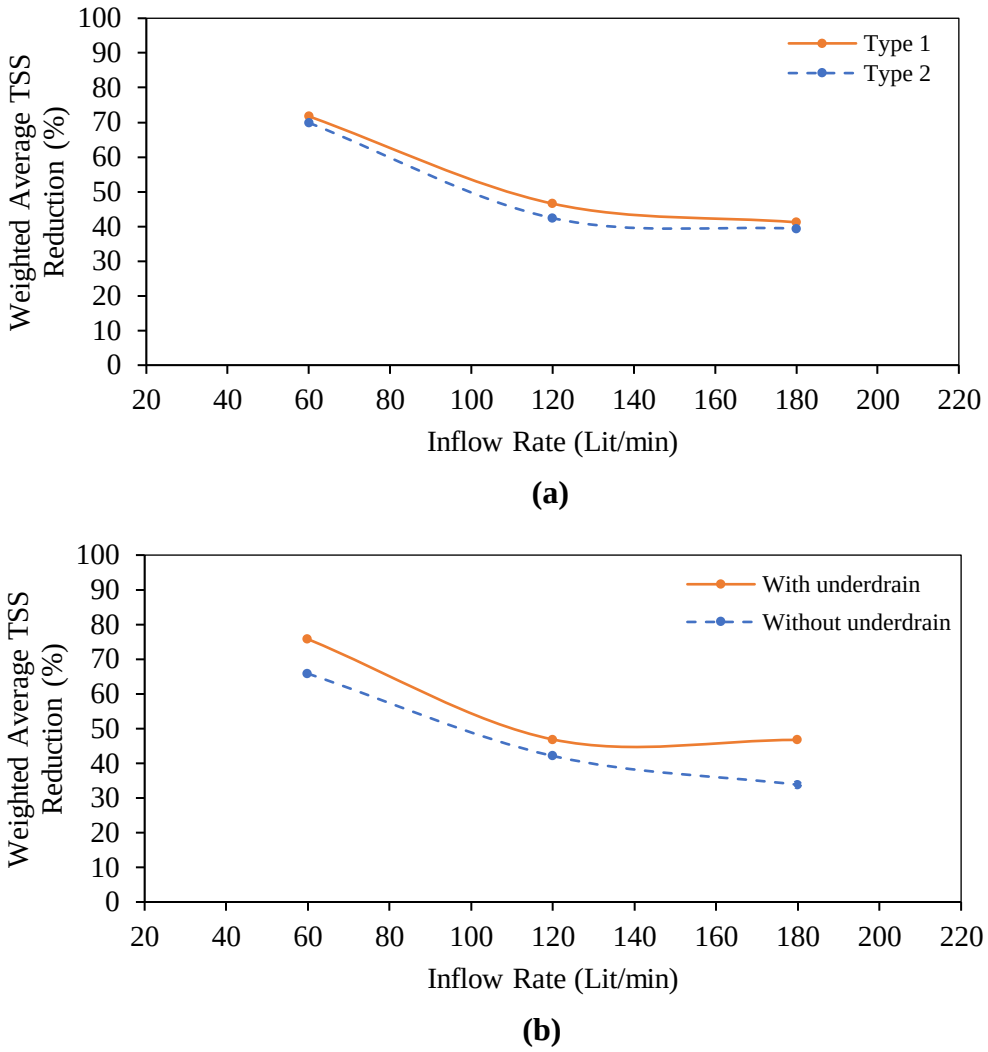

Figure 4.6: Weighted average TSS removal for (a) Types 1 and 2 soil media, (b) with and without underdrain system

4.2.2 Effect of Inflow Rate and Influent Sediment Concentration on TSS Removal

The results from experiments with the same conditions but varying inflow and influent sediment concentrations are compared in Figures 4.7 and Figure 4.8 for soil media Type 1 and Type 2. These figures clearly show that the TSS removal efficiency in underflow and overflow was always higher during low inflows, except for one case (Type 1 media without underdrain, inflow of 60 Lit/min, and influent concentration of 100 mg/L). During the lower inflows, a larger proportion of the water passed through the soil media resulting in more sediment being captured. This better performance during low inflows was more pronounced when the underdrain was active. In such scenarios, even more sediment was captured by the soil media due to infiltration and filtration processes.

The increase in influent concentration from 100 to 200 mg/L did not show any significant impact on the TSS removal efficiency, and no specific relationship between these two was found.

The weighted average TSS reductions of each experiment were calculated, and the results are summarized in Table 4.5 and shown in Figure 4.9. These results also confirm that the overall efficiency of the swale due to infiltration, filtration, and sedimentation processes was higher during low inflows, and the TSS removal efficiency did not change with the increase in incoming sediment load.

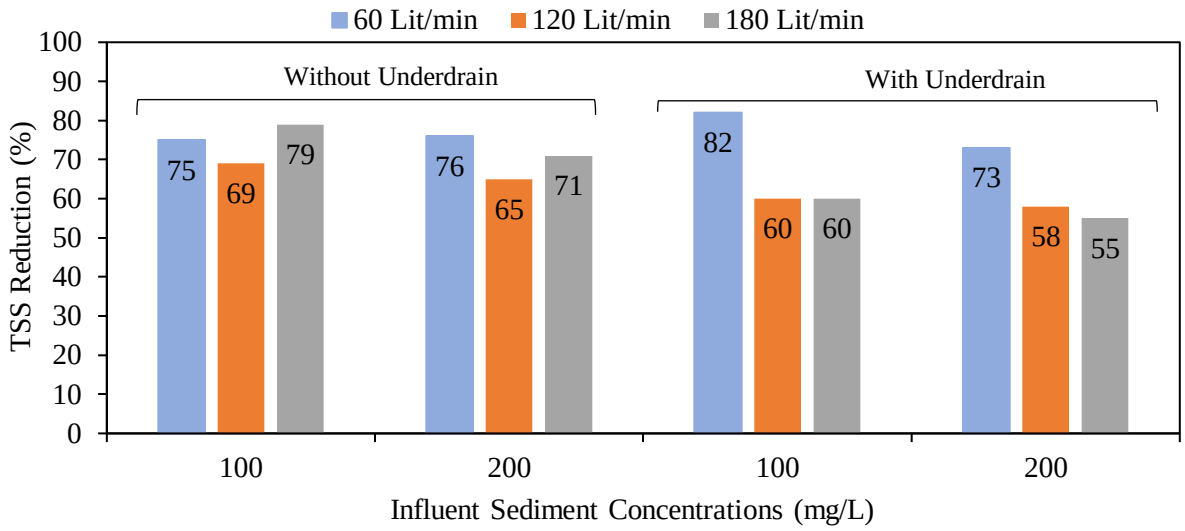

(a)

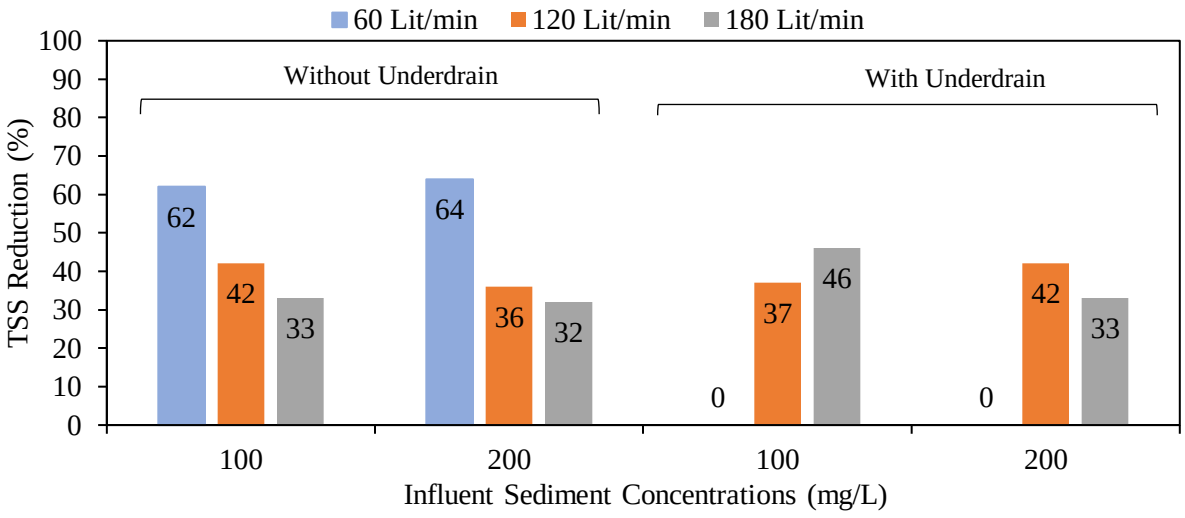

(b)

Figure 4.7*:* Effect of inflow on TSS removal of Type 1 soil media (a) Underflow, (b) Overflow

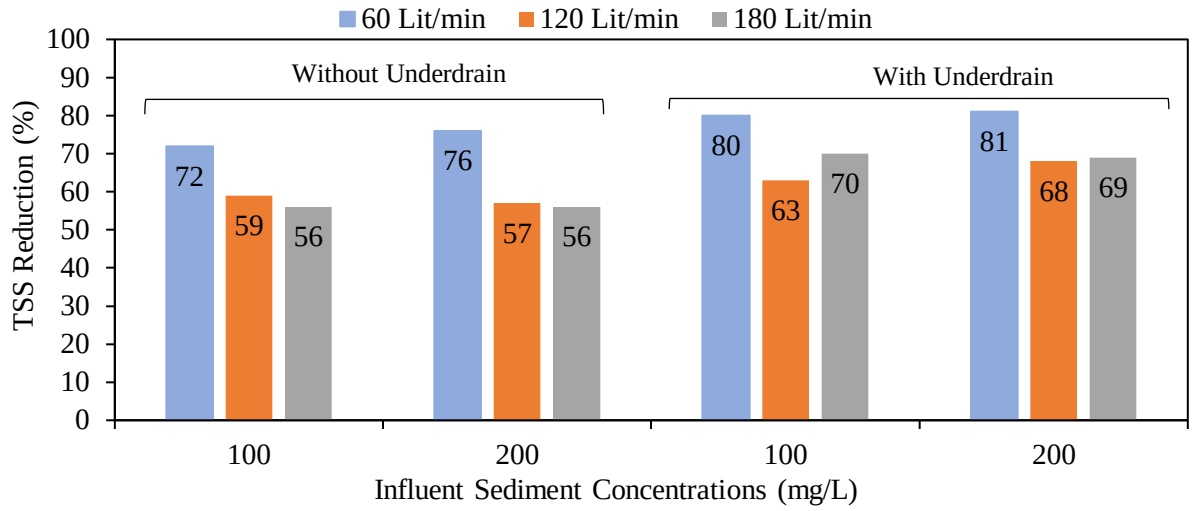

(a)

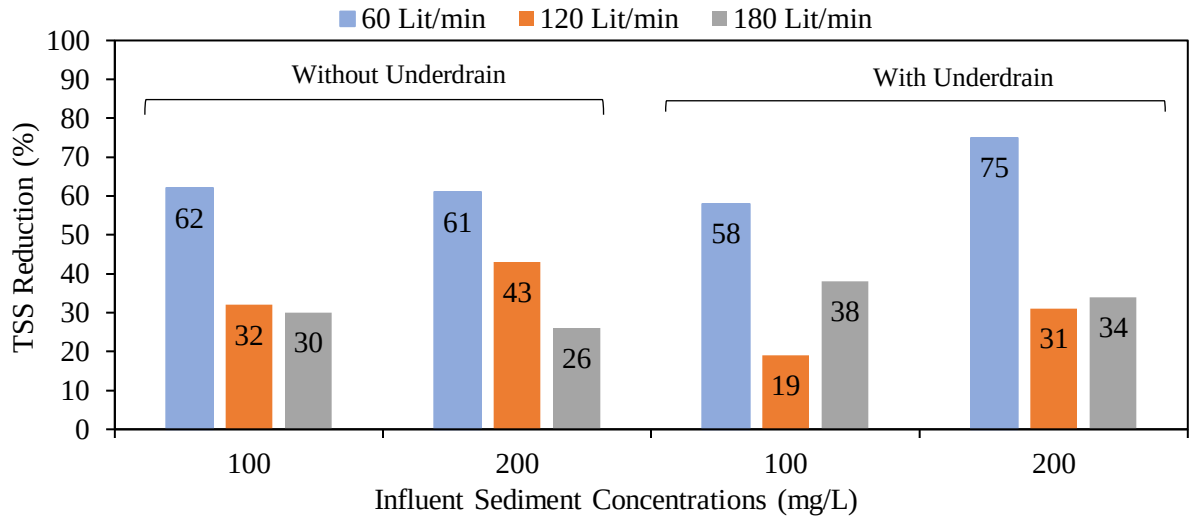

(b)

Figure 4.8*:* Effect of inflow on TSS removal of Type 2 soil media (a) Underflow, (b) Overflow

Table 4.5: Weighted average TSS removal for various inflows and sediment loading

Influent Sediment Concentration	**Weighted Average TSS Removal (%)**		
	60 (Lit/min)	**120 (Lit/min)**	**180 (Lit/min)**
100 mg/L	70	43	43
200 mg/L	71	46	38

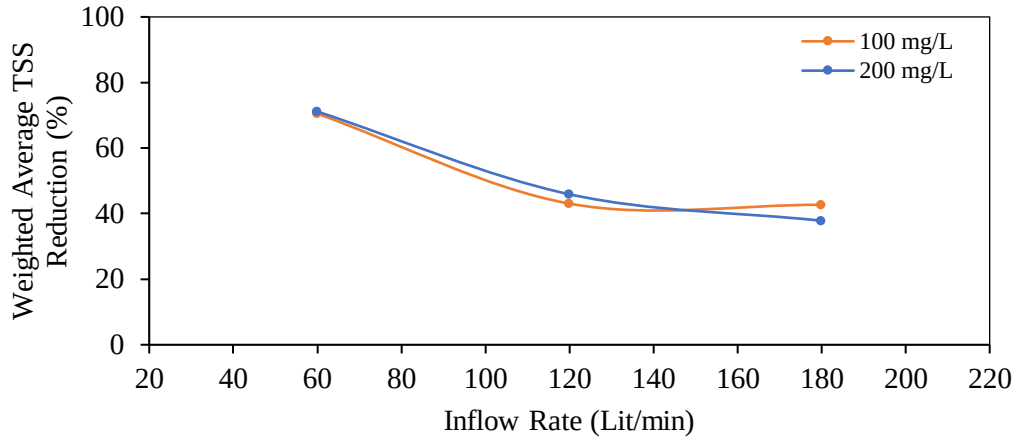

Figure 4.9*:* Weighted average TSS removal for various inflows and sediment loading

4.2.3 TSS Removal Efficiency at Sampling Locations

The overall TSS removal efficiency of the swale was calculated at each TSS sampling location. For this purpose, all scenarios were grouped based on the sampling location and irrespective of other conditions. The percentage of TSS removal in the middle section of the flume, overflow, and underflow were calculated by averaging the results of all experiments. The overall average and range of TSS removal at the sampling locations are summarized in Table 4.6.

These results show that on average, 42% of suspended sediment reduction occurred within the upstream half length of the flume, 43% in the water overflowing the downstream weir, and 68% in the water flowing through the soil media and underdrain system (underflow). The range of TSS removal at these locations was 20-75%, 19-75%, and 55-82%, respectively. These results show that the TSS decreased at a higher rate along the first half-length of the flume and at a much smaller rate in the second half. However, the rate at which TSS dropped varied with the inflow rate. The reduction in TSS concentration for three different inflows is shown in Figure 4.10. The rate of drop in TSS was much faster in the low inflow (60 Lit/min) than in the high inflow (180 Lit/min). The higher the inflow, the higher the flow velocity in the flume which means that the sediment would travel longer along the flume before it settles out.

Table 4.6: Overall mean and range of TSS removal efficiency at sampling locations

Location	Average TSS Removal Efficiency (%)	Range of TSS Removal Efficiency (%)
Middle section	42	20 - 75
Overflow	43	19 - 75
Underflow	68	55 - 82
Mean*	52	30 - 82

*** Including all the experiments*

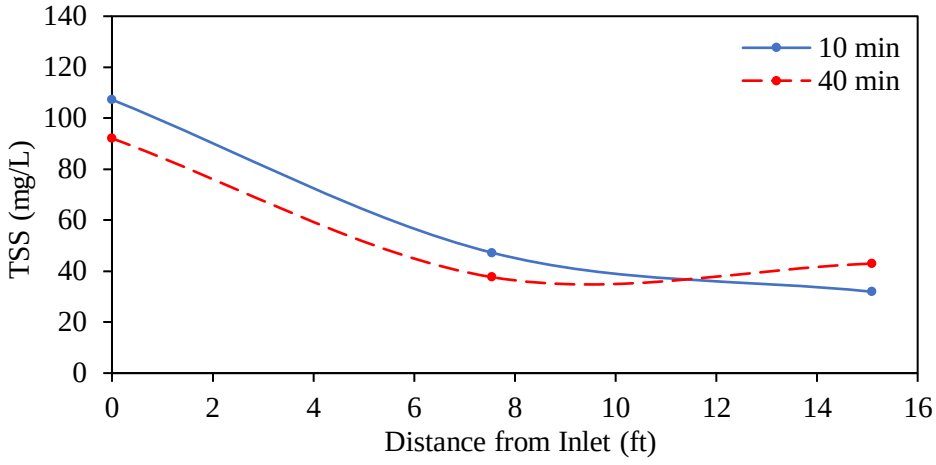

(a)

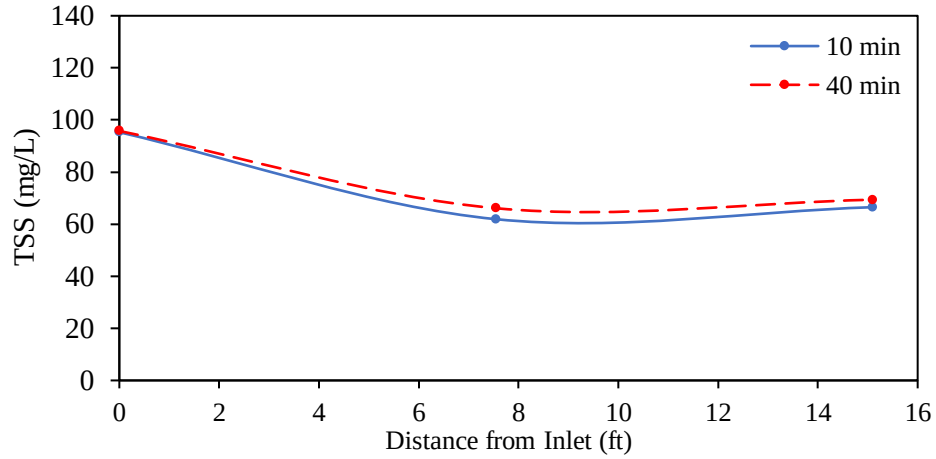

(b)

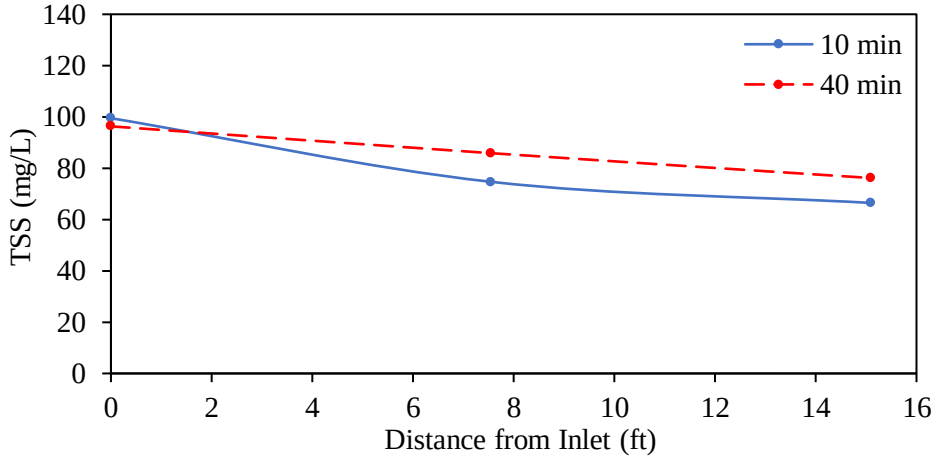

(c)

Figure 4.10*:* Reduction in TSS concentration along the flume in experiments with Type 2 soil media, without underdrain, influent concentration of 100 mg/L, and inflow of (a) 60 Lit/min, (b) 120 L/min, and (c) 180 Lit/min (solid lines and dash lines represent the results for samples taken 10 and 40 min after the experiments started)

4.2.4 Turbidity Removal

The efficiency of the swale in removing turbidity (Tu) at different locations in the flume under different soil media types, drainage conditions, inflows, and influent sediment concentrations are assessed, and the results are discussed in the following sections.

4.2.4.1 Effect of Soil Media Type and Drainage Condition on Tu Removal Efficiency

The Tu reductions in underflow and overflow were measured for soil media Type 1 and 2, with and without the underdrain system, and the results are depicted in Figures 4.11 and 4.12. Also, the weighted average Tu reduction of each experiment was calculated, and the results are summarized in Table 4.7 and depicted in Figure 4.13.

In experiments without the underdrain, Type 1 performed better than in reducing Tu in underflow and overflow during low and high inflow rates regardless of influent sediment concentration but Type 2 performed better in average inflow (i.e., 120 Lit/min) (Figure 4.11a,b). During the average inflow the Tu in the overflow was higher than in the inlet resulting in a negative Tu reduction percentage. Also, in some experiments, an increase in Tu was observed from the middle section of the flume to the overflow. Such variation in Tu could be due to the resuspension of the settled-out sediments or the change in the composition of suspended sediment that became finer along the flow. This phenomenon is further discussed in Section 4.2.3.

Activating the underdrain system for both soil media types resulted in an overall higher Tu removal. Figure 4.12 shows the effect of the underdrain system on Tu removal efficiency in Type 1 and Type 2 soil media. Type 2 showed higher Tu reduction in underflow in all scenarios, except for 60 Lit/min & 100 mg/L (Figure 4.12a). However, Type 1 had better performance in Tu removal from the overflow during low inflow conditions (Figure 4.12b).

Comparing the weighted average Tu reduction in all experiments shows that both soil media types had the same Tu removal percentage regardless of the inflow condition. Also, in experiments with active underdrain, the weighted average Tu removal was higher than that in the experiments without the underdrain, regardless of the inflow conditions (Table 4.7 and Figure 4.13).

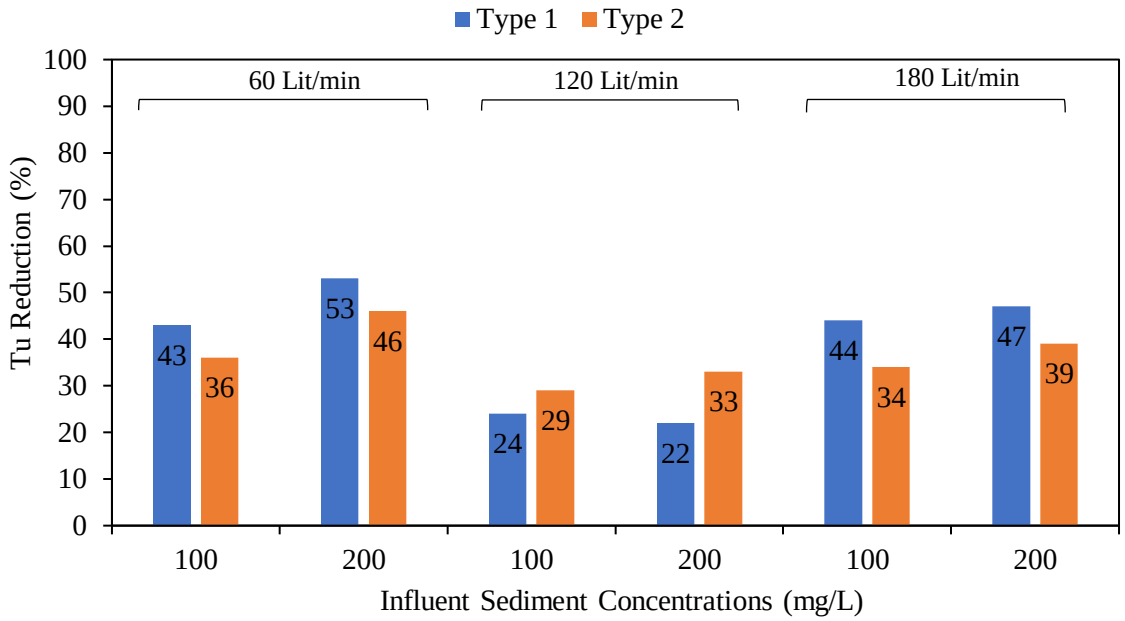

(a)

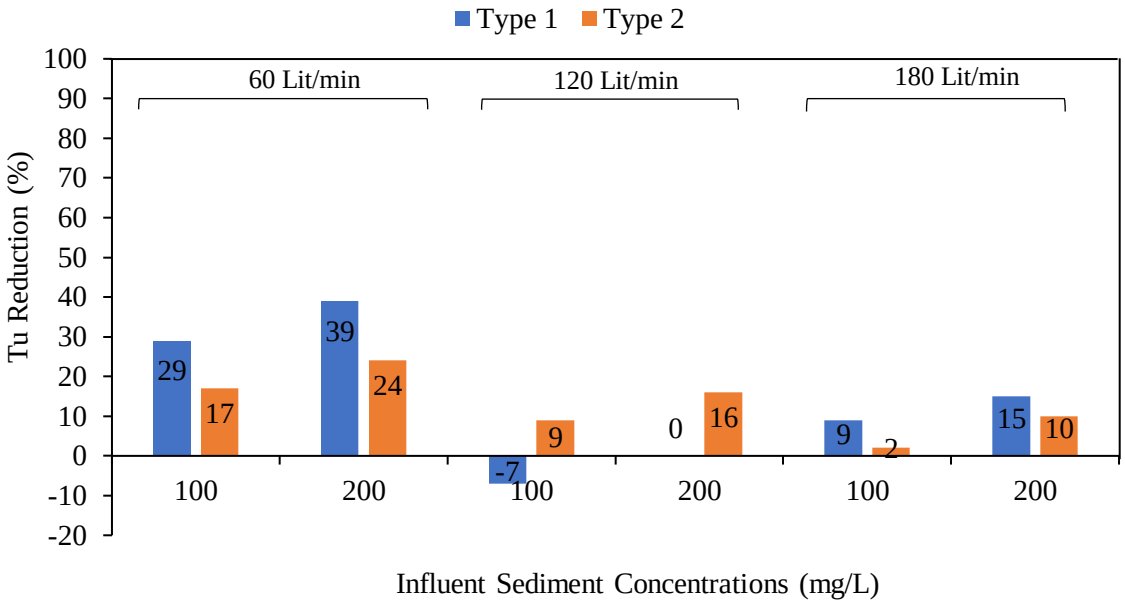

(b)

Figure 4.11*:* Effect of soil media type on Tu removal: (a) Underflow, (b) Overflow (without underdrain system)

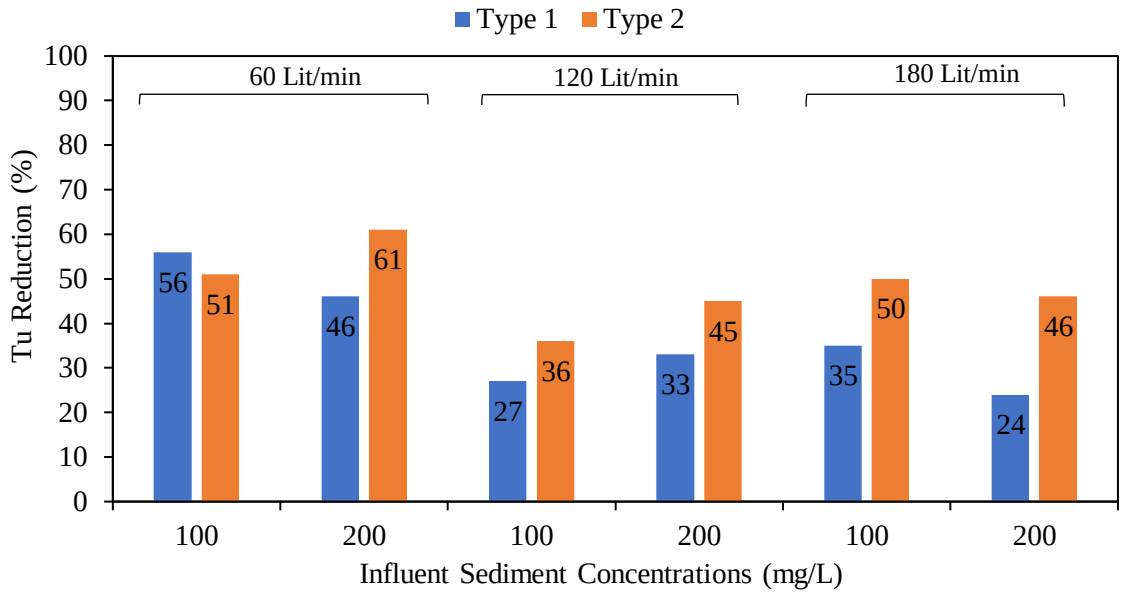

(a)

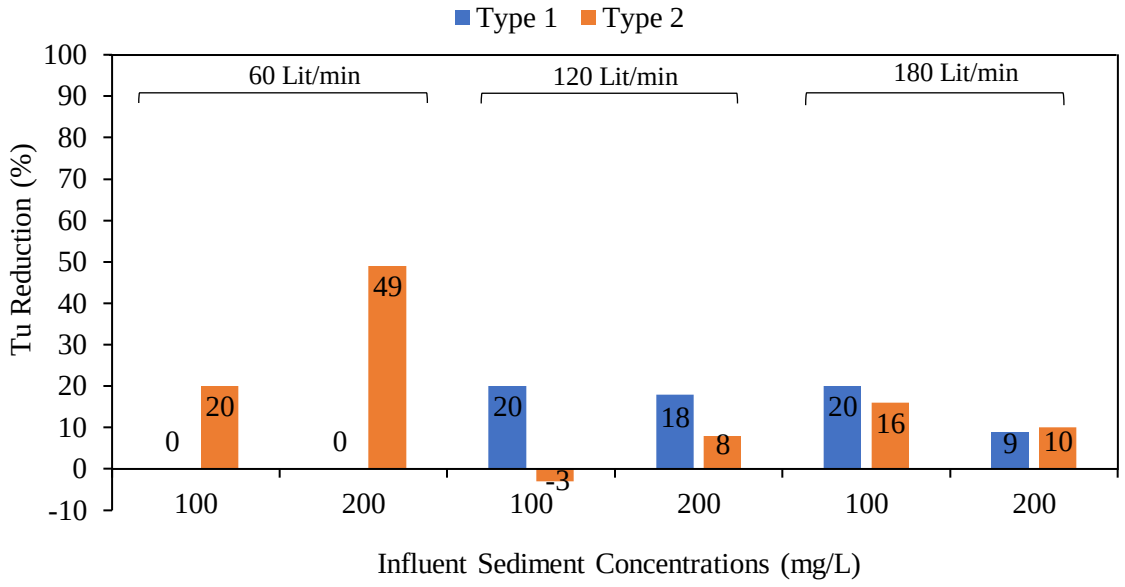

(b)

Figure 4.12*:* Effect of soil media type on Tu removal: (a) Underflow, (b) Overflow (with underdrain system)

Table 4.7: Weighted average Tu removal for Types 1 and 2 soil media, and with and without underdrain system

Media Type/ Drainage Condition	Weighted Average Tu Removal (%)		
	60 (Lit/min)	120 (Lit/min)	180 (Lit/min)
Type 1	37	18	18
Type 2	37	17	17
Without underdrain	32	12	12
With underdrain	46	22	22

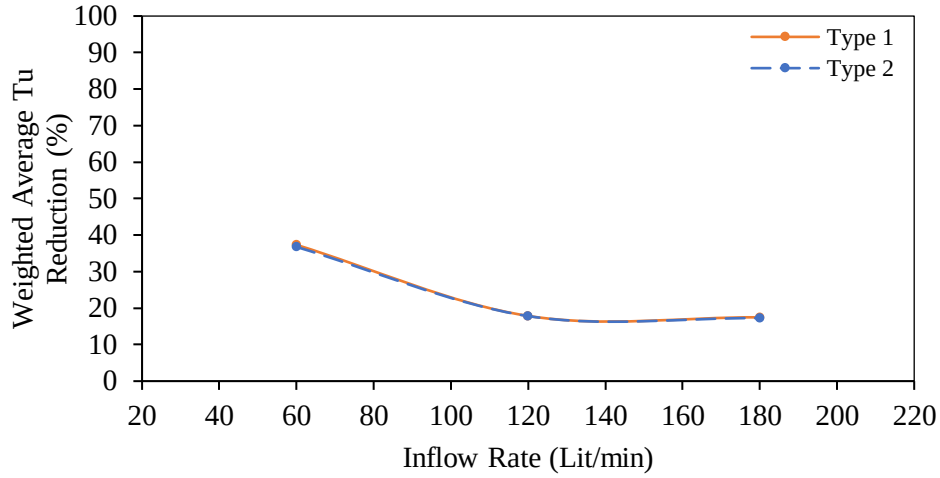

(a)

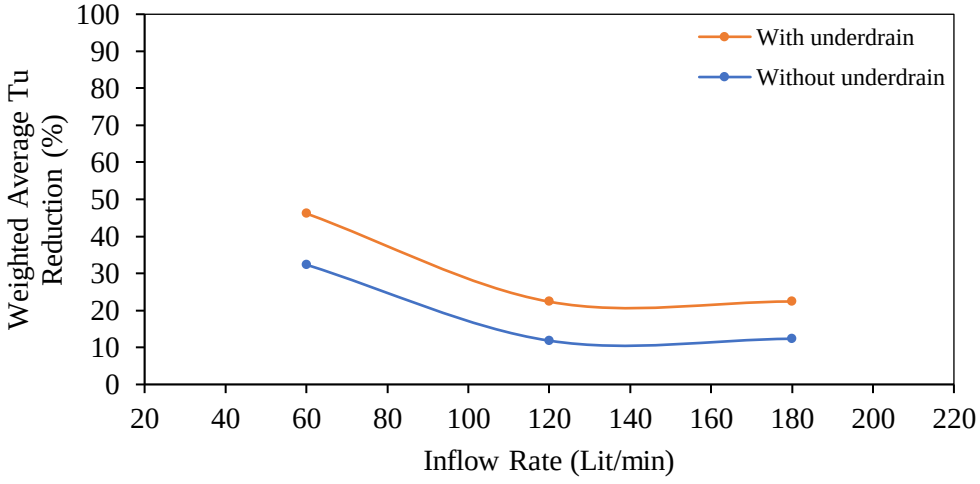

(b)

Figure 4.13*:* Weighted average Tu removal for (a) Types 1 and 2 soil media, (b) with and without underdrain system

4.2.4.2 Effect of Inflow Rate and Influent Sediment Concentration on Tu Removal

The effects of inflow rate and influent sediment concentration of reducing Tu by the swale were assessed and the results are presented in Figure 4.14 and Figure 4.15 for soil media Type 1 and Type 2, respectively. These figures clearly show that the Tu removal efficiency in the underflow and overflow was always higher during low flows. During the low inflows, a larger proportion of the water passed through the soil media and more sediment was captured resulting in lower turbidity in both overflow and underflow. This better performance during low flows was more pronounced when the underdrain was active.

The increase in influent concentration from 100 to 200 mg/L did not show any significant impact on Tu removal efficiency or any specific relationship with influent concentration.

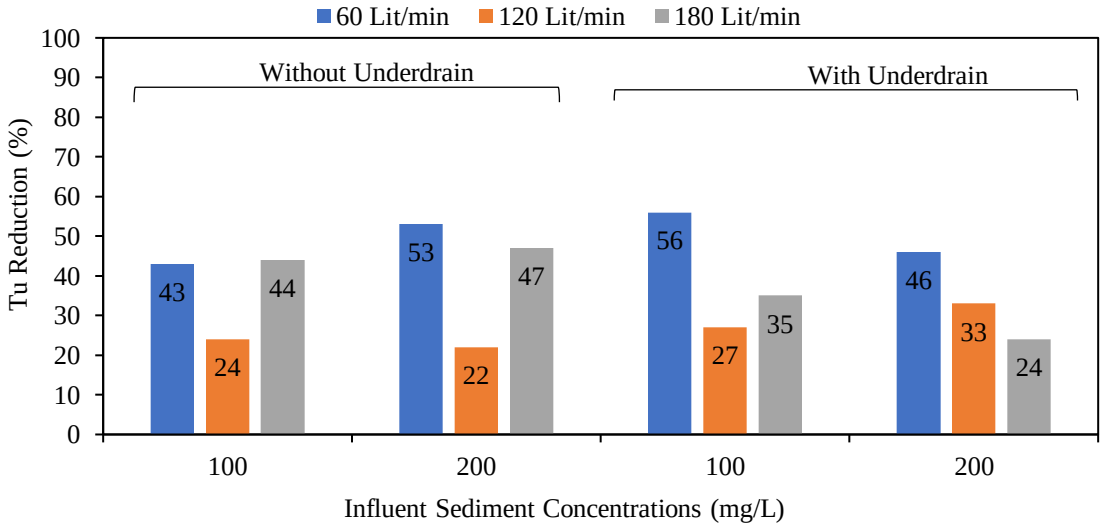

(a)

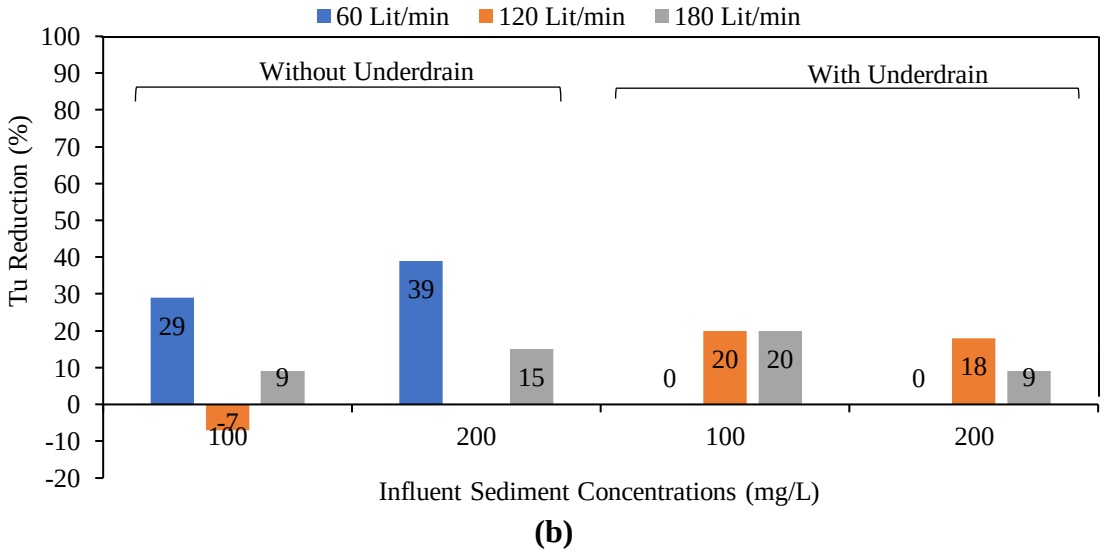

(b)

Figure 4.14*:* Effect of inflow on Tu removal of Type 1 soil media: (a) Underflow, (b) Overflow

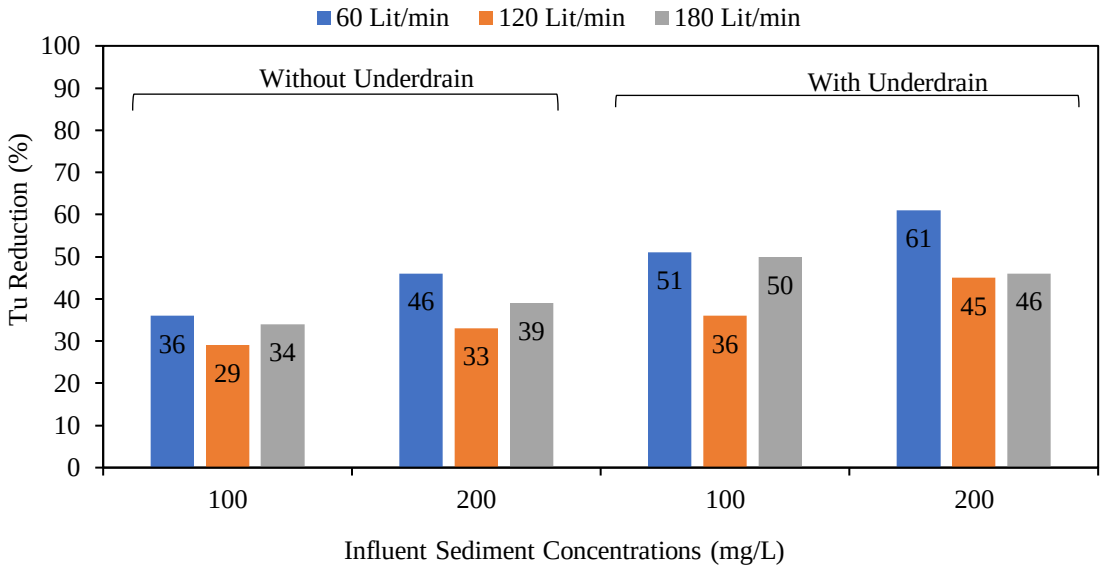

(a)

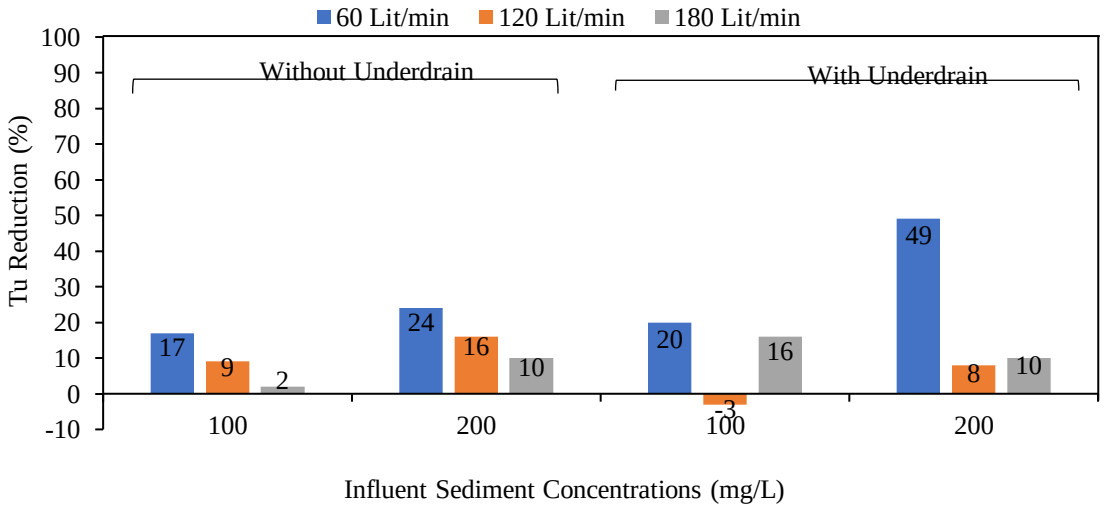

(b)

Figure 4.15*:* Effect of inflow on Tu removal of Type 2 soil media: (a) Underflow, (b) Overflow

The weighted average Tu reductions of each experiment were also calculated, and the results are summarized in Table 4.8 and shown in Figure 4.16. These results also confirm that the overall efficiency of the swale due to infiltration, filtration, and sedimentation was higher during low inflows, and the Tu removal efficiency was higher in low inflows (60 Lit/min) and high influent concentration (200 mg/L).

Table 4.8: Weighted average Tu removal for various inflows and sediment loading

Influent Sediment Concentration	Weighted Average Tu Removal (%)		
	60 (Lit/min)	120 (Lit/min)	180 (Lit/min)
100 mg/L	31	17	18
200 mg/L	43	18	17

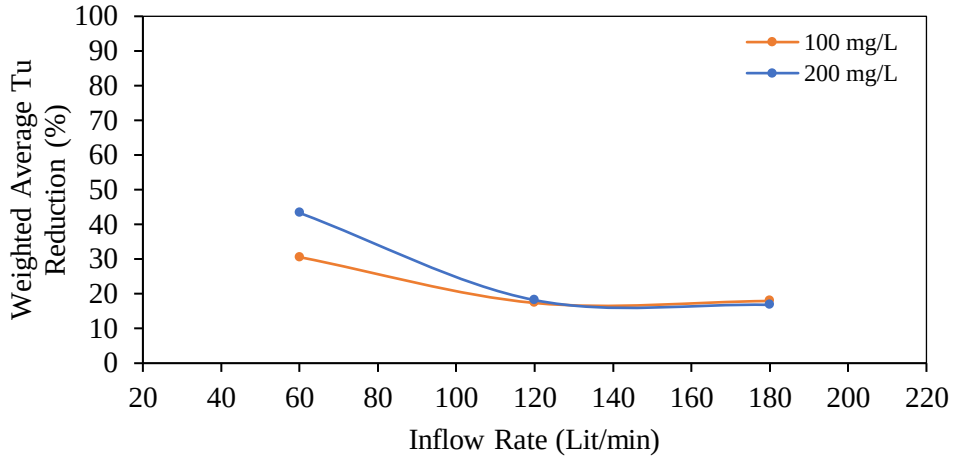

Figure 4.16*:* Weighted average Tu removal for various inflows and sediment loading

4.2.4.3 Tu Removal Efficiency at Sampling Locations

The Tu removal efficiency of the swale was determined at each sampling location. For this purpose, all scenarios were grouped based on the sampling location and irrespective of other conditions. The percentage of Tu removal in the middle section of the flume, overflow, and underflow were calculated by averaging the results of all experiments. The overall average and range of Tu removal at the sampling locations are summarized in Table 4.9. An average reduction in turbidity of 18 % was obtained within the half length of the flume with a range of (–4%) to 43% varying within different experiments. The water infiltrating through soil media (underflow) had an average reduction of 40% while its range was 22% to 61%. The water that overflowed through the downstream weir had 17% turbidity removal, with a range of (–7%) to 49%. In all cases, the turbidity showed a mean weighted average reduction of 24% irrespective of test conditions. The negative weighted average reduction means that the Tu in the overflow was higher than in the inlet area.

As an example, Figure 4.17 displays the reduction in turbidity for three different inflows. The turbidity exhibited a general decreasing trend in the first half of the flume's length for all three inflow cases; however, the results for the second half were inconclusive. A reduction in Tu was observed in the second half of the flow 10 minutes after the experiments started, but it increased when the experiments concluded at t = 40 minutes.

Table 4.9: Overall mean and range of Tu removal efficiency at sampling locations

Location	Average Tu Removal Efficiency (%)	Range of Tu Removal Efficiency (%)
Middle section	18	(–4) - 43
Overflow	17	(–7) - 49
Underflow	40	22 - 61
Mean*	24	(–4) - 56

** Including all the experiments*

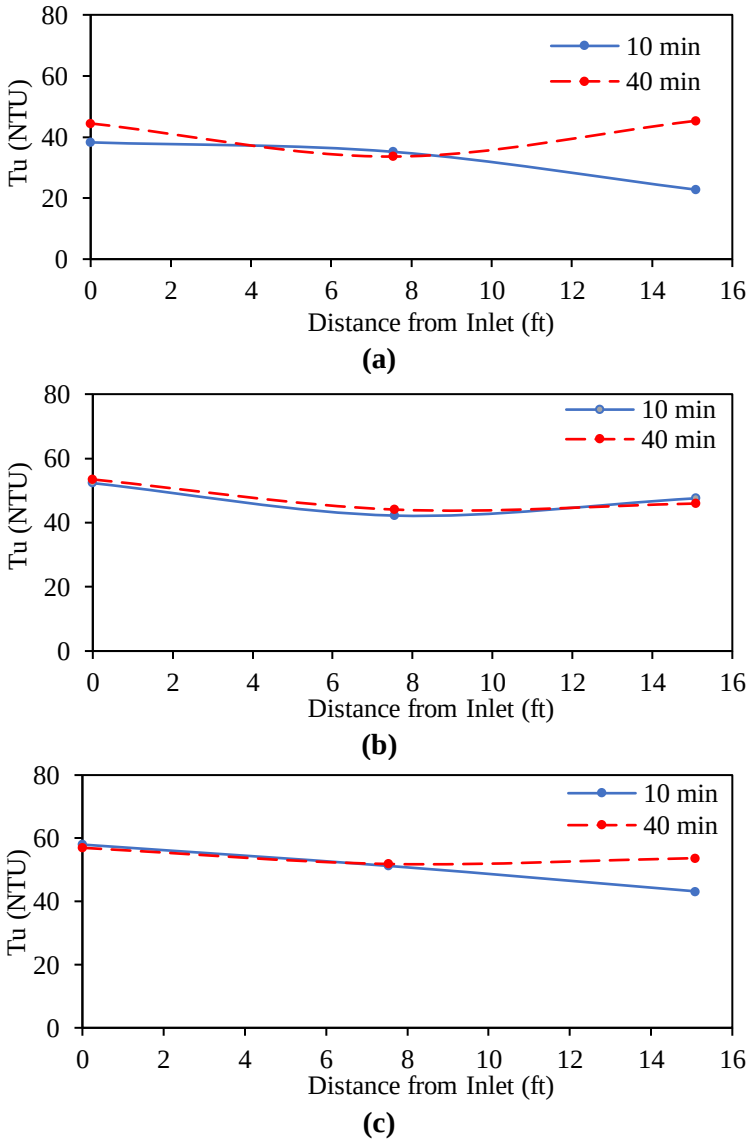

Figure 4.17*:* Reduction in Tu along the flume in experiments with Type 2 soil media without underdrain, influent sediment concentration of 100 mg/L, and inflow rate of (a) 60 Lit/min, (b) 120 L/min, and (c) 180 Lit/min (solid lines and dash lines represent the results for samples taken 10 and 40 min after the experiments started)

4.2.5 Change in Sediment Particle Gradation

Water samples from five experiments were selected to assess the changes in suspended sediment composition by performing particle size gradation tests. The experiments that were considered for the suspended sediment particle size gradation are tabulated in Table 4.10.

Table 4.10: Experiments selected for suspended sediment gradation size tests (6-inch soil media with underdrain)

Soil Media	Inflow (Lit/min)	Influent Sediment Concentration (mg/L)
Type 1	60	100
	180	200
Type 2	60	200
	180	100
	180	200

4.2.5.1 Change in Suspended Sediment Gradation Over Time

The pattern of change in suspended sediment gradation was analyzed for sampling locations with respect to the time of sampling during each experiment. Samples were collected after 10, 20, 30, and 40 min after the experiment was started. Samples collected from the inlet, middle section, overflow, and underflow were analyzed to determine the change in sediment gradation with time. The gradation curves for experiments, conducted with Type 2 soil media (with underdrain), inflow rate of 180 Lit/min, and two different incoming suspended sediment loads, i.e., 100 and 200 mg/L, are shown in Figures 4.18 and 4.19. The gradation curves are prepared for samples collected from the flume's inlet area, middle section, underflow, and overflow. Figures 4.18a and 4.19a show that the sediment injected into the flume had a small variation in size for both low and high sediment loading. Also, except for minor changes in the gradation of suspended sediment in samples taken from the middle section of the flume, all sediment gradation curves at other sampling locations were similar throughout the experiments. This observation suggests that the flow and sediment regime were in equilibrium conditions, and the soil media did not become clogged during the experiments. If there was any change in the performance of the swale, the sediment gradation would have changed with time during the experiments. Nonetheless, the results presented in Figures 4.18 and 4.19 suggest that the sediment load became finer in composition along the flume. The suspended sediment at the inlet had ~10% particles smaller than 1 micron but ~13% in the middle section of the flume and ~20% in the underflow. The sediments in overflow were slightly coarser than in the middle section of the flume. This phenomenon is discussed in detail in the following section.

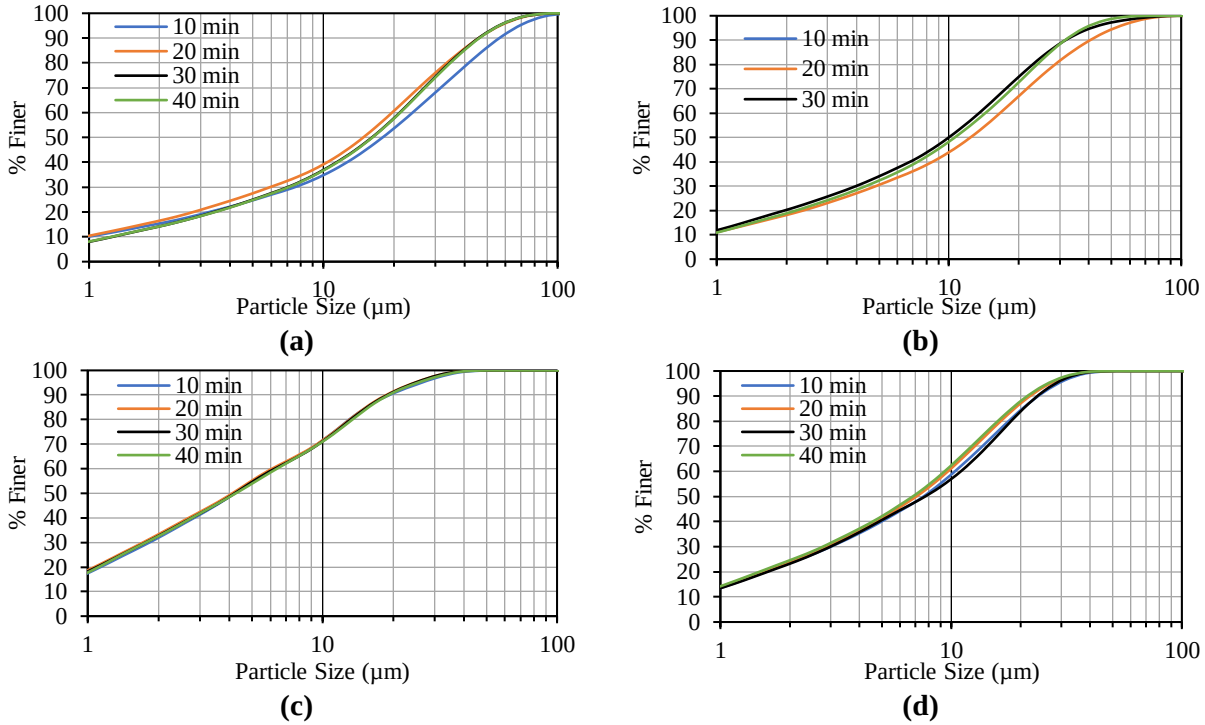

Figure 4.18: Changes in suspended sediment gradation with time at (a) Inlet, (b) Middle section, (c) Underflow, and (c) Overflow (Type 2 media, inflow rate 180 Lit/min, influent sediment concentration 100 mg/L)

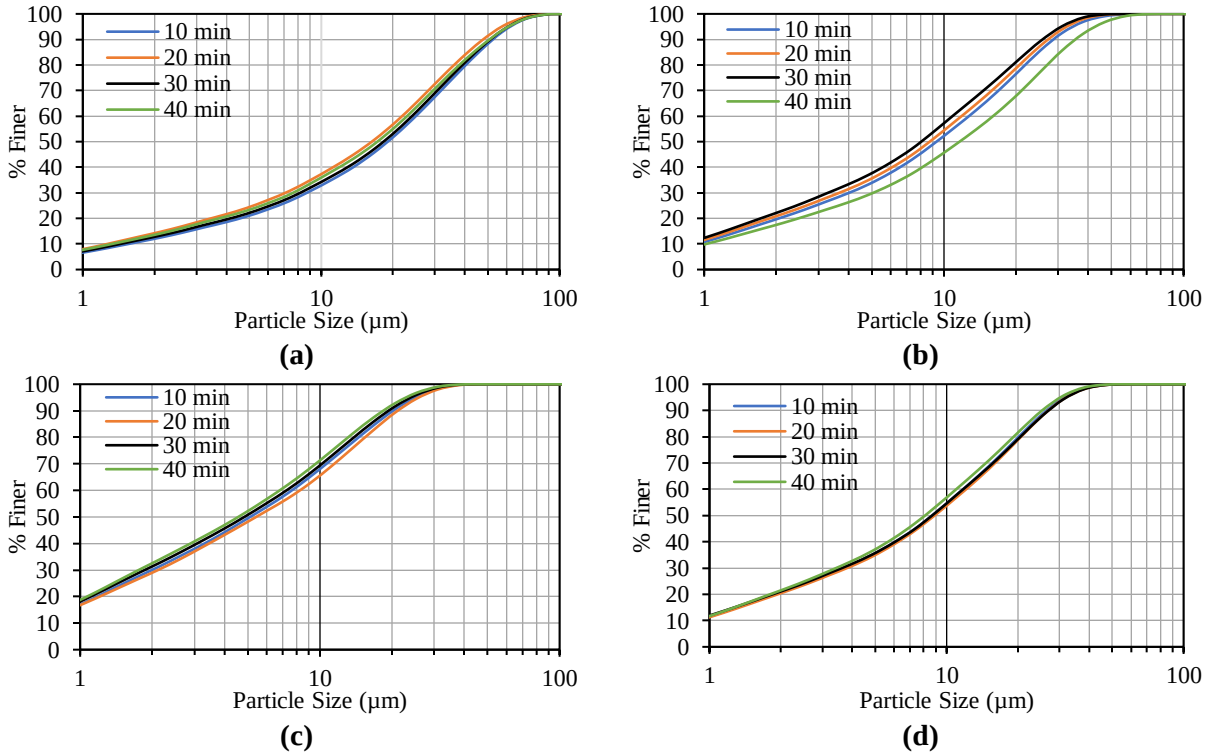

Figure 4.19: Change in suspended sediment gradation with time at (a) Inlet, (b) Middle section, (c) Underflow, and (d) Overflow (Type 2 media, inflow rate 180 Lit/min, influent sediment concentration 200 mg/L)

4.2.5.2 Effects of Soil Media Type on Suspended Sediment Gradation

The gradation test results were compared based on two types of soil media. The results are illustrated in Figure 4.20. In this figure, the average of two experiments with Type 1 and three experiments with Type 2 (as listed in Table 4.10) are presented irrespective of the inflow rate and sediment concentration. The results show that the type of soil media did not have any effects on sediment size in the underflow. In both media types, the mean particle size (d_{50}) in the inflow changed from ~15-17 µm to ~4.5 µm. It can be concluded that both types are capable of removing all sediment classes coarser than clay size, i.e., ~4 µm.

In Type 2, the suspended sediment in the middle section was coarser than in the overflow (d_{50} of ~6.5 µm in the middle section vs. ~5 µm in the overflow). This pattern of sediment becoming finer in the flow direction was intuitively expected. However, in Type 1 experiments, the suspended sediment in the middle section was finer than in the overflow (~6 µm in the middle section compared to ~8 µm in the overflow). This atypical pattern prompts a need for additional investigation. Since the gradation curves in Figure 4.20 were developed by averaging results from low and high inflows, it was speculated that the inflow rate may have skewed the results.

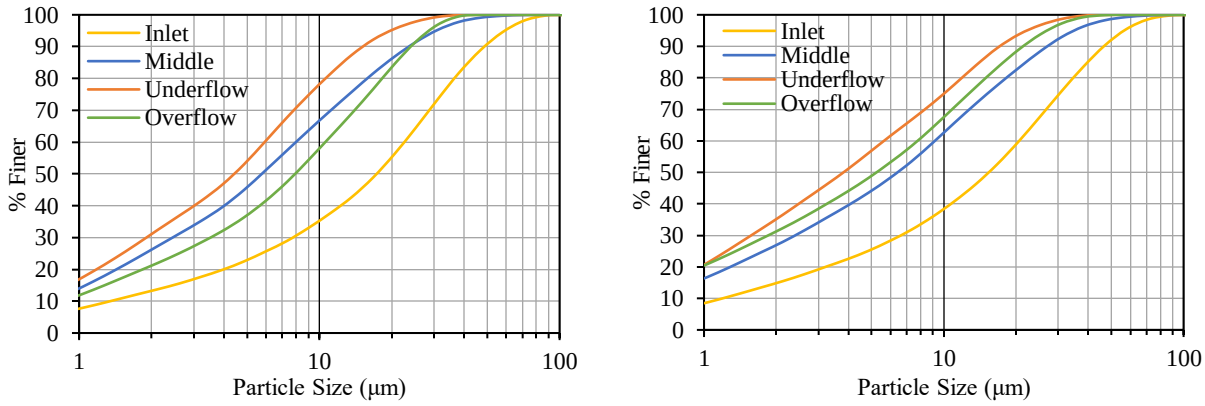

Figure 4.20: Change in suspended sediment gradation with soil media type: (a) Type 1, (b) Type 2

4.2.5.3 Effects of Inflow Rate on Suspended Sediment Gradation

The gradation curves for experiments with low inflow (60 Lit/min) and high inflow (180 Lit/min) are prepared and presented in Figure 4.21. As shown, the change in sediment composition along the flow is very different in these two inflow conditions.

A significant change in particle size was observed during low inflow conditions such that the d_{50} decreased from ~15 µm (at the inlet) to ~3-4 µm within the half length of the flume (Figures 4.21a and b). Apart from this, the particle size of the underflow and the middle section were similar. However, the d_{50} in the overflow was finer (2 µm) than the particles in the underflow/middle

section(3-4 μm), possibly due to lower flow velocity and higher hydraulic residence time in the low inflow experiments. For these reasons, the flow had enough time to drop off coarser particles.

During the high inflow experiments, particles in the underflow had the smallest d_{50} than any other sampling locations (Figures 4.21c, and d). Also, sediments in the overflow were finer than in the middle section. The d_{50} was 15-17 μm at the inlet and reduced to 9-11 μm in the middle section of the flume. The overflow had a slightly smaller d_{50} of 7-8.5 μm compared to the middle section. The underflow had the smallest sediment size with d_{50} = 4-5 μm than at any other locations. This result shows that flow did not have enough time to settle out the coarser particles during high inflows due to higher flow velocity in the flume and shorter hydraulic residence time. Unlike during the low inflow experiments, in which particles in the overflow were finer than in the middle section, high inflow conditions resulted in coarser particles in overflow. Also, no drastic change in particle size was observed during high inflow experiments as observed during low inflows.

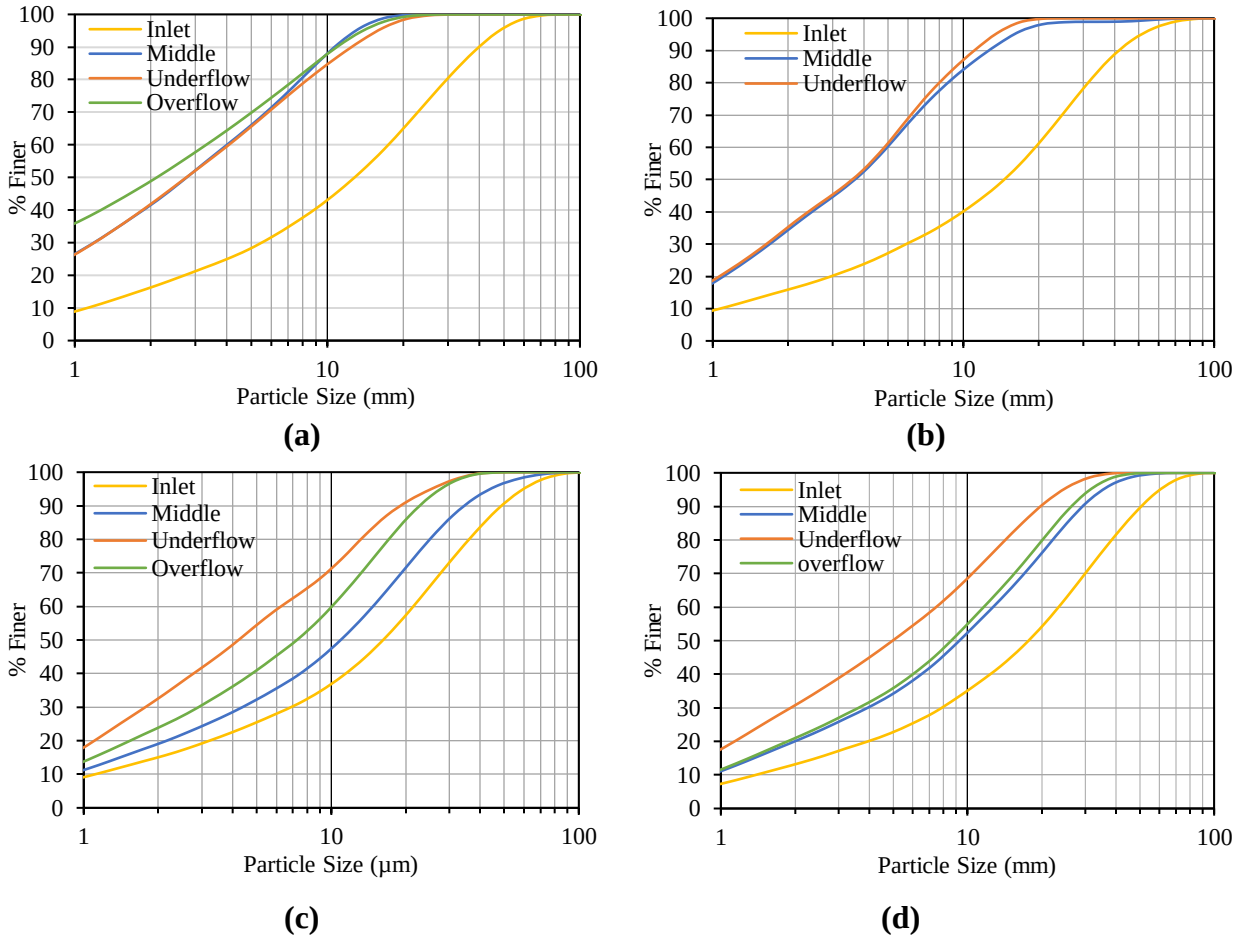

Figure 4.21: Change in suspended sediment gradation with inflow rate (a) 60 Lit/min, 200 mg/L, and (b) 60 Lit/min, 100 mg/L (note: since there was no overflow in this experiment, the gradation curve is not prepared), (c) 180 Lit/min, 100 mg/L, and (d) 180 Lit/min, 200 mg/L

4.3 Chemical Experiments

4.3.1 Removal Efficiency Based on Hydraulic Residence Time

In experiments 1 to 6, the efficiency of chemical removal was evaluated under various conditions. These experiments were run for a period equal to the calculated hydraulic residence time (*HRT*) to study the efficiency of chemical removal in situations that do not have continuous influx of pollutants. The initial results showed that the percentage reduction in chemicals was not significant in the in the overflow samples, and even in some cases an increase was observed in the chemical concentrations. Apparently, the *HRT* of the experiments was not long enough to allow the absorption of the chemicals moving along the surface of the soil media. On the contrary, the chemical reduction in the underflow (flow passing through the soil media) was considerable. Therefore, in the following sections, the effectiveness of the soil media in removing nitrogen, phosphorus, and zinc in the underflow samples are presented.

Total nitrogen, phosphorus, and zinc removal efficiencies are shown in Figures 4.22a to c. Overall, the experiments with underdrain show better removal efficiencies compared to those without underdrain. However, at 60 L/min, both nitrogen and zinc removal efficiencies were slightly better in tests without underdrain compared to those with underdrain.

Nitrogen removal exhibits a decreasing trend for experiments without underdrain as the inflow rate increases, while it remains relatively constant in experiments with the underdrain (Figure 4.22a).

For phosphorus, the removal efficiency in experiments without underdrain significantly decreased at the inflow rate of 120 Lit/min compared to 60 Lit/min and 180 Lit/min. However, it remained constant for all three inflow rates in tests with underdrain (Figure 4.22b).

Similarly, for zinc, the efficiency shows a similar behavior to phosphorus in tests without underdrain. The removal efficiency was nearly the same for 120 Lit/min and 180 Lit/min with underdrain (almost 50%), whereas at 60 Lit/min, it reached to only 24% removal efficiency (Figure 4.22c).

The results show an intriguing relationship between flow rate and chemical removal efficiency. In the presence of the underdrain system, 120 Lit/min and 180 Lit/min inflows exhibit similar efficiency in removing phosphorus and zinc. However, all three inflows were equally effective in removing nitrate. In contrast, in the absence of the underdrain system, nitrogen removal efficiency decreased as the inflow rate increased. However, the 120 Lit/min inflow rate did not significantly affect the soil media's ability to remove zinc and phosphorus. In fact, the concentration of zinc and phosphorus in the underflow was higher than in the inlet (negative removal efficiencies in Figures 4.22b and c). One possible explanation for this peculiar phenomenon is the flow circulation and backwater effect caused by the presence of the check dam, which may lead to an increase in chemical concentration in the middle of the flume. Nevertheless, this speculation requires further

investigation. The effects of the check dam on the flow dynamics in the flume are discussed in Section 5.

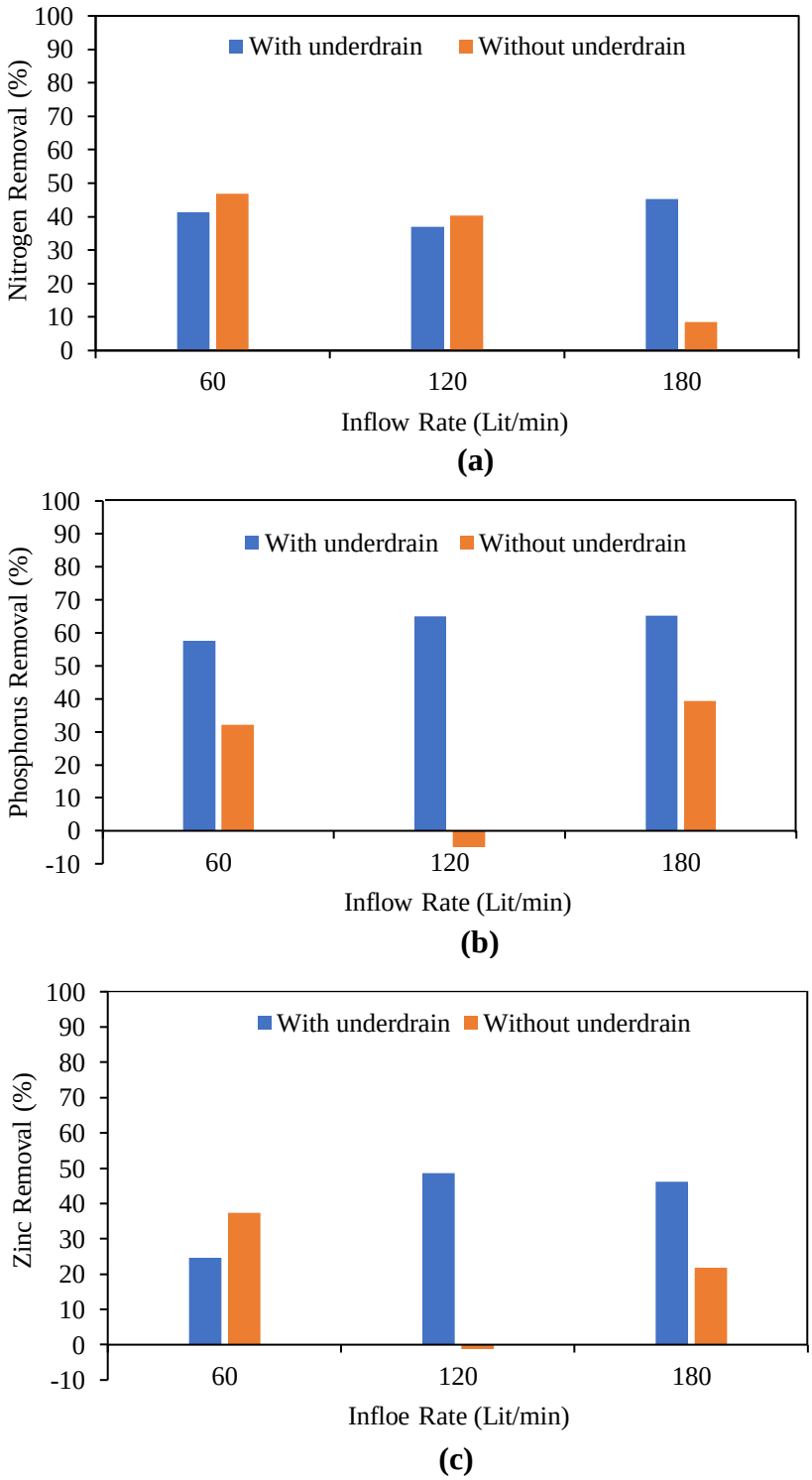

Figure 4.22: Effect of inflow on removal efficiency of (a) Nitrogen, (b) Phosphorus, and (c) Zinc

4.3.2 Removal Efficiency with Continuous Influx of Chemical

In Experiment 7, the inflow rate was 120 Lit/min, while for Experiment 8, the inflow rate was 60 Lit/min. Both experiments were conducted for a duration of 40 minutes with an active underdrain. Figure 4.23 shows the chemical removal efficiency over time in these experiments. In general, the removal efficiency of nitrogen and zinc decreased over time. Notably, the removal efficiencies of nitrogen and zinc were higher at the inflow rate of 60 Lit/min compared to 120 Lit/min. Regarding phosphorus removal efficiency, it decreased over time at 60 Lit/min, whereas at 120 Lit/min, it peaked at 20 min and remained relatively constant thereafter.

In Experiments 9 and 10, the inflow control was implemented to prevent any overflow through the downstream weir. Experiment 9 was conducted with an underdrain, while Experiment 10 was conducted without an underdrain, both lasting 40 minutes. In these experiments the inflow rates were 30 Lit/min and 12 L/min, respectively. These experiments aimed to assess the efficiency of chemical removal in scenarios where all stormwater passed through the filter media without any overflow. Figure 4.24 show the chemical removal efficiency over time for Experiments 9 and 10.

The removal efficiency of nitrogen, phosphorus, and zinc at a flow rate of 30 Lit/min with an underdrain (Experiment 9) initially decreased from 10 minutes to 30 minutes but showed a significant increase at 40 minutes. A similar trend was observed in nitrogen removal efficiency in Experiment 10 (with inflow at 12 L/min). However, phosphorus and zinc efficiencies became negative, indicating higher concentrations at the outlet than at the inlet.

Overall, the removal efficiency was greater compared to the previous experimental conditions, likely attributed to the reduced inflows and absence of the overflow. The removal efficiency at 10 minutes was lower in experiment with an underdrain compared to the without underdrain experiment, but at 40 minutes, the experiment with underdrain condition exhibited significantly higher removal efficiency.

Further investigation is needed to determine whether the increased efficiency is a result of the absence of overflow or the reduced inflows.

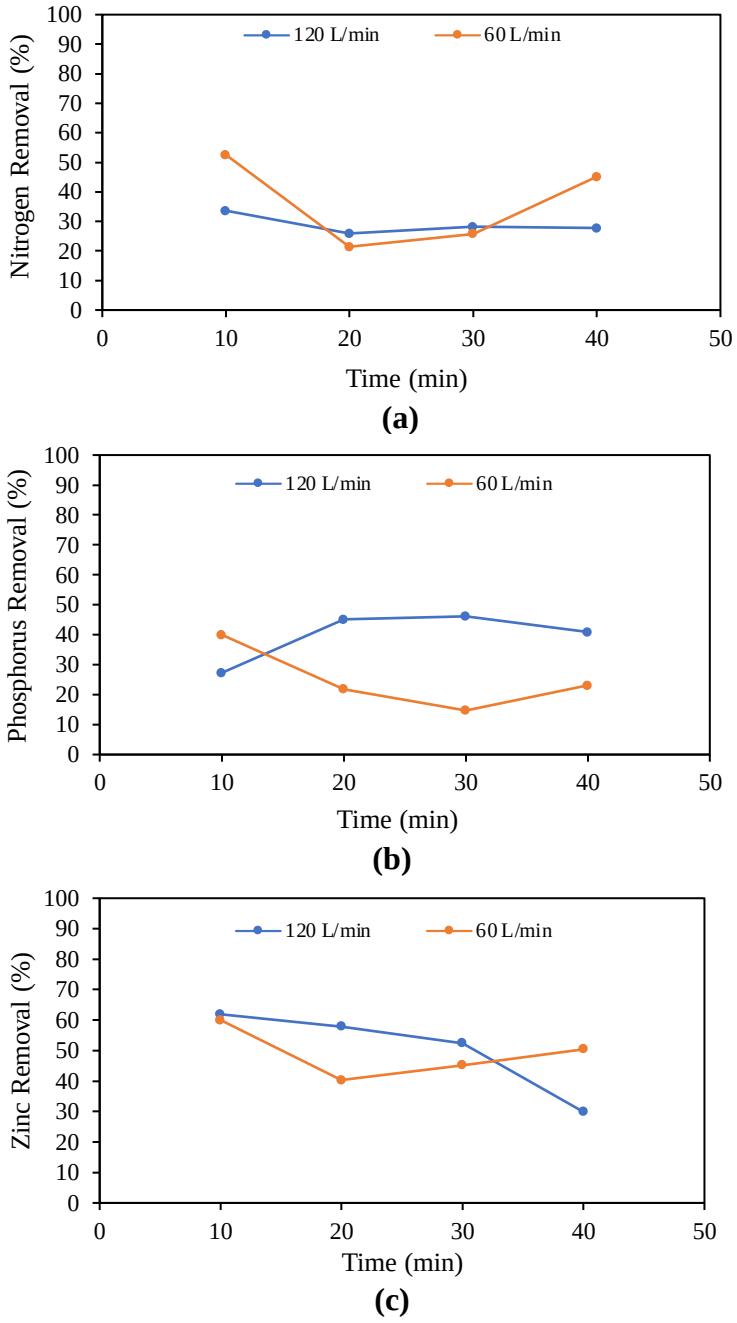

Figure 4.23: Removal efficiency of chemicals in 120 Lit/min and 60 Lit/min with underdrain experiments (a) Nitrogen, (b) Phosphorus, and (c) Zinc

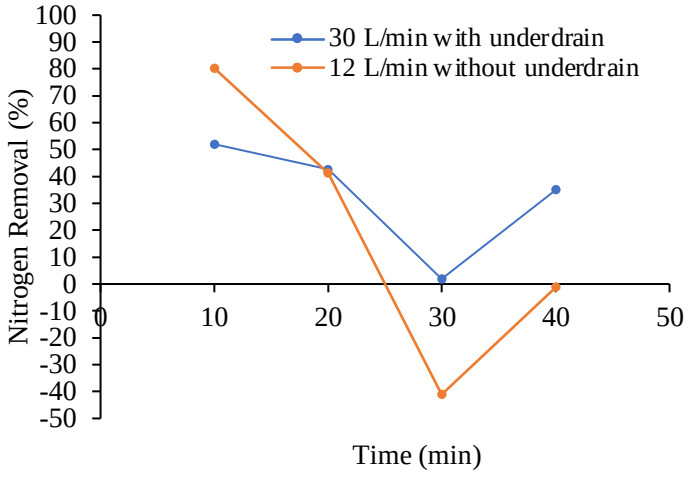

(a)

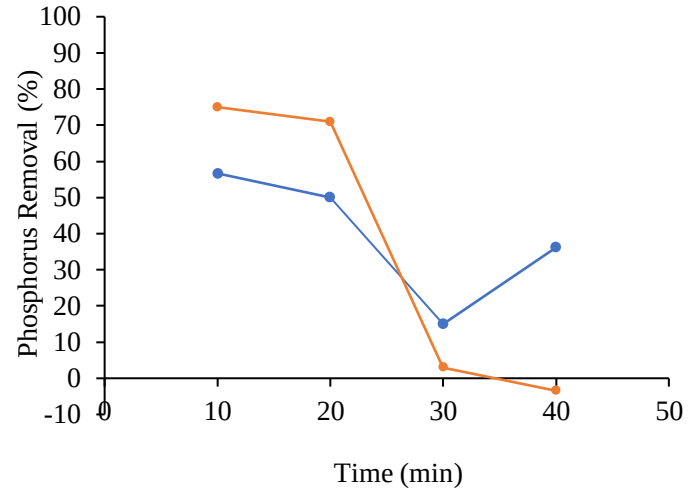

(b)

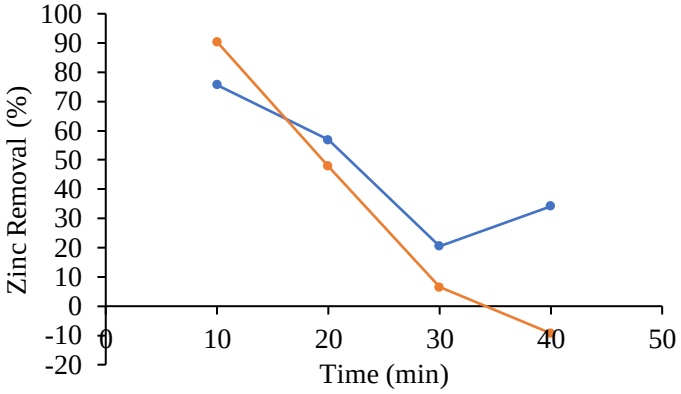

(c)

Figure 4.24: Removal efficiency of chemicals in 12 Lit/min without underdrain and 30 Lit/min with underdrain experiments (zero overflow) (a) Nitrogen, (b) Phosphorus, and (c) Zinc

4.3.3 Chemical Removal Efficiency at Sampling Locations

Figure 4.25 illustrates the average concentrations of nitrate nitrogen, phosphate phosphorus, and zinc along the length of the flumes for Experiments 9 and 10. The concentration gradient along the length of the flume exhibits a consistent decreasing trend, as depicted in Figure 4.25 for both Experiments 9 and 10. Specifically, the concentration in the middle of the flume closely resembles that at the inlet, while the concentration at the underflow is notably lower than at the inlet. The experimental results unequivocally demonstrate the swales' efficiency in removing nitrogen, phosphorus, and zinc. This reduction in concentration can be attributed to the adsorption of these chemicals through the filtering media.

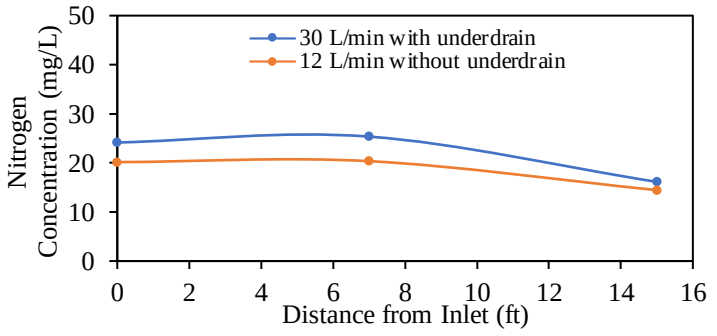

(a)

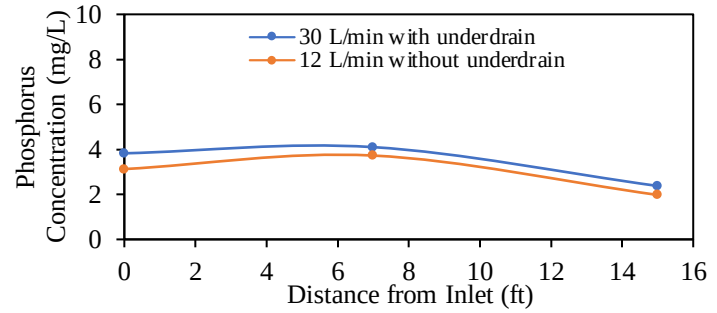

(b)

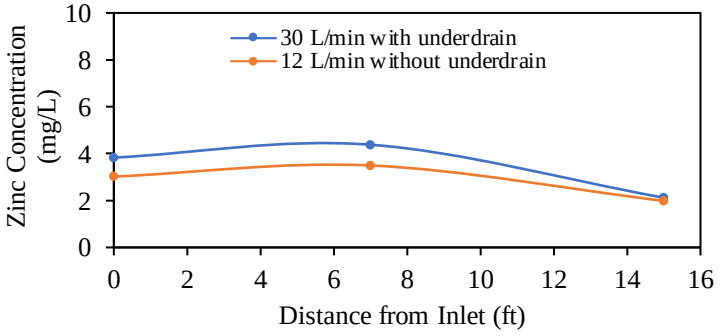

(c)

Figure 4.25: Change in chemicals concentration over the length of the flume in 12 Lit/min without underdrain and 30 Lit/min with underdrain experiments (zero overflow) (a) Nitrogen, (b) Phosphorus, and (c) Zinc

5. FLOW VISUALIZATION EXPERIMENTS

The flow dynamics over the soil media was studied by the flow visualization technique. Particle Image Velocimetry (PIV) was employed to collect flow pattern data at various locations along the experimental flume. A basic PIV setup typically involves the use of a laser, tracer particles, and a high-speed camera to capture a series of images over time within a specified illuminated region. This process yields valuable insights into fluid characteristics such as velocity vectors, streamlines, and shear stresses.

In this study, PIV was utilized to visualize the local flow velocity information along the flume. The flow dynamics in the flume were investigated over Type 2 soil media under inflow rates of 60 and 120 Lit/min. A total of six sets of PIV data were collected: at three locations for each inflow rate. The first location was positioned approximately 65 inches from the flume's inlet, serving as the most upstream point. The second location was situated around the middle of the flume, roughly 105 inches from the inlet. The third location was near the downstream end, close to the flume's outlet, approximately 140 inches from the inlet. The data collection locations are highlighted with red (X) markers in Figure 5.1. It should be noted that no sediment or chemicals were introduced into the inflow during these experiments.

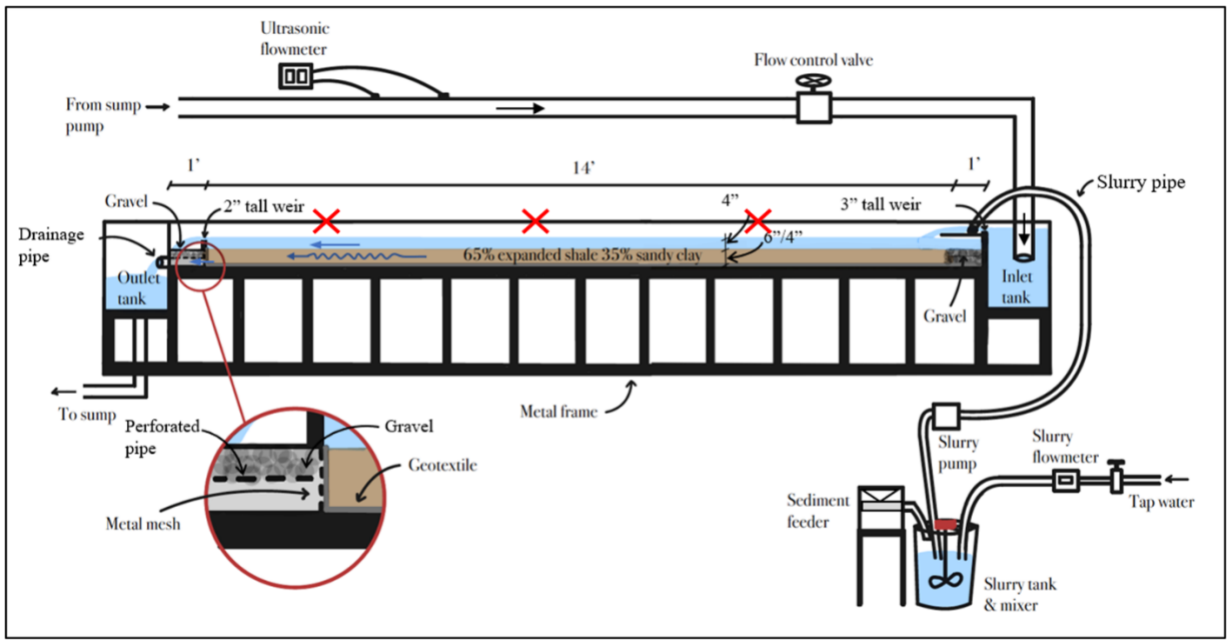

Figure 5.1: Location of the data collection spots in the flume highlighted with red cross (X) mark

The PIV configuration employed for this study consisted of a laser light source and a camera. Specifically, a 1-watt green laser was affixed to a frame positioned atop the flume, and it was coupled with a cylindrical lens to generate a 2-mm thick laser sheet within the test section. As for the tracer particles, sediment naturally present in the flume water served this purpose. To capture

images, a high-speed GoPro Hero 5 action video camera was utilized, which was configured with a 28-mm focal length and a narrow field of view (FOV) to maximize the frame rate (240 Hz) at a pixel resolution of 1280 × 720. Each acquisition run lasted for 10 seconds, producing a total of 2400 images (240 frames per second). The camera was securely mounted on a tripod at one side of the test section to provide a view of the vertical plane, with the laser sheet situated 6 inches away from the flume wall. To optimize data recording quality, a dim lighting condition was maintained in the laboratory during the experiments.

PIVlab, a MATLAB extension, served as the post-processing tool for extracting velocity data by analyzing the video recordings captured during the experiments. PIVlab employs cross-correlation analysis to determine the displacement of tracer particles within the flow field. This analysis extracts particle displacement within a known time interval, enabling the determination of particle direction and velocity on a point-by-point basis [97].

The images were captured in the XZ or vertical planes, where X represents the streamwise coordinate direction, and Z represents the depth-wise coordinate direction. The positive X direction was set as the flow direction, with flow depth serving as the reference distance for calibrating each frame. This calibration provided valuable information, such as the distance per pixel or the relationship between the pixel-to-frame ratio and distance-to-time ratio.

The PIV setup in this study was used to obtain velocity distribution in the area of interest. During image preprocessing, Contrast-Limited Adaptive Histogram Equalization (CLAHE) was enabled to enhance local image contrast [98],[99].

5.1 PIV Experiment Observations

Figure 5.2. presents the flow velocity field in the flume at three selected areas. Figures 5.2a to c show the velocity pattern for a 60 Lit/min flow experiment, and Figures 5.2d to f show the flow patterns for the 120 Lit/min experiment.

In the upstream area, velocity vectors alighted with the flow directions, i.e., from upstream to downstream during both inflows (Figures 5.2c and 5.2f). As expected, the flow velocity at the inlet area was higher during the experiment with higher inflow. In both inflow conditions, the flow velocity near the water surface was the highest, while it approached zero near the bed level.

In the middle section of the flume, the general direction of the velocity vectors was opposite to the inflow direction for both inflow conditions. In the 60 Lit/min experiment, the velocity vectors initially displayed an upward direction, then became horizontal, and eventually moved downward, resembling the formation of vertical vortices rolling towards upstream (Figure 5.2b). This phenomenon could be attributed to the presence of the check dam, which creates a backwater effect and causes the flow to rebound as it reaches the downstream section of the flume. However, in the experiment with the 120 Lit/min inflow, the flow bounces back so strongly that the velocity vectors exhibit a horizontal direction towards upstream without the flow rolling up. Unlike the upstream

area, the velocity was higher near the free surface and the bottom of the flume, and gradually decreased towards the mid-depth of the flow (Figure 5.2e).

In the downstream areas of the flume, the velocity vectors aligned with the flow direction in the 60 Lit/min experiment. As the flow approached the check dam, it gradually lifted up to pass over the downstream weir, as indicated by the direction of velocity vectors in the near-bed area. Additionally, a reverse flow could be observed close to the water surface, pushing the flow back upstream and creating vertical vortices in the middle section of the flume, as discussed earlier. In the 120 Lit/min experiment, the strong incoming flow generated an even more powerful reverse flow, with a velocity magnitude equal to that of the incoming flow in the inlet area but in the opposite direction. However, in contrast to the inlet area, the maximum velocity was observed close to the bed rather than in the surface flow area.

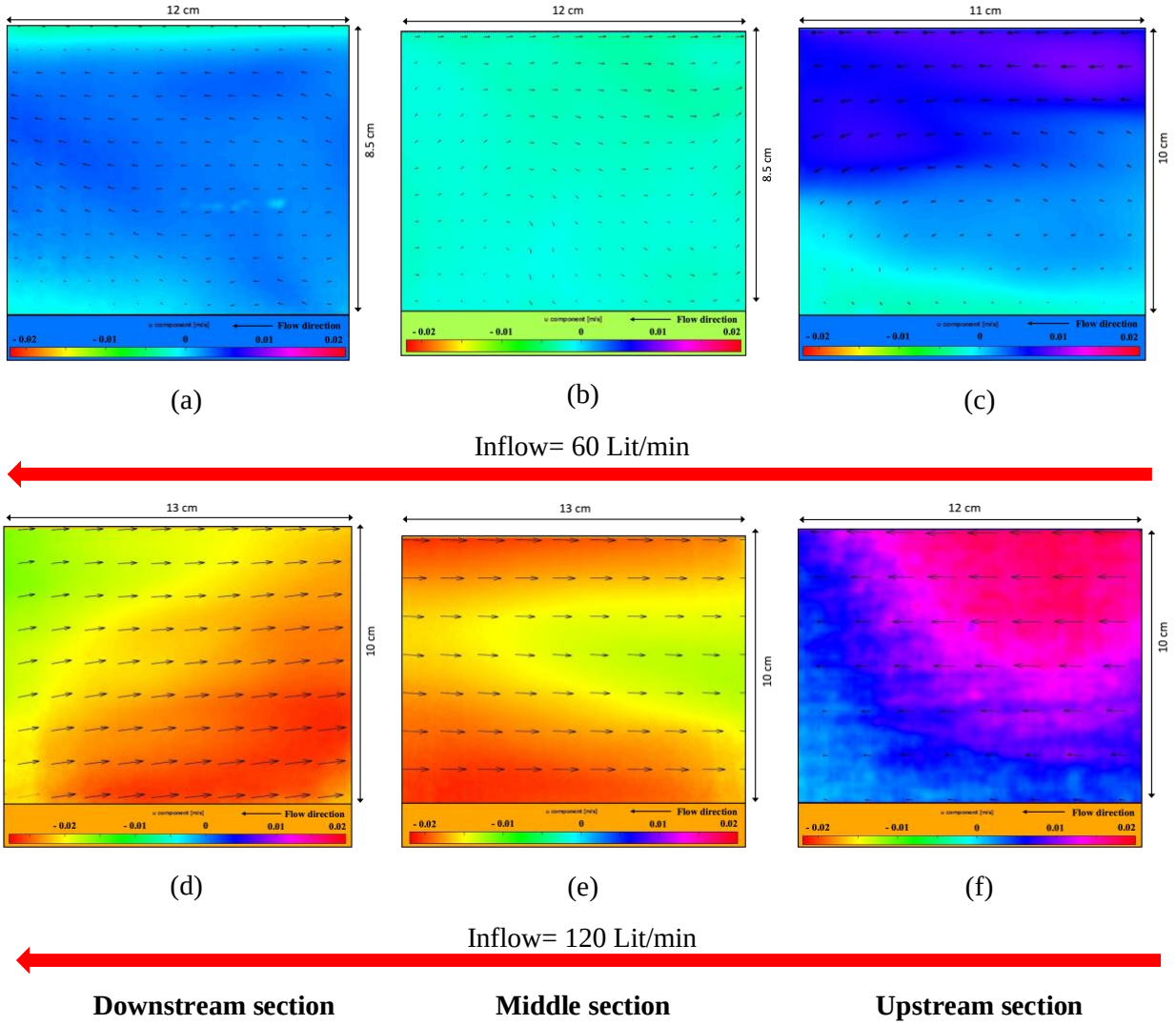

Figure 5.2: Observed flow field and velocity pattern in experiments with 60 Lit/min inflow (a-c) and 120 L/min (d-e). The general inflow direction was from right to left

6. NUMERICAL MODELING

This chapter focuses on investigating sediment transport and flow dynamics in the soil medium using computer simulations. It is important to note that this research had specific objectives, and the scope of the numerical modeling was limited. The study did not attempt to comprehensively address the intricate and multifaceted dynamics of flow and sediment movement within bioswales. Instead, its aim was to gain insights into sediment transport and fluid dynamics within a soil environment. Deliberately, it did not tackle the entire spectrum of challenges associated with studying flow and sediment transport within bioswales.

6.1 Methodology

In recent years, computational fluid dynamics (CFD) simulations have gained significant prominence in flow simulation and sediment transport. Several researchers have studied the application of CFD models in various areas of water resources engineering, including but not limited to investigations of fluid-structure interactions [100],[101],[102], wave and coastal simulations [103],[104],[105], and sediment transport and scouring analysis [106],[107],[108]. Among various CFD models, such as Ansys Fluent, Ansys CFX, OpenFoam, and Flow-3D Hydro, the exceptional performance exhibited by the Flow-3D Hydro model across various aspects of hydraulic and sediment transport problems has positioned this model as the robust commercial CFD model of choice for application within the present study.

6.1.1 Flow-3D CFD Model

The hydraulic analysis in the present study was conducted using the Flow-3D numerical model. This model can accommodate diverse solid geometry design scenarios, simplifying the process of importing the geometry and integrating the solid model into the software. The Navier-Stokes equations, i.e., a set of three-dimensional mass and momentum conservation equations (Equations 6.1 to 6.4), are the primary equations solved by the Flow-3D model to simulate the flow field in various conditions. Flow-3D utilizes the Finite Volume Method (FVM) to discretize the Navier-Stokes equation.

$$V_F \frac{\partial \rho}{\partial t} + \frac{\partial}{\partial x}(\rho u A_x) + \frac{\partial}{\partial y}(\rho v A_y) + \frac{\partial}{\partial z}(\rho w A_z) = 0 \tag{6.1}$$

$$\frac{\partial \mathrm{u}}{\partial t} + \frac{1}{\mathrm{V}_F}\left\{uA_x \frac{\partial \mathrm{u}}{\partial \mathrm{x}} + vA_y \frac{\partial \mathrm{u}}{\partial \mathrm{y}} + wA_z \frac{\partial \mathrm{u}}{\partial \mathrm{z}}\right\} = -\frac{1}{\rho}\frac{\partial p}{\partial x} + G_x + f \tag{6.2}$$

$$\frac{\partial \mathrm{v}}{\partial t} + \frac{1}{\mathrm{V}_F}\left\{uA_x \frac{\partial \mathrm{v}}{\partial \mathrm{x}} + vA_y \frac{\partial \mathrm{v}}{\partial \mathrm{y}} + wA_z \frac{\partial \mathrm{v}}{\partial \mathrm{z}}\right\} = -\frac{1}{\rho}\frac{\partial p}{\partial y} + G_y + f \tag{6.3}$$

$$\frac{\partial \mathrm{w}}{\partial t} + \frac{1}{\mathrm{V}_F}\left\{uA_x \frac{\partial \mathrm{w}}{\partial \mathrm{x}} + vA_y \frac{\partial \mathrm{w}}{\partial \mathrm{y}} + wA_z \frac{\partial \mathrm{w}}{\partial \mathrm{z}}\right\} = -\frac{1}{\rho}\frac{\partial p}{\partial z} + G_z + f \tag{6.4}$$

To model the turbulent regime in the flume of the present study, the K-ε turbulence model was implemented. This model has been utilized in various studies to simulate sediment transport in open channels using the Flow-3D [109],[110],[111]. The solid geometry regions within the grids

in the Flow-3D model are defined using the Fractional Area/Volume Obstacle Representation (FAVOR) method, where 0 < FAVOR < 1. In this representation, 0 represents void cells, and 1 represents cells that are entirely filled with fluid [112],[113].

6.1.2 Geometry and Mesh Size

The geometry of the model in this study consists of solid and porous media elements, representing the flume's solid structure and the soil media, respectively. These geometry elements were designed in AutoCAD 3D to achieve a Froude similarity of 1 compared to the experimental setup. Figure 6.1 illustrates the model's geometry, which was imported into the Flow-3D Hydro for simulating various hydraulic and sediment entrainment scenarios.

The flume itself has dimensions of 4.9 meters (16 ft) in length and 1.2 meters (4 ft) in width. The downstream weir has a width of 0.3 meters (1 ft), and the drainage pipe has a diameter of 5 cm (2 inches).

As shown in Figure 6.1, two porous media elements were incorporated into the model. Porous Media I (brown color area in Figure 6.1) represents the soil media with an average porosity of 0.2. Porous Media II (yellow color area in Figure 6.1) represents the gravel box located before the drainage pipe, with a porosity of 0.9.

A total of 94,080 mesh cells were employed within the mesh domain. The optimal mesh count was determined through trial-and-error processes, involving an examination of mesh domain aspect ratios in all three directions of the models and the FAVOR method's ability to accurately capture the model's geometry. Additionally, mesh independence tests were conducted to assess the impact of mesh cell count on the model's results.

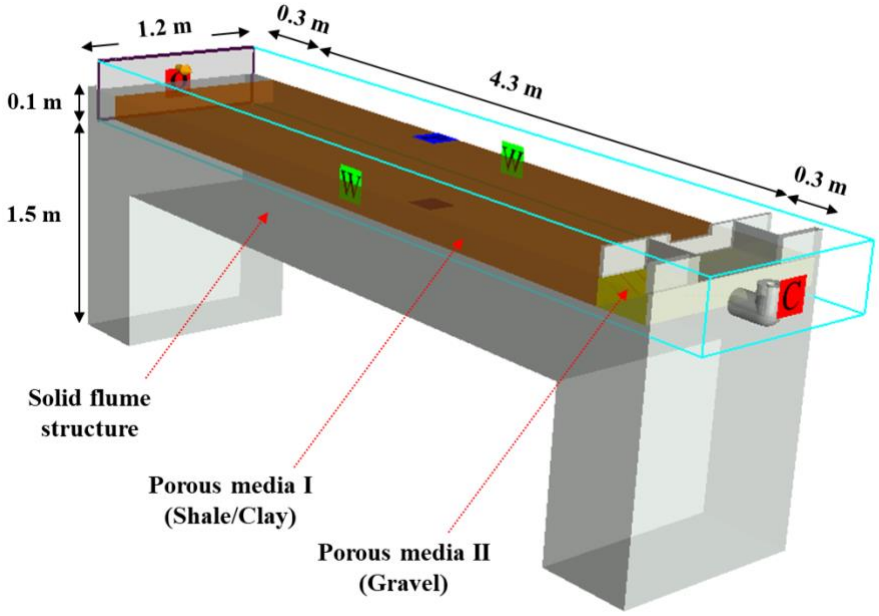

Figure 6.1: Geometry of experimental setup in Flow-3D

6.1.3 Boundary and Initial Conditions

Figure 6.2 illustrates the boundary conditions considered in the CFD model. The inlet and sidewall boundaries were set to a wall condition, while the outlet surface boundary was set to continuous flow conditions to simulate drainage downstream of the flume. To model water-air interactions, an air-water interface was implemented at the upper surface boundary using atmospheric pressure. Additionally, two rectangular flow and sediment sources were introduced at the inlet surface boundary to simulate the flow and sediment discharge into the flume from the inlet surface of the mesh domain.

This study investigated sediment transport in the flume both with and without soil media. In the *without soil media* scenario, the bottom of the model was set as solid. It should be emphasized that a solid bed model represents a clogged swale that does not allow infiltration and only removes sediment through depositional processes. The solid bed models were specifically employed with the primary objective of enhancing our understanding of the intricate dynamics governing flow patterns and sedimentation processes within the swale. To model scenarios without soil media, the porosity values for Porous Media I and II were set to 0 to represent a solid condition. To aid in model convergence and reduce simulation time, an initial fluid volume was considered at t =0, thereby reducing the time required for the model to fill the flume.

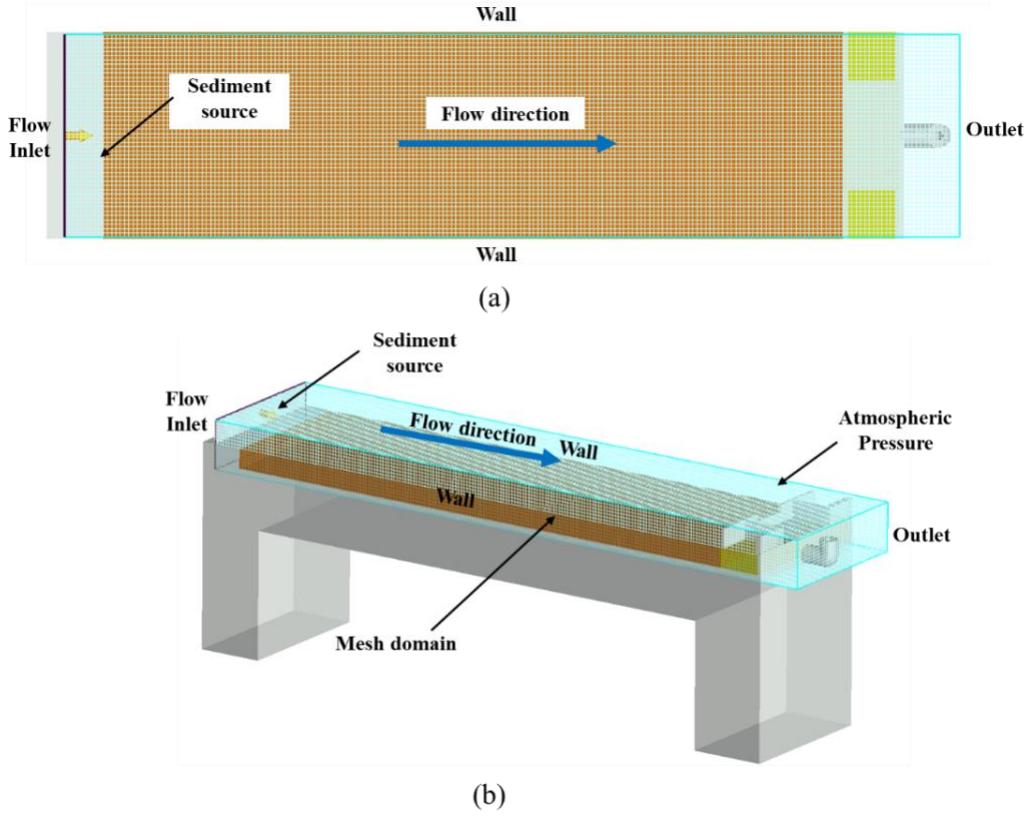

Figure 6.2: Mesh domain and boundary conditions for CFD model (a) plan view, and (b) isometric view.

6.1.4 Optimum Simulation Time

Once the optimal number of mesh cells was determined, the simulation time was assigned to the model based on specific requirements and convergence conditions. To ensure the establishment of steady-state conditions in the model, an examination of temporal fluctuations in flow rate was conducted. It was observed that for low-flow scenarios (60 Lit/min), temporal fluctuations in flow rate became negligible after approximately t = 725 seconds of simulation time. Conversely, in high-flow scenarios (180 Lit/min), temporal fluctuations in flow rate became negligible from approximately t = 310 seconds. Therefore, a simulation time of 1000 seconds was chosen for modeling purposes to ensure that both low and high flow scenarios reach steady-state conditions.

6.1.5 Hydraulic and Sediment Transport Scenarios

Eight scenarios were considered to model sediment transport in the flume. Table 6.1 summarizes each modeling scenario, including the inflow rate and influent sediment concentration. Consistent with the laboratory experiments, a high-concentration slurry was introduced into the flume's inlet at a constant rate. Therefore, the total inflow in each scenario comprises the flow rate at the inlet (with zero sediment concentration) and the slurry flow. The slurry discharge remained fixed at 6 Lit/min for all scenarios, but two different flow rates at the inlet were considered: 54 Lit/min for low inflow scenarios and 174 Lit/min for high inflow scenarios.

It is important to highlight that the Flow-3D model exclusively takes into account a single sediment size when considering the sediment concentration in the influent. Therefore, the sediment size of 20 µm, which corresponds to the d50 of the suspended sediment found at the inlet of the experimental flume as described in Section 4.2.3, was introduced to the model.

The models were run for two different cases: one with a solid bed and the other with a porous bed (soil media). In the models with a solid bed, changes in suspended sediment concentration were solely attributed to the depositional process. However, in the models with a porous bed, both sediment deposition and sediment capture by the soil media contributed to variations in suspended sediment concentration along the flume.

It should be noted that in the experiments involving a solid bed, the drainage system and outlet pipe (as depicted in Figure 6.2) were not part of the model. Consequently, the only outlet point on the downstream side of the flume was the downstream weir.

In model runs #1 to #4 with a solid bed, the change in suspended sediment concentration due to deposition along the flume was assessed. In run #1, a low inflow condition (60 Lit/min) with an influent sediment concentration of 100 mg/L was simulated. For this purpose, the flow and slurry rates at the inlet boundary were set to 0.0009 m^3/s (equivalent to 54 Lit/min) and 0.0001 m^3/s (6 Lit/min). Additionally, the slurry concentration was set to 1 kg/m^3 (equivalent to 1000 mg/L). A simulation time of 1000 seconds was used to reach steady-state conditions in the model. Once the simulation was completed, suspended sediment concentration along the flume was obtained. In run #2, everything was kept the same as in run #1, except the slurry concentration was set to 2000

mg/L. For runs #3 and #4, the total inflow was 180 Lit/min in both experiments, but the concentration was selected as 3000 mg/L and 6000 mg/L, respectively.

Runs #5 to #8 were similar to runs #1 to #4 in terms of the initial solid bed condition, but they were conducted with a porous bed. A summary of the hydraulic and sediment conditions of these runs is presented in Table 6.1.

Table 6.1: Summary of hydraulic and sediment transport conditions used in Flow-3D model

Run No.	Flow Rate at inlet (Lit/min)	Slurry Rate (Lit/min)	Slurry Concen. (mg/L)	Inflow Rate[1] (Lit/min)	Influent Concen.[2] (mg/L)	Remark
1	54	6	1000	60	100	Solid bed
2	54	6	2000	60	200	
3	174	6	3000	180	100	
4	174	6	6000	180	200	
5	54	6	1000	60	100	Porous bed (soil media)
6	54	6	2000	60	200	
7	174	6	3000	180	100	
8	174	6	6000	180	200	

[1] *Inflow rate is the sum of the flow rate at the inlet and the slurry rate in each scenario*

[2] *Influent sediment concentration is calculated based on the flow rate at the inlet with zero sediment concentration and slurry rate with sediment concentration in each scenario*

6.2 Model Validation

The solid models were not validated against experimental results because these scenarios were not simulated in the laboratory, and there was no available data for model validation. Instead, a comparison was made between the water depths recorded at the downstream weir location and those observed in the CFD models, as shown in Table 6.2.

Table 6.2: Comparison between observed and simulated water depth at the outlet of flume

Run No.	Target Inflow (Lit/min)	Experimental Model	CFD Model
		Flow Depth (cm)	Flow Depth (cm)
1	60	10.06	10.11
2	60	10.06	10.11
3	180	10.69	10.71
4	180	10.69	10.71

The overflow and underflow values measured in the drainage experiments were used to validate the results from the CFD models with a porous bed (soil media). The porosity of the porous bed was adjusted through a trial-and-error process to achieve consistent values for overflow and underflow in both the physical model and the CFD model. The comparison between observed flow rates in the laboratory experiments and the numerical model is presented in Table 6.3.

Table 6.3: Comparison between observed and simulated overflow and underflow

Run No.	Target Inflow (Lit/min)	Experimental Model		CFD Model	
		Overflow (Lit/min)	Underflow (Lit/min)	Overflow (Lit/min)	Underflow (Lit/min)
5	60	11.5	48	-	59.20
6	60	11.5	48	-	59.24
7	180	127	55.2	127.06	54.30
8	180	127	55.2	126.22	53.10

6.3 Results

6.3.1 Models with Solid Bed

Figure 6.3 depicts the temporal distribution of suspended sediment concentration (SSC) along the flume for run #1 at four time steps: 0, 100, 500, and 1000 seconds. As the sediment plume travels downstream in the flume, the suspended sediment concentration increases in the direction of flow. This increase is attributed to the continuous injection of sediment into the flume and sediment settling along its length, resulting in higher SSC values near the inlet and a gradual decrease toward the outlet.

The SSC distribution for runs #2 to #4 at t = 1000 seconds are shown in Figure 6.4. As the sediment concentration of the slurry increases in runs #3 and #4, the SSC in the flume also increases.

To provide a clearer visualization of the changes in SSC along the flume, Figure 6.5 illustrates the change in suspended sediment concentration (SSC) distribution for runs #1 to #4 at t = 1000 seconds, presenting the depth-averaged SSC. As seen in Figure 6.5, SSC decreases along the flume from the inlet to the downstream weir location, following an exponential trend.

Table 6.4 summarizes the inlet and outlet SSC values, along with the percentage change in suspended sediment concentration for all runs. Notably, the reduction in SSC is significantly higher for low inflow scenarios (88-89%) compared to high inflow scenarios (49-54%). These results were expected because of the lower flow velocity and longer hydraulic residence time (*HRT*) in low inflow runs. Importantly, these findings are consistent with those observed in the laboratory experiments.

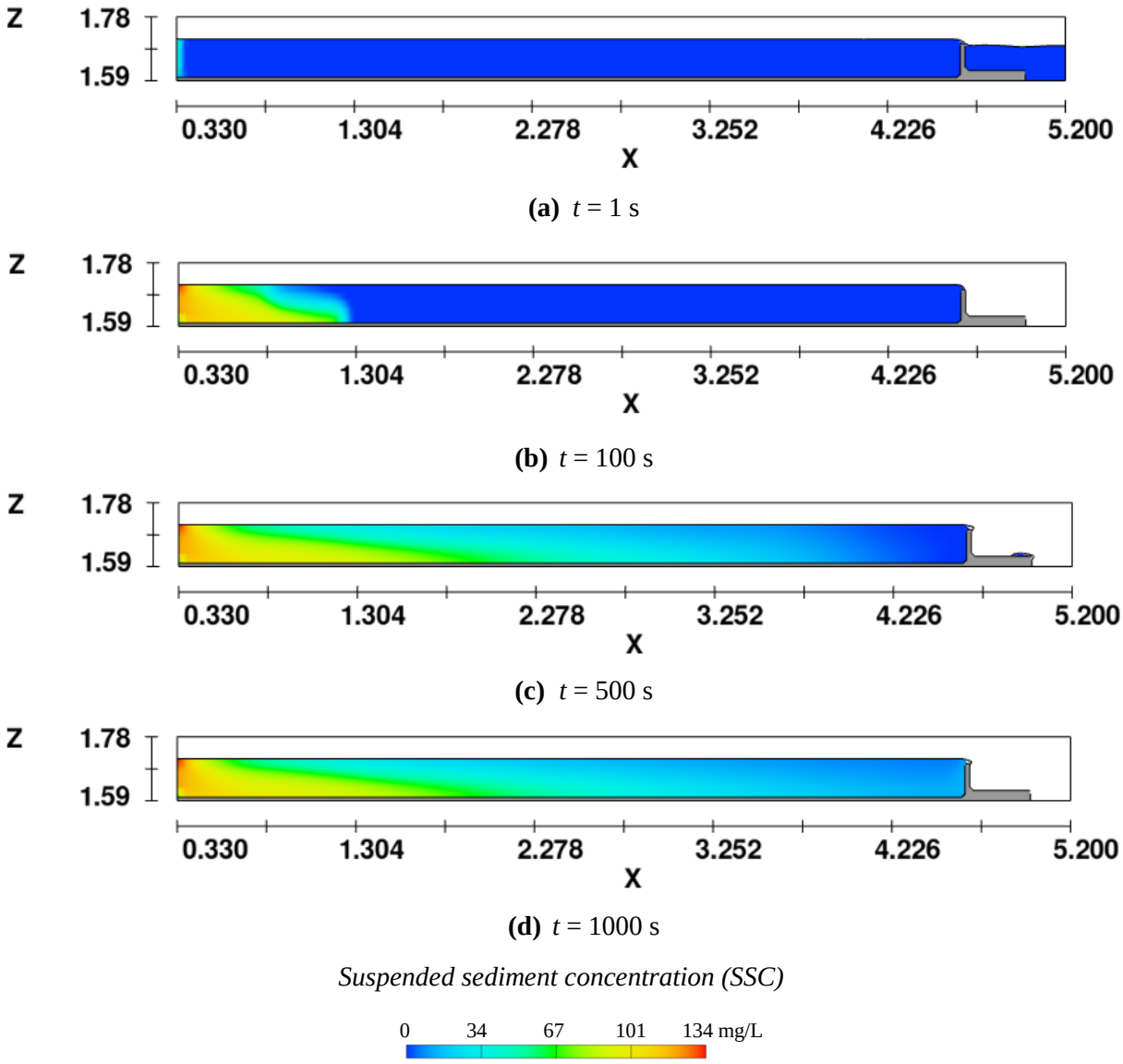

Figure 6.3: Suspended sediment concentration distribution along the flume over the solid bed for different simulation times (Inflow =60 Lit/min, Influent sediment concentration = 100 mg/L)

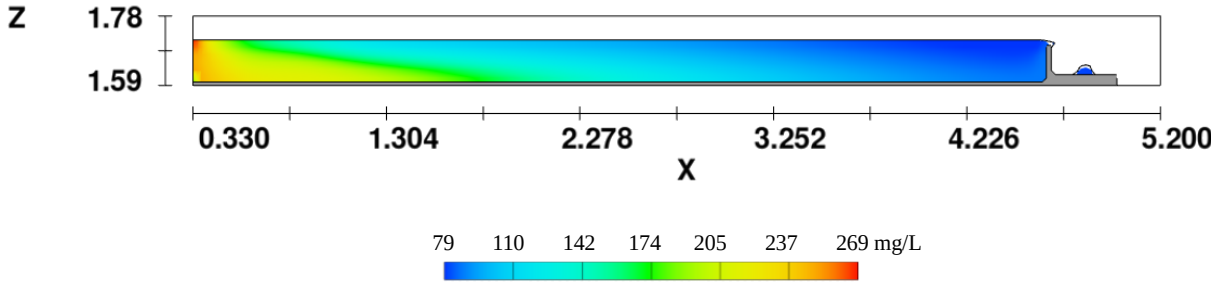

(a) Run # 2: 60 Lit/min, 200 mg/L

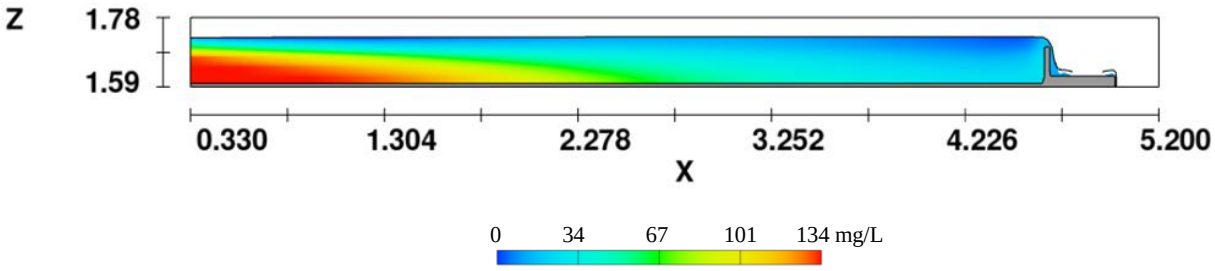

(b) Run # 3: 180 Lit/min, 100 mg/L

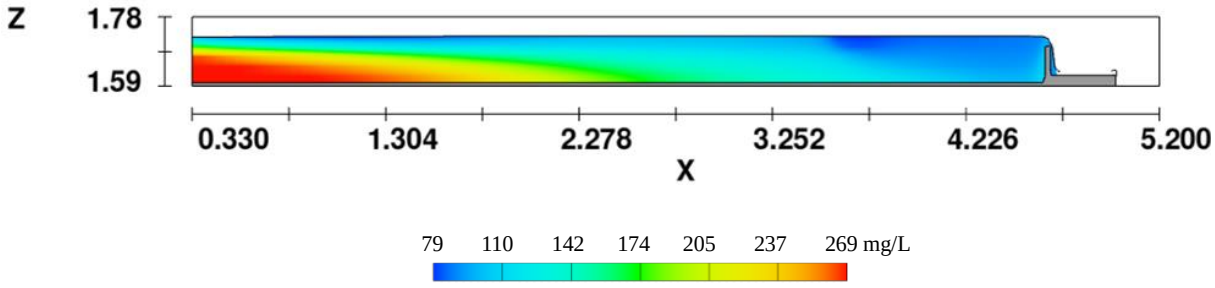

(c) Run # 4: 180 Lit/min, 200 mg/L

Figure 6.4: Suspended sediment concentration distribution along the flume over the solid bed for Runs # 2 to # 4 at t = 1000 seconds

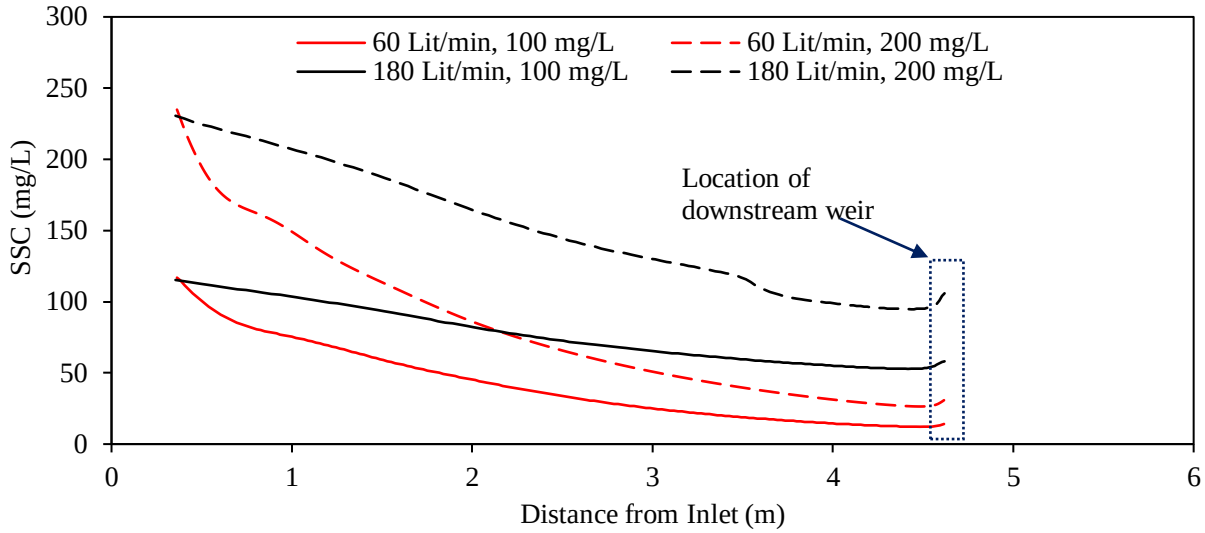

Figure 6.5: Depth averaged suspended sediment concentration (SSC) distribution along the flume with solid bed for scenarios #1 to 4 at t = 1000 seconds

Table 6.4: Summary of suspended sediment concentration (SSC) at inlet and outlet areas and percentage reduction in SSC

Run No.	Inflow (Lit/min)	Target Influent Concen. (mg/L)	Inlet SSC (mg/L)	Outlet SSC (mg/L)	SSC Reduction (%)
1	60	100	117	13	89
2	60	200	235	29	88
3	180	100	115	58	49
4	180	200	230	106	54

6.3.2 Models with Porous Bed (Soil Media)

In this section, the results of the CFD model for runs #5 to #8 are presented. In these scenarios, a porous media bed with an average porosity of 0.2 was incorporated into the model. Figure 6.6 shows the suspended sediment concentration (SSC) distribution for various flow and slurry conditions at time t = 1000 seconds. The SSC distribution in water flowing over and through the soil media is depicted in this figure. In the low inflow scenarios (runs #5 and #6), no overflow occurred through the downstream weir; instead, the flow passed through the soil media and exited the flume via the drainage outlet pipe. In the high inflow scenarios (runs #7 and #8), approximately 1/3 of the inflow passed through the soil media and exited through the outlet pipe (underflow), while the remaining 2/3 flowed over the downstream weir (overflow) (see Table 6.3).

In Figure 6.6, it can be observed that the distribution of SSC is significantly different in these scenarios and varies substantially due to changes in the inflow rate and influent sediment concentration.

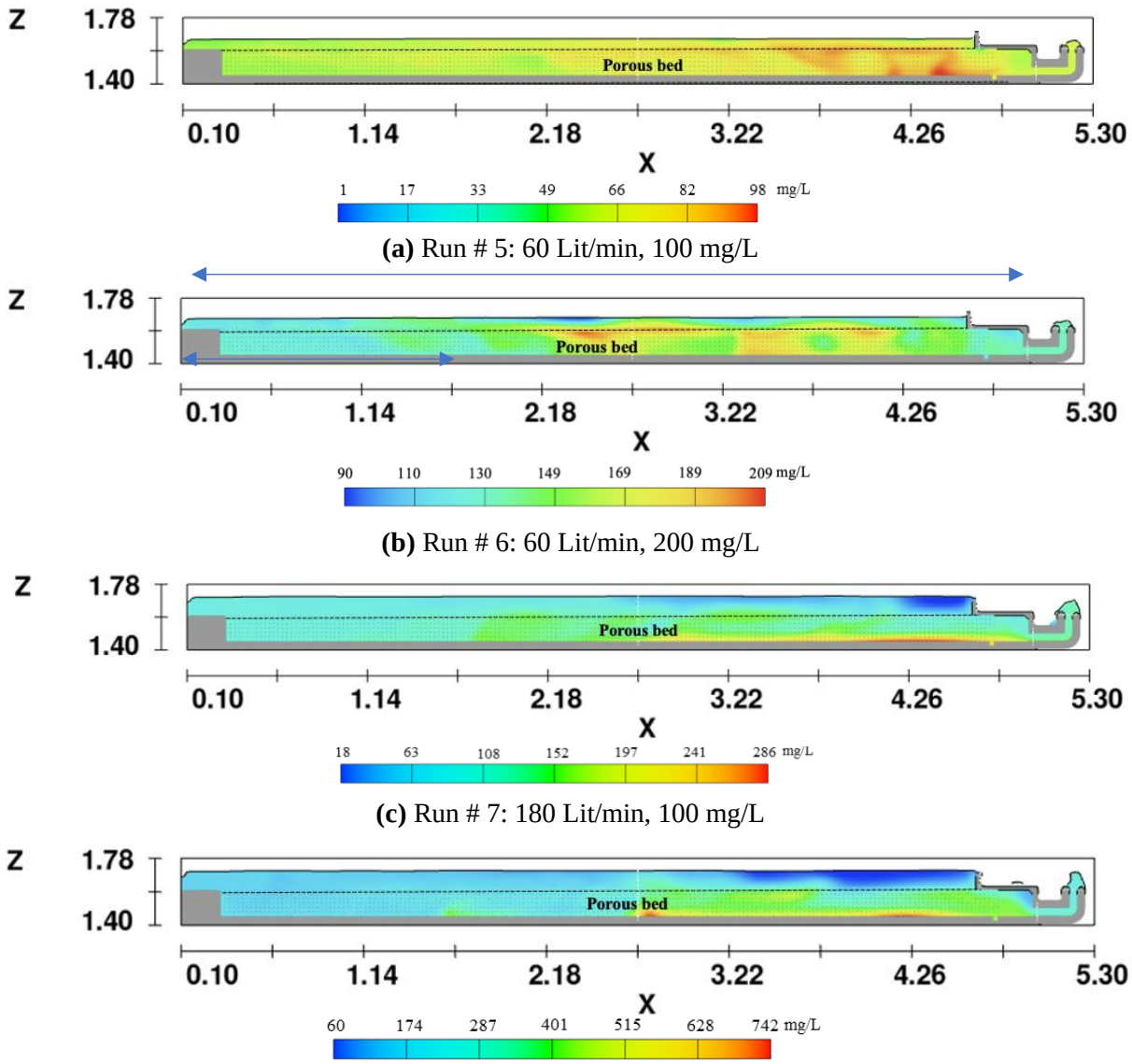

(a) Run # 5: 60 Lit/min, 100 mg/L

(b) Run # 6: 60 Lit/min, 200 mg/L

(c) Run # 7: 180 Lit/min, 100 mg/L

(d) Run # 8: 180 Lit/min, 200 mg/L

Figure 6.6: Suspended sediment concentration distribution along the flume with porous bed for Runs #5 to 8 at t = 1000 seconds

The variations in SSC along the flume, in the water moving over the soil media, and through it are separately depicted in Figures 6.7a and b. These figures present the depth-averaged SSC through the water column and soil media.

Figure 6.7a shows variation in SSC in water flowing over the soil media. From this figure, it can be observed that SSC decreased along the flume due to the deposition of sediment over the bed. A sharp decrease in SSC was observed at the inlet area during low inflow scenarios. This decrease was more prominent when the influent concentration was higher, i.e., 200 mg/L. In low inflow scenarios, the flow velocity was much smaller than in high inflow cases, resulting in sediment

deposition. During high inflows, the change in SSC was more gradual; however, the overall decrease in SSC was less significant. The higher velocity in the flume due to the increased inflow rate resulted in less sediment deposition in the flume and more suspension of sediment.

Figure 6.7b shows the variation in SSC in water flowing through the soil media. From this figure, it is evident that SSC increased along the flume due to sediment being captured by the soil media. The low flow velocity through the soil media resulted in accumulation of suspended sediment and an increase in SSC.

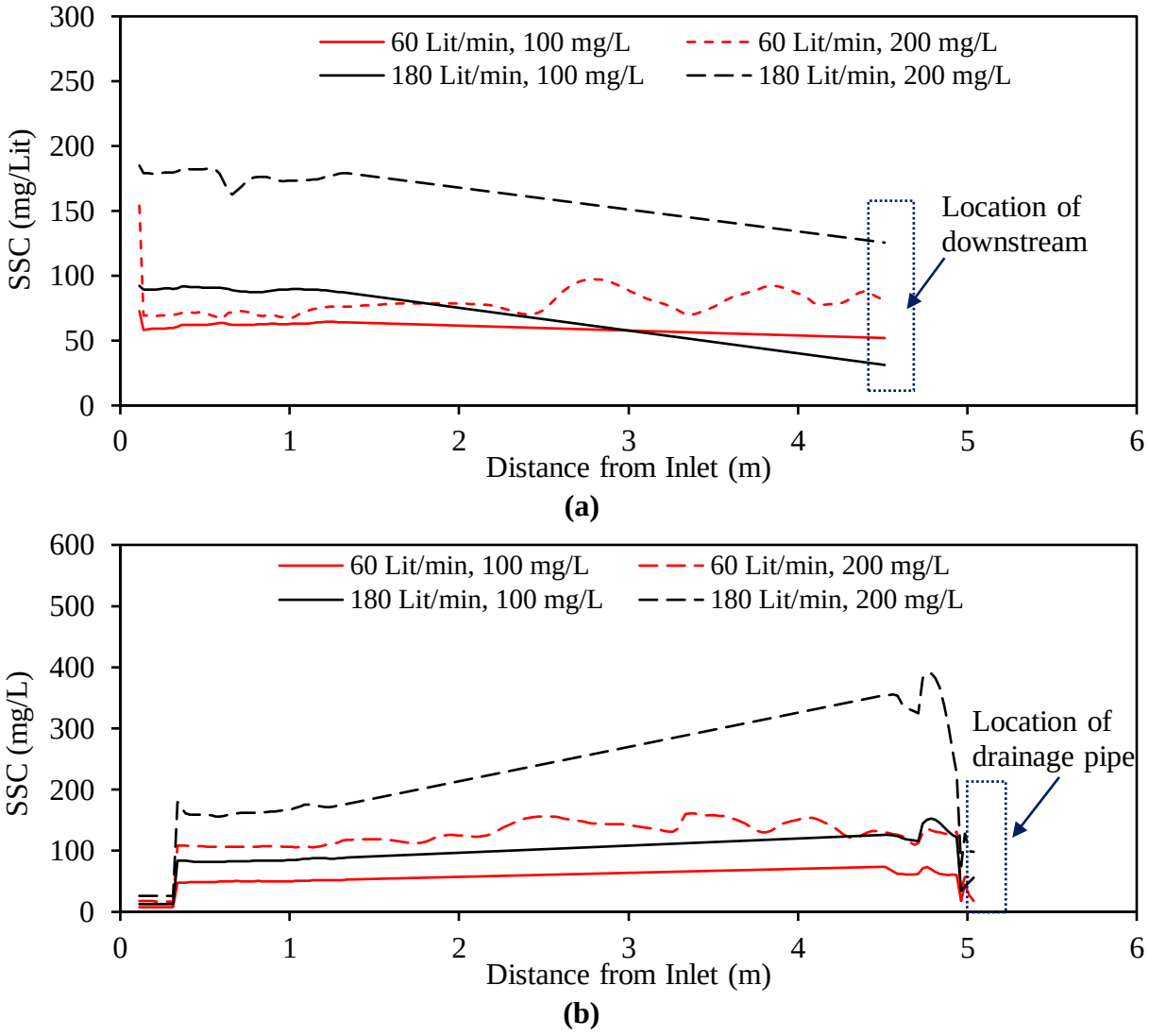

Figure 6.7: Depth-averaged suspended sediment concentration (SSC) distribution along the flume with porous bed for scenarios #5 to 8 at t = 1000 seconds (a) Flow through the downstream weir (overflow) and (b) Flow through soil media (underflow)

The SSC values at the inlet, overflow, and underflow in runs #5 to #8 are summarized in Table 6.5. The percentage reduction of SSC in the overflow and underflow is calculated and shown in this table. In general, the reduction in SSC in water flowing through the soil media was much higher than in water flowing over the soil media (51-82% vs. 10-59%). Additionally, during low inflow conditions, the reduction in SSC was higher than during high inflow conditions, both in the overflow (48-59% vs. 10-14%) and in the underflow (71-82% vs. 44-51%). No conclusive relationship was found between the inlet sediment concentration and the reduction in SSC in the underflow and overflow. These results are consistent with observations made in laboratory experiments.

Table 6.5: Summary of suspended sediment concentration (SSC) at inlet and outlet areas and percentage reduction in SSC

Run No.	Inflow (Lit/min)	Influent Concen. (mg/L)	Overflow SSC (mg/L)	Underflow SSC (mg/L)	SSC Redu. in Overflow (%)	SSC Redu, in Underflow (%)
5	60	100	52*	18	48	82
6	60	200	81*	57	59	71
7	180	100	86	56	14	44
8	180	200	179	98	10	51

**Since there was no overflow in 60 Lit/min experiments, the SSC upstream of the outlet weir was considered for the overflow SSC*

6.3.3 Flow Dynamics

In Figure 6.7, valuable insights into the flow field and velocity patterns during two distinct scenarios with varying inflow rates can be obtained: one scenario is represented by run #7, with a 60 L/min inflow, and the other by run #8, with a higher inflow rate of 180 L/min. The formation of eddies along the flume in both of these flow scenarios is illustrated in this figure. Swirling currents of fluid, or eddies, are often generated along the flume in response to changes in flow velocity and direction caused by the presence of the check dam. A crucial role in the transport and distribution of suspended solids within the water is played by these eddies, highlighting their significance.

Furthermore, a notable observation in Figure 6.7 is the presence of reverse flow, where water appears to move from downstream to upstream, particularly pronounced during the low inflow condition. This reverse flow is an intriguing phenomenon, as it suggests complex flow patterns within the system that can have important implications for sediment transport and deposition along the swale.

These observations align with findings obtained through Particle Image Velocimetry (PIV), the technique used to visualize and analyze fluid flow in this study (See Chapter 5). The use of PIV allowed for tracking the movement of particles within a fluid and understanding its velocity

distribution. However, PIV has its limitations, and one of these is its inability to provide comprehensive insights into the flow dynamics through the soil media. However, the results from CFD provide the flow dynamics both over and within the soil media simultaneously, offering insights that would be otherwise challenging or impossible to obtain through experimental techniques alone. A comprehensive understanding of the complex flow patterns and interactions occurring within the soil media is gained by employing CFD, thereby shedding light on the intricate processes that are influenced by sediment transport and deposition.

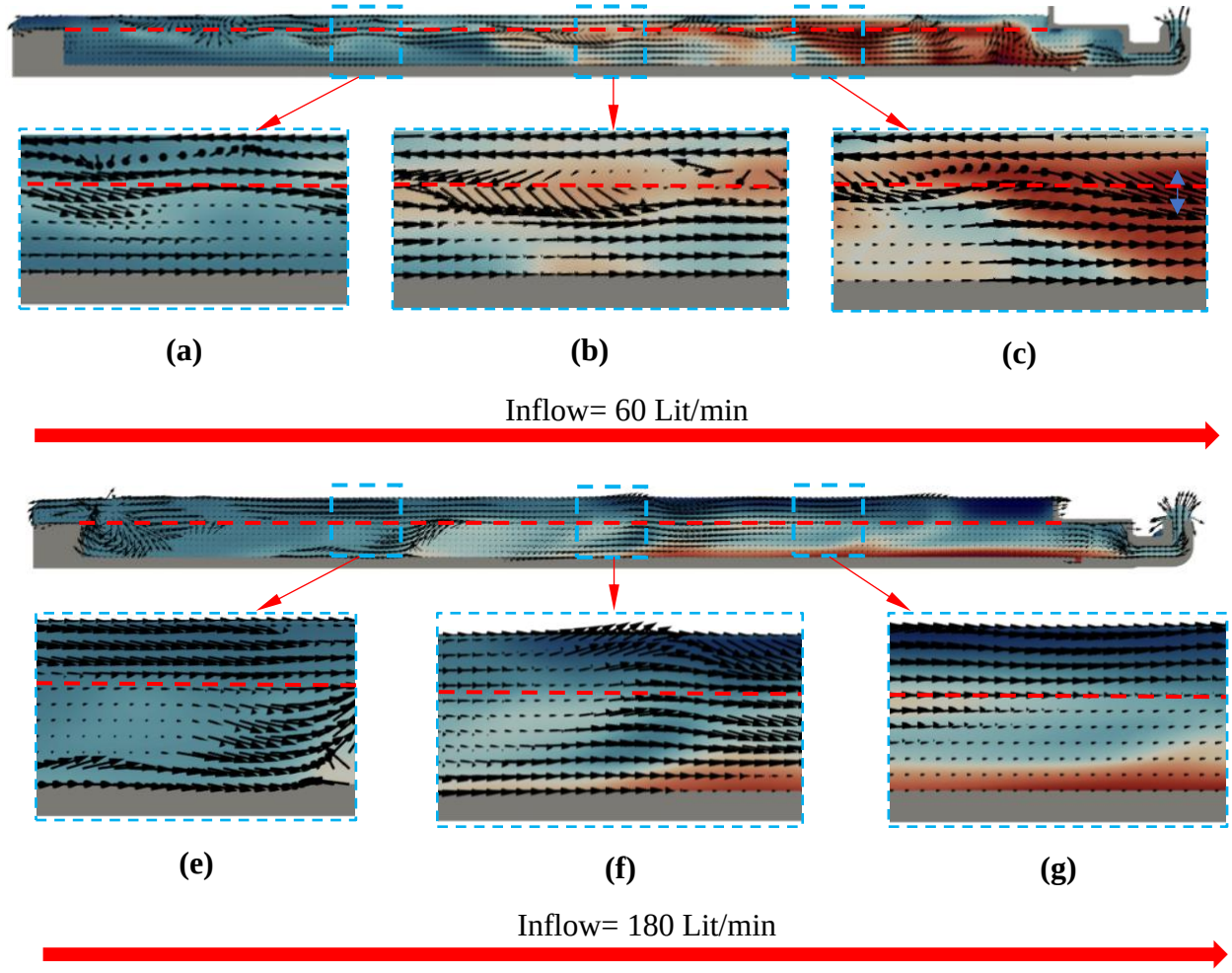

Figure 6.8: Simulated flow field and velocity pattern in scenarios with 60 Lit/min inflow (a-c) and 180 L/min (d-e). The general inflow direction was from left to right. The blow-up areas correspond to where PIV results are presented.

7. CONCLUSIONS, IMPLEMENTATION RECOMMENDATIONS, AND FUTURE WORK

Bioswales, frequently utilized as Best Management Practices (BMPs), are specifically engineered for the purpose of functioning as treatment systems for water quality and for mitigating peak flows during extreme events. The evaluation of BMP effectiveness hinges on their ability to minimize pollutants. To attain optimal efficiency in bioswales, it is imperative to possess a comprehensive grasp of the mechanisms responsible for pollutant removal.

The primary aim of this study was to assess the treatment efficiency of expanded shale when employed as an infiltration medium in bioswales. To accomplish this objective, a small-scale model of an expanded shale engineered infiltration layer was installed and subjected to rigorous testing within a carefully controlled laboratory environment. The primary objective of this testing was to assess the performance of the expanded shale layer in terms of its ability to effectively remove total suspended solids (TSS), turbidity, and other water quality pollutants such as nitrogen, phosphorus, and zinc from stormwater runoff.

To comprehensively evaluate its performance, expanded shale engineered infiltration layer was tested under a range of varying conditions. These conditions included different infiltration thicknesses and gradation, drainage condition, hydraulic loading rates, and pollutant concentrations. Throughout the testing process, samples were continuously taken for both the inflows and outflows into and out of the swale. Additionally, the rates of infiltration through the shale media were carefully monitored and recorded.

The quality of the water was closely examined as well. The effluent, which represents the water leaving the system, was analyzed in terms of its total suspended solids, turbidity, nitrogen, phosphorus, and zinc. This thorough and systematic testing allowed for a detailed assessment of how the expanded shale layer performed in different scenarios, providing valuable insights into its effectiveness as a component of stormwater management practices.

Furthermore, to gain a comprehensive understanding of the bioswales' performance, a combination of flow visualization and numerical modeling techniques was employed to investigate the flow and sediment dynamics within these systems.

Flow visualization allowed for the direct observation of how water moved within the bioswales, providing a visual representation of flow patterns, velocities, and interactions with the surrounding media. This technique helped to visualize how stormwater runoff traversed the bioswales and how sediment particles were transported and settled within the system.

In conjunction with flow visualization, Flow-3D numerical model was utilized. This computational fluid dynamic model allowed for a more quantitative analysis of flow and sediment dynamics. By inputting data and parameters from the laboratory experiments into the numerical model, additional comprehension was gained on how stormwater would behave within the bioswales

under various conditions. This approach provided valuable insights into the complex interactions between water, sediment, and the bioswale's design elements.

7.1 Conclusions

The following conclusions are made based on the laboratory experiments, flow visualization, and numerical simulations.

7.1.1 Suspended Sediment Experiments

- A 6-inch thickness of expanded shale consistently outperformed the 4-inch thickness in terms of TSS reduction along the entire channel length, regardless of the scenarios tested. This suggests that a thicker layer of expanded shale is more effective at sediment removal. Previous studies have also shown that greater infiltration thickness led to a higher reduction in inflow volume and higher pollutant removal (e.g. [47], [114]).
- Coarser mix of expanded shale generally exhibited better performance than finer mix when the underdrain system was active. However, under inactive underdrain conditions, both coarser and finer mixes performed similarly. The inclusion of an underdrain system significantly enhanced pollutant removal efficiency compared to systems without one. The underdrain system improved drainage, allowing for increased contact between water and the expanded shale media, thus enhancing sediment adsorption. This result aligns with the existing literature findings (e.g., [51], [59]), which indicate that the pollutant removal efficiency is directly related to the degree of infiltration. Additionally, the integration of *internal water storage* (IWS) is considered as a potential design modification to enhance the BMP's performance by mitigating overflow and boosting overall pollutant removal efficiency. This design approach is based on the concept of retaining and temporarily storing stormwater within the system rather than allowing it to immediately overflow. It is reported that the efficiency of nutrient removal was significantly improved when IWS was incorporated into a bioretention system. This suggests that the presence of IWS has a positive impact on the removal of pollutants from stormwater [55]. Therefore, it can be inferred that bioswales, may achieve higher pollutant removal rates when infiltration is promoted by integrating an underdrain system. By enhancing water retention and infiltration capabilities, such design modifications can contribute to more effective stormwater treatment and improved water quality outcomes within bioswales.
- The study's findings indicated a notable trend in the efficiency of TSS and turbidity removal as inflow rates increased. Specifically, as the inflow rates increased, the overall effectiveness of removing TSS and Tu decreased. This observation underscores the critical importance of taking inflow rates into account when formulating stormwater management strategies. This trend aligns with similar findings reported for TSS and Tu removal in bioswales [115]. The consistency in these observations suggests that the relationship between pollutant removal efficiency and flow rates is a crucial factor to consider when designing and implementing stormwater management measures, particularly within bioswales. In practical terms, these

findings imply that stormwater management strategies should not only focus on the design and performance of treatment systems but also take into account the variability in flow rates to optimize pollutant removal effectiveness and ensure the overall success of stormwater management efforts.

- While TSS and turbidity showed similar reduction patterns in most scenarios, the results showed that swale was less effective in reducing turbidity. Even in some scenarios, an increase in Tu was observed from the middle section of the flume to the overflow. Such variation in Tu was attributed to the resuspension of the settled-out sediments caused by the presence of the check dam or the change in the composition of suspended sediment that became finer along the flow. Higher turbidity in overflow than infiltrated water was previously reported in the bioswales [64].
- Although, the overall TSS and Tu removal efficiencies were the same for low and high influent sediment concentration, the individual experiments had differences in TSS removal at the outflow (infiltrated water). It was observed that when the influent concentration was doubled from 100 to 200 mg/L, the effluent concentration range was also approximately doubled. This observation agrees with previous studies that showed the efficiency of the bioswales is dependent on the influent concentration [31].
- The results showed that the TSS decreased at a higher rate along the first half-length of the flume, and at a much smaller rate in the second half. This observation is in line with the previous studies which showed that TSS concentration reduces exponentially along the flow (e.g., [117], [118]).
- The particle size gradation analysis indicated that coarser particles settled in the upstream part of the swale, resulting in a higher reduction in TSS and turbidity within half of the flume's total length. Also, while the particle gradation change along the flume length remained relatively constant over time, the gradation in the middle and overflow samples varied with changes in the inflow rate. The results showed that the flow did not have enough time to settle out the coarser particles during high inflows due to higher flow velocity in the flume and shorter hydraulic residence time. Unlike during the low inflows experiments, in which particles in the overflow were finer than in the middle section, high inflow conditions resulted in coarser particles in overflow. Also, no drastic change in particle size was observed during high inflow experiments as observed during low inflows. The findings of this study regarding change in suspended sediment gradation during low inflow scenarios align with the observations made in earlier studies where decrease in sediment size along the length of swales was also noted (e.g. [117], [118]).

7.1.2 Chemical Experiments

- The results from chemical experiments indicated that chemical reduction in the overflow (flow passing over the downstream weir) was not significant, and in some cases, concentrations even increased. This suggests that the hydraulic residence time (*HRT*) in the

experiments might not have been sufficiently long to allow for the absorption of chemicals on the soil media's surface. In contrast, chemical reduction in the underflow (flow passing through the soil media) was substantial.

- Generally, the efficiency of nutrient removal was higher when an underdrain was incorporated into the system compared to scenarios without an underdrain. The presence of an underdrain likely improves drainage and, as a result, increases the exposure of stormwater to the bioswale's treatment media, facilitating more effective nutrient removal.
- The chemical concentrations decreased along the flume length. Typically, the middle of the flume had a concentration similar to the inlet, while the undertrained flow showed a significantly lower concentration. This demonstrates shale's effectiveness in chemical removal.
- The study's results indicate that the bioswale has the capacity to reduce nitrogen, phosphorus, and zinc, though the outcomes vary under different flow conditions. Particularly noteworthy is the finding that reducing the inflow rate led to a substantial increase in the removal efficiency of these chemicals. In low inflow experiment conditions (without overflow), the bioswale demonstrated maximum removal efficiencies of 80% for nitrogen, 75% for phosphorus, and 90% for zinc. This suggests that a controlled, slower inflow rate through the bioswale enhances its ability to effectively remove these chemicals from stormwater runoff. The literature does not provide conclusive evidence regarding the effectiveness of various BMPs in removing nitrogen, phosphorus, and zinc (see Table 2.3). For example, the reported effectiveness of a dry swale ranged from (–49.2%) to 68.7% for total phosphorus, (–25.6%) to 85.6% for total nitrogen, and 18% to 92.6% for heavy metals (lead, copper, zinc, and cadmium) [49]. In the case of bioswales, these values were reported as 31%, 32%, and 31%-60%, respectively [60].
- The study observed that the efficiency of chemical removal remained stable over time. This suggests that the bioswale's performance in removing these chemicals reached a consistent level of effectiveness after a certain duration of operation. This stability is an important aspect to consider when evaluating the long-term performance and reliability of bioswales in stormwater management systems.

7.1.3 Flow Visualization and Numerical Modeling

- The results from flow visualization and numerical modeling showed that the flow dynamics within the swale exhibited significant variations between low and high inflow conditions. In both scenarios, the presence of the check dam induced a backwater effect, causing the flow to rebound as it approached the downstream section of the flume. However, during the high inflow experiment, this rebound effect was much more pronounced compared to the low inflow case. Consequently, vertical eddies formed in the downstream area and propagated towards the inlet, leading to a reversal of the typical flow direction. Velocity vectors indicated an upstream movement caused by these eddies.

- The formation of these eddies and the reversal of flow had notable implications for sediment dynamics within the swale. Some of the suspended sediment particles that had initially reached the swale's outlet were redirected back toward the upstream region. This phenomenon had dual effects. On one hand, it potentially prolonged the hydraulic residence time within the swale, thereby enhancing sediment removal through sedimentation processes. On the other hand, the vertical eddies might have resuspended sediments that had already settled on the swale's bed, allowing the flow to transport them out of the swale through the downstream weir. This resuspension effect could potentially diminish the overall efficiency of the swale in sediment removal.
- The presence of vertical eddies and the reversal of flow direction created a complex interplay between sediment retention and re-suspension processes within the swale. These dynamics had a substantial impact on the swale's effectiveness in mitigating sediment-related issues in stormwater runoff, highlighting the importance of considering flow variations in swale design and operation.

7.2 Implementation Recommendations

Based on the findings of this study, several implementation recommendations are proposed for the design of bioswales using expanded shale as the filtration media:

Enhancing Treatment Effectiveness: The study suggests that incorporating expanded shale into the soil alongside vegetation can significantly enhance the treatment effectiveness of bioswales. This combination not only improves pollutant removal but also promotes increased vegetation growth, which further contributes to the overall effectiveness of the bioswale in mitigating water pollution.

Bioswale Sizing: Instead of using the Aberdeen equation for sizing bioswales, it is recommended to consider a sizing method based on hydraulic residence time (*HRT*), as recommended by Caltrans [26]. This approach can potentially result in more efficient and appropriately sized bioswales, avoiding the creation of unnecessarily long channels.

Residence Time for Chemical Removal: While the hydraulic residence time calculated for sediment removal from stormwater may be adequate, it may not be long enough for the effective removal of certain chemicals such as nitrogen, phosphorus, and zinc. To address this, it is suggested that bioswales designed for the removal of these pollutants should be constructed with longer hydraulic residence times to allow for better absorption by the expanded shale media.

Direct Measurement of TSS: To accurately assess the suspended sediment removal efficiency of bioswales, it is recommended to directly measure total suspended solids (TSS) at both the inlet and outlet of the bioswale. This approach is preferred over using turbidity as a surrogate for TSS, as it provides a more precise estimate of removal efficiency.

Media Depth: When using expanded shale as the filter media, it is advisable to use a filter bed with a minimum depth of at least 6 inches. Additionally, for optimal performance, consider mixing

expanded shale with native soil or sandy clay soil in a ratio of 2/3 expanded shale and 1/3 soil. This combination offers a balance between effective filtration and vegetation support.

Strategic Placement of Check Dams: When designing bioswales, carefully determine the location of check dams based on the size of the swale and the expected inflow rate. It is recommended to utilize numerical modeling techniques to calculate the appropriate spacing between check dams. This ensures that they effectively control the flow, prevent erosion, and maximize treatment efficiency.

Underdrain System: The inclusion of an underdrain system is highlighted as a significant enhancement for pollutant removal efficiency within a shorter treatment area. Such a system allows for efficient collection and removal of treated water, preventing the buildup of pollutants in the treatment area. This contributes to consistent and efficient pollutant removal, making it a valuable addition to bioswale design.

By implementing these recommendations, designers and engineers can optimize the performance of bioswales using expanded shale as a filtration medium, enhancing their effectiveness in mitigating stormwater pollution and promoting sustainable urban water management.

7.3 Recommendations for Future Work

The following recommendations for future work based on the findings of this study offer valuable directions for expanding our understanding of the use of expanded shale as a filtration medium in stormwater management.

Impact of Clogging: Investigating the long-term impact of clogging on expanded shale media is crucial. While in this study no clogging was observed, more extensive experiments are needed to assess how it affects pollutant removal efficiency over an extended period. Understanding the factors leading to clogging and its mitigation strategies can inform the design and maintenance of sustainable stormwater systems.

Effects of Inflow Patterns: This recommendation suggests conducting studies that incorporate different inflow patterns, including lateral flows. The current experimental facilities had limitations in simulating diverse inflow scenarios. By exploring the effects of various inflow patterns, insights can be gained into how different flow dynamics influence the performance of expanded shale-based stormwater management systems.

Influence of Vegetation: In real-world stormwater management scenarios, natural vegetation can play a significant role in affecting flow dynamics and pollutant removal efficiency. Investigating the combined effect of vegetation and expanded shale media is essential for practical applications. Research in this area can help optimize the design of bioswales and similar systems that incorporate vegetation as part of their pollutant removal strategies.

Cost-Benefit Analysis: Conducting a cost-benefit analysis comparing expanded shale as a filter media with existing filter media is critical for assessing the economic feasibility of using expanded shale in stormwater management. This analysis can provide decision-makers with valuable

information regarding the financial implications of adopting expanded shale and its potential advantages over traditional filter media.

Comprehensive Field Experiment: Expanding the research beyond laboratory experiments to include comprehensive field experiments is essential. Field experiments should consider volume reduction through the bottom and sides of the treatment area, simulating real-world conditions more accurately. This approach allows for a better assessment of the actual efficiency of expanded shale in stormwater treatment and management.

Technology Transfer and Site Implementation: Collaborating with local authorities, such as the, for potential site implementations is a crucial step in bringing laboratory-tested technologies to practical use. Transferring technology from the lab to the field involves pilot projects and real-world implementations, ensuring that research findings are applied effectively to improve stormwater management practices.

Incorporating these recommendations into future research efforts will not only advance our understanding of expanded shale as a stormwater management tool but also contribute to more effective and sustainable urban water management practices. This research can lead to innovative solutions for addressing water quality and environmental challenges in urban areas.

REFERENCES

1. Washington State Department of Ecology. 2019. *Stormwater Management Manual for Western Washington*, Water Quality Program, Publication No. 10-10-021, Washington, D.C.
2. Johnson, K., Cai, M., Patelke, M., Saftner, D., & Swanson, J. 2017. Comparing Properties of Water Absorbing/Filtering Media for Bioslope/Bioswale Design. Minnesota Department of Transportation, St. Paul, Minnesota. Accessed Sep 4, 2023. https://core.ac.uk/download/pdf/211352841.pdf
3. Yang, D., Y. Yang, and J. Xia. 2021. Hydrological cycle and water resources in a changing world: A review. Geography and Sustainability, 2 (2): 115–122. https://doi.org/10.1016/j.geosus.2021.05.003.
4. Sun, N., Limburg, K. E., & Hong, B. 2019. The Urban Hydrological System. In Understanding Urban Ecology. https://doi.org/10.1007/978-3-030-11259-2_6
5. McGrane, S. J. 2016. Impacts of urbanization on hydrological and water quality dynamics, and urban water management: a review. Hydrological Science Journal, 61 (13): 2295–2311. Taylor & Francis. https://doi.org/10.1080/02626667.2015.1128084.
6. Pringle, C. M. 2000. Managing riverine connectivity in complex landscapes to protect remnant natural areas. SIL Proc. 1922-2010, 27 (3): 1149–1164. Taylor & Francis. https://doi.org/10.1080/03680770.1998.11901419.
7. Akan, A. O., and R. J. Houghtalen. 2003. Urban Hydrology, Hydraulics, and Stormwater Quality: Engineering Applications and Computer Modeling. John Wiley & Sons.
8. Thorpe, A., and R. M. Harrison. 2008. Sources and properties of non-exhaust particulate matter from road traffic: A review. Science of Total Environment, 400 (1): 270–282. https://doi.org/10.1016/j.scitotenv.2008.06.007.
9. Environmental Protection Agency (EPA). 2017. National Water Quality Inventory Report to Congress." Reports and Assessments. Accessed June 16, 2023. https://www.epa.gov/waterdata/2017-national-water-quality-inventory-report-congress.
10. Brinkmann, W. L. F. 1985. Urban stormwater pollutants: Sources and loadings. Geo Journal, 11 (3): 277–283. https://doi.org/10.1007/BF00186341.
11. Björklund, K., M. Bondelind, A. Karlsson, D. Karlsson, and E. Sokolova. 2018. Hydrodynamic modelling of the influence of stormwater and combined sewer overflows on receiving water quality: Benzo(a)pyrene and copper risks to recreational water. J. Environ. Manage., 207: 32–42. https://doi.org/10.1016/j.jenvman.2017.11.014.
12. Lee, H., X. Swamikannu, D. Radulescu, S. Kim, and M. K. Stenstrom. 2007. Design of stormwater monitoring programs. Water Research, 41 (18): 4186–4196. https://doi.org/10.1016/j.watres.2007.05.016.

13. Zhang, W., J. Li, H. Sun, and W. Che. 2021. Pollutant first flush identification and its implications for urban runoff pollution control: a roof and road runoff case study in Beijing, China. Water Science and Technology, 83 (11): 2829–2840. https://doi.org/10.2166/wst.2021.157.

14. Wang, Y., H. Yin, Z. Liu, and X. Wang. 2022. A Systematic Review of the Scientific Literature on Pollutant Removal from Stormwater Runoff from Vacant Urban Lands." Sustainability, 14 (19): 12906. https://doi.org/10.3390/su141912906.

15. Dang, D. P. T., L. Jean-Soro, and B. Bechet. 2023. Pollutant characteristics and size distribution of trace elements during stormwater runoff events. Environmental Challenges, 11: 100682. https://doi.org/10.1016/j.envc.2023.100682.

16. Maniquiz-Redillas, M., M. E. Robles, G. Cruz, N. J. Reyes, and L.-H. Kim. 2022. First Flush Stormwater Runoff in Urban Catchments: A Bibliometric and Comprehensive Review. Hydrology, 9 (4): 63. Multidisciplinary Digital Publishing Institute. https://doi.org/10.3390/hydrology9040063.

17. Lee, J. H., K. W. Bang, L. H. Ketchum, J. S. Choe, and M. J. Yu. 2002. First flush analysis of urban storm runoff. Sci. Total Environ., 293 (1): 163–175. https://doi.org/10.1016/S0048-9697(02)00006-2.

18. U.S. Department of Agriculture (USDA). 2020. Stormwater Runoff Control (Ac.) (570) Conservation Practice Standard, Natural Resources Conservation Service. Accessed July 28, 2023. https://www.nrcs.usda.gov/sites/default/files/2022-10/Stormwater_Runoff_Control_570_CPS_9_2020.pdf.

19. Xiao, Q., and G. McPherson. 2011. Performance of engineered soil and trees in a parking lot bioswale. Urban Water Journal 84 241-253, 8 (4): 241–253. https://doi.org/10.1080/1573062X.2011.596213.

20. Integrated Stormwater Management (iSWM) 2014. iSWM Technical Manual, Water Quality. Accessed July 3, 2023. https://iswm.nctcog.org/Documents/technical_manual/Water%20Quality_9-2014.pdf

21. Bertrand-Krajewski, J.-L. 2021. Integrated urban stormwater management: Evolution and multidisciplinary perspective. J. Hydro-Environment Research, Sustainable Urban Drainage, 38: 72–83. https://doi.org/10.1016/j.jher.2020.11.003.

22. Environmental Protection Agency (EPA). What is Green Infrastructure? Green Infrastructure. Accessed July 29, 2023. https://www.epa.gov/green-infrastructure/what-green-infrastructure

23. Fletcher, T. D., W. Shuster, W. F. Hunt, R. Ashley, D. Butler, S. Arthur, S. Trowsdale, S. Barraud, A. Semadeni-Davies, J. L. Bertrand-Krajewski, P. S. Mikkelsen, G. Rivard, M. Uhl, D. Dagenais, and M. Viklander. 2015. SUDS, LID, BMPs, WSUD and more - The evolution

and application of terminology surrounding urban drainage. Urban Water Journal, 12 (7): 3–20. https://doi.org/10.1080/1573062X.2014.916314.

24. Environmental Protection Agency (EPA). 2014. Best Management Practices (BMPs) Siting Tool. Overviews and Factsheets. Accessed June 16, 2023. https://www.epa.gov/water-research/best-management-practices-bmps-siting-tool.

25. Brander, K. E., K. E. Owen, and K. W. Potter. 2004. Modeled Impacts of Development Type on Runoff Volume and Infiltration Performance1. JAWRA Journal of the American Water Resources Association, 40 (4): 961–969. https://doi.org/10.1111/j.1752-1688.2004.tb01059.x.

26. California Department of Transportation (Caltrans) 2020. Biofiltration Swale Design Guidance, Caltrans Division of Design, Office of Hydraulics and Stormwater Design, Sacramento, CA. https://dot.ca.gov/-/media/dot-media/programs/design/documents/2_dg-biofiltration_swale_ada.pdf

27. Environmental Protection Agency (EPA). 1999. Preliminary Data Summary of Urban Storm Water Best Management Practices. Office of Water. Accessed July 18, 2023. https://www.epa.gov/sites/default/files/2015-11/documents/urban-stormwater-bmps_preliminary-study_1999.pdf

28. Environmental Protection Agency (EPA). 2022. NPDES, National Menu of Best Management Practices (BMPs) for Stormwater. Accessed July 29, 2023. https://www.epa.gov/npdes/national-menu-best-management-practices-bmps-stormwater

29. Osouli, A., A. A. Bloorchian, M. Grinter, A. Alborzi, S. L. Marlow, L. Ahiablame, and J. Zhou. 2017. Performance and Cost Perspective in Selecting BMPs for Linear Projects. Water, 9 (5): 302. Multidisciplinary Digital Publishing Institute. https://doi.org/10.3390/w9050302.

30. Riverside County 2020. LID BMP Handbook. Watershed Protection, Accessed May 7, 2023. https://rcwatershed.org/permittees/riverside-county-lid-bmp-handbook/

31. Barrett, M. E., L. B. Irish, J. F. Malina, and R. J. Charbeneau. 1998. Characterization of Highway Runoff in Austin, Texas, Area. J. Environmental Engineering, 124 (2): 131–137. American Society of Civil Engineers. https://doi.org/10.1061/(ASCE)0733-9372(1998)124:2(131).

32. Environmental Protection Agency (EPA). 2012. Green Infrastructure, Western Ecology Division. Office of Research and Development. Accessed July 25, 2023. https://nepis.epa.gov/Exe/ZyPURL.cgi?Dockey=P100Z2P1.txt

33. Eckart, K., Z. McPhee, and T. Bolisetti. 2017. Performance and implementation of low impact development –A review. Science of The Total Environment, 607–608: 413–432. https://doi.org/10.1016/j.scitotenv.2017.06.254.

34. Ekka, S. A., H. Rujner, G. Leonhardt, G.-T. Blecken, M. Viklander, and W. F. Hunt. 2021. Next generation swale design for stormwater runoff treatment: A comprehensive approach.J. Environmental Management, 279: 111756. https://doi.org/10.1016/j.jenvman.2020.111756.

35. Clar, M. L., B. J. Barfield, and T. P. Connor. 2004. Stormwater Best Management Practices Design Guide Volume 2 - Vegetative Biofilters. US Environmental Protection Agency, 2.

36. Ekka, S. and Hunt, B. 2020. Swale Terminology for Urban Stormwater Treatment, Urban Waterway Series, NC State Extension, North Carolina State University. Assessed June 14, 2023). https://content.ces.ncsu.edu/swale-terminology-for-urban-stormwater-treatment.

37. North Carolina Department of Transportation (NCDOT). 2014. Stormwater Best Management Practices Toolbox. n.d. Accessed July 28, 2023. https://connect.ncdot.gov/resources/hydro/HSPDocuments/2014_BMP_Toolbox.pdf

38. Integrated Stormwater Management (iSWM) 2015. iSWM Criteria Manual for Site Development and Construction. Accessed July 3, 2023. https://iswm.nctcog.org/Documents/iSWM_Criteria_Manual_01142015.pdf

39. Iowa Storm Water Management Manual (iSWMM). 2009. Design Standards Chapter 9- Vegetated Swale Systems. Accessed Sep. 3, 2023. https://www.iowadnr.gov/Portals/idnr/uploads/water/stormwater/manual/iswmm_chapter09.pdf.

40. Minnesota Pollution Control Agency, Minnesota Stormwater Manual- Terminology for swales. Available online at: https://stormwater.pca.state.mn.us/index.php?title=Terminology_for_swales, (Accessed Dec. 15, 2022)

41. Mustaffa, N., N. A. Ahmad, and M. A. M. Razi. 2016. Variations of roughness coefficients with flow depth of grassed swale. *IOP Conference Series: Materials Science and Engineering*, vol. 136, no. 1, p. 012082. IOP Publishing.

42. Gibb, T., *Bioswales Can Improve Water Quality Resource.* 2015. Michigan State University Extension, Michigan State University. East Lansing, MI, June 10.

43. Environmental Protection Agency (EPA). 2021. Stormwater Best Management Practice, Grassed Swales. NPDES. Accessed July 29, 2023, https://www.epa.gov/system/files/documents/2021-11/bmp-grassed-swales.pdf

44. Nuamah, L. A., Y. Li, Y. Pu, A. S. Nwankwegu, Z. Haikuo, E. Norgbey, P. Banahene, and R. Bofah-Buoh. 2020. Constructed wetlands, status, progress, and challenges. The need for critical operational reassessment for a cleaner productive ecosystem. Journal of Cleaner Production, 269: 122340. https://doi.org/10.1016/j.jclepro.2020.122340.

45. Caflisch, M. and K. Giacalone. 2015. An Introduction to Bioswales, Clemson University.

46. Natural Resources Conservation Service (NRCS). 2005. Bioswales. Accessed July 28 2023 https://mostcenter.umd.edu/sites/default/files/2020-04/NRCS_Bioswale_Fact_Sheet.pdf

47. Brown, R. A., and W. F. Hunt. 2012. Bioretention Performance in the Upper Coastal Plain of North Carolina. 1–10. American Society of Civil Engineers. https://doi.org/10.1061/41009(333)95.

48. Wang, R., X. Zhang, and M.-H. Li. 2019. Predicting bioretention pollutant removal efficiency with design features: A data-driven approach. Journal of Environmental Management, 242: 403–414. https://doi.org/10.1016/j.jenvman.2019.04.064.

49. Stagge, J. H., A. P. Davis, E. Jamil, and H. Kim. 2012. Performance of grass swales for improving water quality from highway runoff. Water Res., 46 (20): 6731–6742. https://doi.org/10.1016/j.watres.2012.02.037.

50. Liu, Y., B. A. Engel, D. C. Flanagan, M. W. Gitau, S. K. McMillan, and I. Chaubey. 2017. A review on effectiveness of best management practices in improving hydrology and water quality: Needs and opportunities. Science of Total Environment, 601–602: 580–593. https://doi.org/10.1016/j.scitotenv.2017.05.212.

51. Clark, M., and Acomb, G. 2008. Bioswales/Vegetated Swales. Accessed July 19, 2023, https://buildgreen.ifas.ufl.edu/fact_sheet_bioswales_vegetated_swales.pdf

52. Minnesota Pollution Control Agency. 2017. Overview of stormwater infiltration https://stormwater.pca.state.mn.us/index.php?title=Overview_of_stormwater_infiltration

53. Ekka, S. A., H. Rujner, G. Leonhardt, G.-T. Blecken, M. Viklander, and W. F. Hunt. 2021. Next generation swale design for stormwater runoff treatment: A comprehensive approach. J. Environmental Management, 279: 111756. https://doi.org/10.1016/j.jenvman.2020.111756.

54. Hunt, W. F., A. R. Jarrett, J. T. Smith, and L. J. Sharkey. 2006. Evaluating Bioretention Hydrology and Nutrient Removal at Three Field Sites in North Carolina. Journal of Irrigation and Drainage Engineering, 132 (6): 600–608. American Society of Civil Engineers. https://doi.org/10.1061/(ASCE)0733-9437(2006)132:6(600).

55. Kim, H., E. A. Seagren, and A. P. Davis. 2003. Engineered bioretention for removal of nitrate from stormwater runoff. Water Environment Research, Publication: Water Environment Federation, 75 (4): 355–367. https://doi.org/10.2175/106143003x141169.

56. King County 1995. Evaluation of Water Quality Ponds and Swales in the Issaquah/East Lake Sammamish Basins. Accessed July 4, 2023. https://your.kingcounty.gov/dnrp/library/1995/kcr853.pdf.

57. Seters, T., D. Smith, and G. MacMillan. 2006. Performance Evaluation of Permeable Pavement and a Bioretention Swale. http://www.sept.org/techpapers/1304.pdf

58. Fardel, A., P.-E. Peyneau, B. Bechet, A. Lakel, and F. Rodriguez. 2019. Analysis of swale factors implicated in pollutant removal efficiency using a swale database. Environmental Science and Pollution Research, 26 (2): 1287–1302. https://doi.org/10.1007/s11356-018-3522-9.

59. Stagge, J. H., A. P. Davis, E. Jamil, and H. Kim. 2012. Performance of grass swales for improving water quality from highway runoff. Water Res., 46 (20): 6731–6742. https://doi.org/10.1016/j.watres.2012.02.037.

60. Hunt, W. F., J. T. Smith, S. J. Jadlocki, J. M. Hathaway, and P. R. Eubanks. 2008. Pollutant Removal and Peak Flow Mitigation by a Bioretention Cell in Urban Charlotte, N.C. Journal of Environmental Engineering, 134 (5): 403–408. American Society of Civil Engineers. https://doi.org/10.1061/(ASCE)0733-9372(2008)134:5(403).

61. Brown, R. A., and W. F. Hunt. 2011. Underdrain configuration to enhance bioretention exfiltration to reduce pollutant loads. Journal of Environmental Engineering 137, no. 11 1082-1091.

62. Knight, E. M. P., W. F. Hunt, and R. J. Winston. 2013. Side-by-side evaluation of four level spreader–vegetated filter strips and a swale in eastern North Carolina. Journal of Soil Water Conservation, 68 (1): 60–72. Soil and Water Conservation Society. https://doi.org/10.2489/jswc.68.1.60.

63. Anderson, B. S., B. M. Phillips, J. P. Voorhees, K. Siegler, and R. Tjeerdema. 2016. Bioswales reduce contaminants associated with toxicity in urban stormwater. Environmental Toxicology and Chemistry, 35 (12): 3124–3134. https://doi.org/10.1002/etc.3472.

64. Purvis, R. A., Winston, R. J., Hunt, W. F., Lipscomb, B., Narayanaswamy, K., McDaniel, A., Lauffer, M.S. & Libes, S. 2018. Evaluating the water quality benefits of a bioswale in Brunswick County, North Carolina (NC), USA. *Water*, *10*(2), 134.

65. Hunt, W. F., E. A. Fassman-Beck, S. A. Ekka, K. C. Shaneyfelt, and A. Deletic. 2020. Designing Dry Swales for Stormwater Quality Improvement Using the Aberdeen Equation. Journal of Sustainable Water in the Built Environment, 6 (1): 05019004. American Society of Civil Engineers. https://doi.org/10.1061/JSWBAY.0000886.

66. Zeiringer, B., C. Seliger, F. Greimel, and S. Schmutz. 2018. River Hydrology, Flow Alteration, and Environmental Flow. Riverine Ecosystem Management, Aquatic Ecology Series, S. Schmutz and J. Sendzimir, eds., 67–89. Cham: Springer International Publishing.

67. U.S. Department of Agriculture (USDA). 2020. Stormwater Runoff Control (Ac.) (570) Conservation Practice Standard, Natural Resources Conservation Service.Accessed July 28, 2023. https://www.nrcs.usda.gov/sites/default/files/2022-10/Stormwater_Runoff_Control_570_CPS_9_2020.pdf

68. City of San Diego (n.d.) Bioswale, Clairemont Boys and Girls Club Accessed 7/4/2023 https://www.sandiego.gov/sites/default/files/legacy/thinkblue/pdf/bioswalelidcard.pdf

69. Anderson, C., J. Klett, J. Bousselot, and K. Barbarick. 2017. Expanded shale as a soil amendment for the Rocky Mountain region. Text. Colorado State University. https://www.proquest.com/openview/83adea18df9ebbd8ebfc432346b5f003/1?pq-origsite=gscholar&cbl=18750

70. Pennsylvania Stormwater (StormwaterPA) 2006. Best Management Practices Manual-Chapter 6. Accessed June 16, 2023. https://www.stormwaterpa.org/bmp-manual-chapter-6.html.

71. Illinois State Toll Highway Authority.2020. Drainage Design Manual. Assessed July 4, 2023 https://www.illinoistollway.com/documents/20184/238191/Drainage+Design+Manual_Mar2020.pdf/498191e4-6457-43a5-b4b3-5c601d4c2478?version=1.4

72. Environmental Protection Agency (EPA). 1999. Storm Water Technology Fact Sheet Vegetated Swales. Office of Water. Accessed July 29, 2023. https://nepis.epa.gov/Exe/ZyPDF.cgi/200044A8.PDF?Dockey=200044A8.PDF

73. North Carolina Department of Environmental Quality (NCDEQ). 2017. Stormwater BMP manual. Assessed July 4, 2023. https://files.nc.gov/ncdeq/Energy%20Mineral%20and%20Land%20Resources/Stormwater/BMP%20Manual/C-11_Treatment_Swale.pdf

74. Chaudhry, M. H. 2022. Channel Design. Open-Channel Flow, M. H. Chaudhry, ed., 283–303. Cham: Springer International Publishing.

75. Winston, R. J., J. T. Powell, and W. F. Hunt. 2019. Retrofitting a grass swale with rock check dams: hydrologic impacts. Urban Water Journal, 16 (6): 404–411. Taylor & Francis. https://doi.org/10.1080/1573062X.2018.1455881.

76. Deletic, A., and T. D. Fletcher. 2006. Performance of grass filters used for stormwater treatment—a field and modeling study. Journal of Hydrology., 317 (3): 261–275. https://doi.org/10.1016/j.jhydrol.2005.05.021.

77. Environmental Protection Agency (EPA). 2016. Summary of State Post Construction Stormwater Standards. Office of Water. Accessed July 21, 2023. https://www.epa.gov/sites/default/files/2016-08/documents/swstdsummary_7-13-16_508.pdf

78. Mechleb, G., R. Gilbert, M. Christman, R. Gupta, and B. Gross. 2014. Use of Expanded Shale Amendment to Enhance Drainage Properties of Clays. 3454. https://doi.org/10.1061/9780784413272.334

79. Expanded Shale, Clay and Slate Institute (ESCSI). 2018. Expanded Shale, Clay and Slate in Water Filtration, Publication #8676 02-2018. Chicago, IL. Accessed July 29, 2023.

www.escsi.org/wp-content/uploads/2018/03/ESCSI-Water-Treatment-Brochure-1.9-FINAL.pdf

80. Sloan, J. J., Mackay, W. A., Colbaugh, P., George, S. W., & Feagley, S. 2002. The suitability of expanded shale as an amendment for clay soils. *HortTechnology*, *12*(4), 646-651.

81. Forbes, M., K. Dickson, T. Golden, P. Hudak, and R. Doyle. 2004. Dissolved Phosphorus Retention of Light-Weight Expanded Shale and Masonry Sand Used in Subsurface Flow Treatment Wetlands. Environmental Science and Technology, 38: 892–8. https://doi.org/10.1021/es034341z.

82. Forbes, M. G., K. L. Dickson, F. Saleh, W. T. Waller, R. D. Doyle, and P. Hudak. 2005. Recovery and Fractionation of Phosphorus Retained by Lightweight Expanded Shale and Masonry Sand Used as Media in Subsurface Flow Treatment Wetlands. Environmental Science and Technology, 39 (12): 4621–4627. American Chemical Society. https://doi.org/10.1021/es048149o.

83. Hauser, J., J. Curtis, J. Johnston, D. Patel, and M. Keisler. 2005. Small-Scale Pilot Testing of Stormwater Treatment Systems To Meet Numerical Effluent Limits in the Lake Tahoe Basin. Proceedings of Water Environment Federation Technical Exhibition and Conference, 3051–3081. http://dx.doi.org/10.2175/193864705783865271

84. Mateus, D. M. R., and H. J. O. Pinho. 2010. Phosphorus Removal by Expanded Clay-Six Years of Pilot-Scale Constructed Wetlands Experience. Water Environment Research, 82 (2): 128–137. Water Environment Federation. https://doi.org/10.2175/106143009X447894

85. Sloan, J. J., R. I. Cabrera, P. A. Y. Ampim, S. A. George, and W. A. Mackay. 2010. Performance of Ornamental Plants in Alternative Organic Growing Media Amended with Increasing Rates of Expanded Shale. HortTechnology, 20 (3): 594–602. American Society for Horticultural Science. https://doi.org/10.21273/HORTTECH.20.3.594.

86. Sloan, J. J., Ampim, P. A., Cabrera, R. I., Mackay, W. A., & George, S. W. 2011. Moisture and Nutrient Storage Capacity of Calcined Expanded Shale. In *Principles, Application and Assessment in Soil Science*. IntechOpen.

87. Jaber, F., and Sloan, J. 2014. Evaluating Trinity Materials Pave Grow® as Pervious Cover. Texas A&M Agrilife Extension Service, Final Report.

88. Li, J., C. Jiang, T. Lei, and Y. Li. 2016. Experimental study and simulation of water quality purification of urban surface runoff using non-vegetated bioswales. Ecol. Eng., 95: 706–713. Elsevier. https://doi.org/10.1016/j.ecoleng.2016.06.060.

89. New Jersey Department of Environmental Protection (NJDEP) (n.d.). Laboratory Protocol to Access TSS Removal by a Filtration Manufactured Treatment Method. Assessed July 19, 2023. https://dep.nj.gov/wp-content/uploads/stormwater/filter-protocol-final-2022-0114.pdf

90. Tecweigh (n.d.). Volumetric Feeders/Auger Feeders. Accessed July 19, 2023. https://www.tecweigh.com/products/volumetric-feeders/

91. ASTM International. 2017. Standard test methods for Particle-Size Distribution (Gradation) of soils using Sieve analysis. ASTM D6913-04. https://doi.org/10.1520/D6913-04.

92. Barrett, M. E., L. B. Irish, J. F. Malina, and R. J. Charbeneau. 1998. Characterization of Highway Runoff in Austin, Texas, Area. J. Environmental Engineering, 124 (2): 131–137. American Society of Civil Engineers. https://doi.org/10.1061/(ASCE)0733-9372(1998)124:2(131).

93. Claytor, R. A. 1996. Design of stormwater filtering systems. Solomons, MD (P.O. Box 1280, Solomons 20688), Silver Spring, MD (8737 Colesville Rd., Silver Spring 20910): Chesapeake Research Consortium.

94. Environmental Protection Agency (EPA). 2023. Operating Procedure: Wastewater Flow Measurement. Assessed July 25, 2023 https://www.epa.gov/sites/default/files/2015-10/documents/wastewater_flow_measurement109_af.r4.pdf

95. U.S. Geological Survey (USGS). 2006. National Field Manual for the Collection of Water-Quality Data. Accessed July 25, 2023. https://www.usgs.gov/centers/new-england-water-science-center/science/quality-stormwater-runoff-discharged-connecticut.

96. Environmental Protection Agency (EPA). 2017. Total Suspended Solids, EPA Method 160.2 (Gravimetric). https://19january2017snapshot.epa.gov/sites/production/files/2015-06/documents/160_2.pdf

97. Thielicke, W., and E. J. Stamhuis. 2014. *PIVlab* - Time-Resolved Digital Particle Image Velocimetry Tool for MATLAB. https://doi.org/10.6084/m9.figshare.1092508.v19.

98. Thielicke, W., and R. Sonntag. 2021. Particle Image Velocimetry for MATLAB: Accuracy and enhanced algorithms in PIVlab. *JORS*, 9 (1): 12. https://doi.org/10.5334/jors.334.

99. Thielicke, W., and E. J. Stamhuis. 2014. PIVlab – Towards User-friendly, Affordable and Accurate Digital Particle Image Velocimetry in MATLAB. Journal of Open Research Software, 2. https://doi.org/10.5334/jors.bl.

100. Tahar Berrabah, A., Belharizi, M., Laulusa, A., and Bekkouche, A. 2012. Three-Dimensional Modal Analysis of Brezina Concrete Arch Dam, Algeria. *Earth Science Research*, 1(2).

101. Omidi, O., and Lotfi, V. 2017. A symmetric implementation of pressure-based fluid–structure interaction for nonlinear dynamic analysis of arch dams. Journal of Fluids and Structures, 69, 34–55.

102. Zawawi, M. H., Hassan, N. H., Ramli, M. Z., Zahari, N. M., Radzi, M. R. M., Saleha, A., Salwa, A., Sidek, L. M., Muda, Z. C., and Kamaruddin, M. A. 2018. Fluid-structure interactions study on hydraulic structures: A review. 020244.

103. Le Quéré, P. A., Nistor, I., and Mohammadian, A. 2020. Numerical Modeling of Tsunami-Induced Scouring around a Square Column: Performance Assessment of FLOW-3D and Delft3D. Journal of Coastal Research, 36(6).
104. Ibrahim Al Shaikhli, H., and Issa Khassaf, S. 2022. Using of Flow 3D as CFD materials approach in waves generation. *Materials Today: Proceedings*, 49, 2907–2911.
105. Sabeti, R., and Heidarzadeh, M. 2022. Numerical Simulations of Tsunami Wave Generation by Submarine Landslides: Validation and Sensitivity Analysis to Landslide Parameters. Journal of Waterway, Port, Coastal, and Ocean Engineering, 148(2).
106. Man, C., Zhang, G., Hong, V., Zhou, S., and Feng, Y. (2019). Assessment of Turbulence Models on Bridge-Pier Scour Using Flow-3D. World Journal of Engineering and Technology, 07(02), 241–255.
107. Jalal, H. K., and Hassan, W. H. 2020. Effect of Bridge Pier Shape on Depth of Scour. *IOP* Conference Series: Materials Science and Engineering, 671(1), 012001.
108. Gupta, L. K., Pandey, M., and Anand Raj, P. 2023. Numerical simulation of local scour around the pier with and without airfoil collar (AFC) using FLOW-3D. Environmental Fluid Mechanics.
109. Thanh, N. V., Chung, D. H., & Nghien, T. D. (2014). Prediction of the local scour at the bridge square pier using a 3D numerical model. Open Journal of Applied Sciences, 2014.
110. Ghasemi, M., & Soltani-Gerdefaramarzi, S. (2017). The scour bridge simulation around a cylindrical pier using Flow-3D. Journal of Hydrosciences and Environment, 1(2), 46-54.
111. Shahriyar, M. A. 2021. Numerical investigation of local scour around different shaped bridge piers using FLOW-3D software. Doctoral dissertation, Department of Mechanical and Production Engineering *(MPE)*, Islamic University of Technology (IUT), Board Bazar, Gazipur, Bangladesh).
112. Hirt, C., and J. Sicilian. 1985. A porosity technique for the definition of obstacles in rectangular cell meshes. In Proc., 4th Int. Conf. Ship Hydrodynamics. Washington, DC: National Academy of Sciences.
113. Flow Science, Inc., Santa Fe, NM, USA. FLOW-3D® Version 12.0 User's Manual. 2018. [Online]. Accessed Sep. 3, 2023.
114. Li, H., L. J. Sharkey, W. F. Hunt, and A. P. Davis. 2009. Mitigation of Impervious Surface Hydrology Using Bioretention in North Carolina and Maryland. Journal of Hydrologic Engineering, 14 (4): 407–415. American Society of Civil Engineers. https://doi.org/10.1061/(ASCE)1084-0699(2009)14:4(407).
115. Grooves W. G. W.,P. E. Hammer, K. L. Knutsen, S. M. Ryan, and R. A. Schlipf, 1999. Analysis of Bioswale efficiency for Treating Surface Runoff, University of California, Santa Barbara https://bren.ucsb.edu/projects/analysis-bioswale-efficiency-treating-surface-runoff
116. Yu, S., S. Barnes and V. Gerde. 1993. Testing of Best Management Practices for Controlling Highway Runoff, Phase II. Virginia Transportation Research Council. FHWA/VA-94-R21.

117. Deletic, A. 2005. Sediment transport in urban runoff over grassed areas. J. Hydrol., 301 (1): 108–122. https://doi.org/10.1016/j.jhydrol.2004.06.023.

118. Lucke, T., Kachchu Mohamed, M. A., and Tindale, N. 2014. Pollutant removal and hydraulic reduction performance of field grassed swales during runoff simulation experiments.Water,6(7), 1887-1904. http://dx.doi.org/10.3390/w6071887